

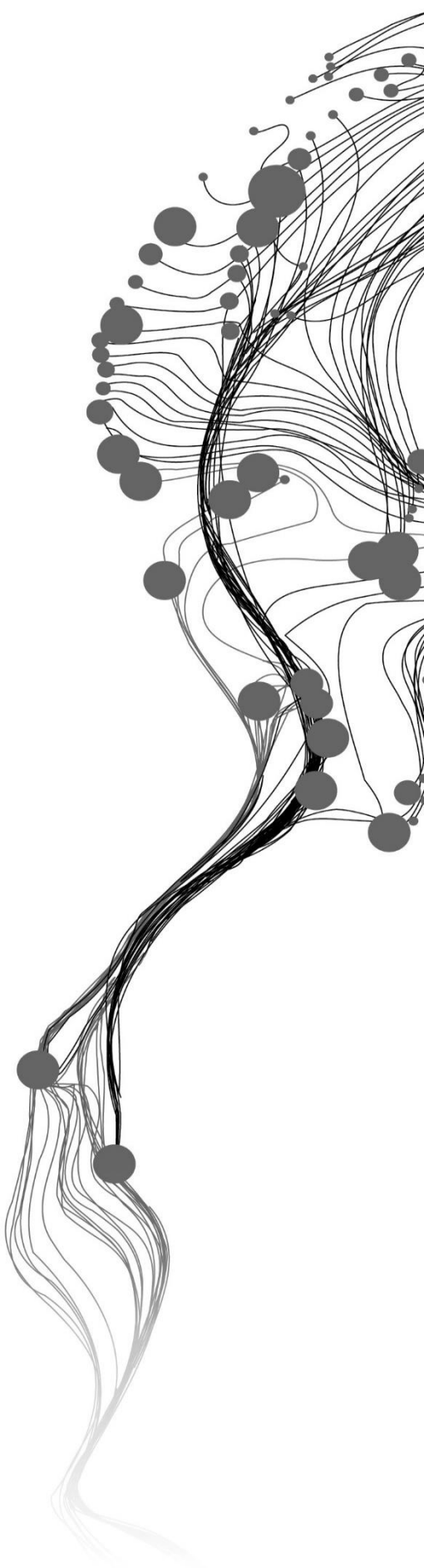
**FLOOD MONITORING AND DAMAGE
ASSESSMENT IN AGRICULTURAL
FIELDS USING SENTINEL-1 SAR IMAGES
AND DIGITAL ELEVATION MODELS: A
CASE STUDY OF THE WHITE VOLTA
RIVER IN GHANA**

RAPHAEL A. GURIBIE

October, 2020

SUPERVISORS:

Prof.dr. V.G. Jetten Victor
Drs. N.C. Kingma



**FLOOD MONITORING AND DAMAGE
ASSESSMENT IN AGRICULTURAL
FIELDS USING SENTINEL-1 SAR
IMAGES AND DIGITAL ELEVATION
MODELS: A CASE STUDY OF THE
WHITE VOLTA RIVER IN GHANA**

RAPHAEL A. GURIBIE

Enschede, The Netherlands, October, 2020

Thesis submitted to the Faculty of Geo-Information Science and Earth Observation of the University of Twente in partial fulfilment of the requirements for the degree of Master of Science in Geo-information Science and Earth Observation. Specialization: Spatial Engineering

SUPERVISORS:
Prof.dr. V.G. Jetten Victor
Drs. N.C. Kingma

DISCLAIMER

This document describes work undertaken as part of a programme of study at the Faculty of Geo-Information Science and Earth Observation of the University of Twente. All views and opinions expressed therein remain the sole responsibility of the author, and do not necessarily represent those of the Faculty.

DECLARATION

I, Raphael A. Guribie, hereby declare that this dissertation entitled “Flood Monitoring and Damage Assessment In Agricultural Fields Using Sentinel-1 Sar Images and Digital Elevation Models: A Case Study of the White Volta River in Ghana” is the result of my own original work, except for reference to the work of others which have been duly acknowledged; and that no part of the work has been presented for another degree in this university or elsewhere and I take full responsibility for all errors.

.....

Raphael A. Guribie

(s2084074)

.....

Date

CERTIFICATION

This dissertation entitled “Flood Monitoring and Damage Assessment In Agricultural Fields Using Sentinel-1 Sar Images and Digital Elevation Models: A Case Study of the White Volta River in Ghana” prepared and submitted by Mr. Raphael A. Guribie in partial fulfilment of the requirements for the award of Master of Science degree in environmental science under our supervision is hereby accepted.

.....

Raphael .A. Guribie
(s208074)

.....

Date

.....

Prof.dr. V.G. Jetten Victor (ESA)
(Supervisor)

.....

Date

.....

Drs. N.C. Kingma (ESA)
(Supervisor)

.....

Date

.....

(Chairperson)

.....

Date

Abstract

Flood is a destructive natural hazard which leads to the loss of lives, properties and resources. Floods are currently predominantly prevalent the world over, resulting in damages worth millions. Northern region of Ghana experiences riverine floods along the White Volta river on annual bases which result in destruction of farms. Geographic Information System (GIS) and remote sensing; optical, Synthetic Aperture Radar (SAR), and Digital Elevation Models (DEMs) have proven over the years to be useful tools in flood monitoring and mapping. This research seeks to monitor flood and assess damage in agricultural fields Using Sentinel-1 SAR Images and Digital Elevation Models; the study also compared the quality of the different DEMs (SPOT, PALSAR and SRTM) used in estimating flood depths and flood extents. The quality of the DEMs were inferior, but the SPOT had better quality compared to the rest, followed by SRTM, and PALSAR DEM had the worse quality. For this study, Sentinel SAR Images from three dates (12th,18th and 24th) of September 2018 were used in monitoring and assessing inundation extent in agricultural fields. Multi Criteria Analysis (MCA) additive model was used in the damage and risk assessment. A composite flood hazard index was developed incorporating variables such as the crops grown, the flood depths, the water tolerance and damage per hector in a GIS environment. The results indicate that the methods used could integrate all the flood hazard causative factors and the components of flood risk in a GIS environment. This led to the generation of various composite maps to assess flood hazard of farms along the White Volta. About 50% of the flooded area is between 0 to 2m depth. Sorghum was considered as the most vulnerable crop to flooding, and rice was the least vulnerable crop. Crops in the lower Volta were also considered as most vulnerable compared to crops grown in the Upper Volta. In terms of calculated damages, sorghum was identified as the crop with high cost and rice was the least. Farmers farming very close to the White Volta River are advised to desist from farming close to the river during the rainy season, as floods occur during this period to evade the floods. Farmers should also adopt the use of early maturing seeds from agricultural extension officers to facilitate early harvesting of crops before the floods come along in late August and early September.

Acknowledgements

First and foremost, I would like to thank the Almighty God for seeing me through the degree programme. I would like to thank my Supervisors, Prof. dr. V.G. Jetten Victor and Drs. N.C. Kingma for their considerable patience, insights and assistance during the entire masters thesis programme. I would also like to thank Mr Seidu Mubarak Kunate for his immerse help with agricultural information. Finally, I would like to thank my family and friends for all their support and understanding during this time.

Contents

DECLARATION	ii
CERTIFICATION	iii
1.0 INTRODUCTION	1
1.1 Application of Radar Satellite and DEM in Flood Monitoring	4
1.2 Research Identification.....	5
1.3 Research objective	5
1.3.1 Specific objectives and research questions.....	6
1.4 Benefit of the study.....	6
2.0 LITERATURE REVIEW	7
2.1 Impacts of floods	7
2.1.1 Damage Function.....	7
2.2 Risk and Hazard	9
2.3 Flood Vulnerability	9
2.4 Methodologies used in flood risk mapping analysis	9
2.5 Basic Operating Principles of Synthetic Aperture Radar (SAR).....	10
2.6 Radar Back Scattering Effect.....	10
2.7 Flood Inundation mapping with radar and optical remote sensing image	11
2.8 Related research in Northern Ghana	12
3.0 STUDY AREA AND DATA DESCRIPTION	13
3.1 Case Study Area description.....	13
3.1.1 Physical features and climate	13
3.2 Soil types.....	17
3.3 Vegetation.....	17
3.4 Data and Method	18
3.4.1 Available Data.....	20
3.5 Data, Tools/ Software Description, and Processing	20
3.5.1 Sentinel-1 Data.....	20
3.6 Pre-processing of Sentinel-1 images and extraction of flood extent	21
3.7 Digital Elevation Model (DEM).....	23
3.7.1 SRTM DEM	23
3.7.2 ALOS Global Digital Surface Model “ALOS World 3D – 30m (AW3D30)”	23
3.7.3 SPOT DEM.....	24
3.8 Ground Control Points (GCP).....	24
4.0 Description of Crops considered in this study	25

4.1 Maize crop.....	26
4.2 Sorghum Crop.....	26
4.3 Millet Crop.....	27
4.4 Rice Crop.....	27
5.0 SENTINEL-1 FLOOD ANALYSIS AND RESULTS.....	29
5.2 Sentinel-2 Processing	37
6.0 Accuracy Assessment of DEMs	40
6.1 Results and Discussion of DEM Accuracy Assessment.....	40
6.2 Landcover Accuracy assessment of DEMs.....	42
7.0Flood Depth Analysis and Digital Elevation Model (DEM) Interpolation Processing	45
7.1 Flood Depth Analysis	45
7.2 DEM Interpolation.....	45
7.3 Trend surface Interpolation	45
7.4 Flood depth analysis.....	46
8.0 Vulnerability, Hazard and Risk Assessment.....	54
8.1 Flood Hazard Mapping.....	54
8.2 Flood Return Period	57
8.3 Vulnerability of crops.....	58
8.4 Risk assessment.....	63
8.5 Discussion	66
9.0 Conclusion	69
9.1 Recommendation	70
9.2 Limitations of the study.....	70
LIST OF REFERENCES.....	72
APPENDIX A: literature review / datasets	84
APPENDIX B: Description of Crops considered in this study	86
APPENDIX C: Flood Depth Analysis and Digital Elevation Model (DEM) Interpolation Processing.....	89
APPENDIX D: Vulnerability, Hazard and Risk Assessment.....	99

LIST OF FIGURES

FIGURE 2.1A: SCHEMATIC STAGE–DAMAGE FUNCTION FOR FLOOD CROP LOSS ASSESSMENT	8
FIGURE 2.1B: RICE CROP DEPTH-DURATION-DAMAGE FUNCTION CURVES.....	8
FIGURE 2.2: SPECULAR REFLECTION	
FIGURE 2.3: DIFFUSE REFLECTION	10
FIGURE 2.4: DRY SOIL REFLECTION	
FIGURE 2.5: WET SOIL REFLECTION	
FIGURE 2.6: FLOODED SOIL	11
FIGURE 3.1: LOCATION OF WHITE VOLTA BASIN IN GHANA	14
FIGURE 3.2: OVERVIEW OF THE VOLTA BASIN IN GHANA.....	15
FIGURE 3.3: ANNUAL AVERAGE RAINFALL AND TEMPERATURE IN THE NORTHERN REGION.	15
FIGURE 3.4 A MAP OF THE STUDY AREA.....	16
FIGURE 3.4B SENTINEL-1 LAND COVER MAP	16
FIGURE 3.5: SOIL MAP OF STUDY AREA	17
FIGURE: 3.6: LANDOVER MAP OF THE STUDY AREA	18
FIGURE3.7: FLOWCHART OUTLINING THE METHOD OF THE RESEARCH PROCESS.....	19
FIGURE 3.9: THE THREE DIFFERENT DIGITAL ELEVATION MODELS OF THE STUDY AREA	24
FIGURE 4.1: MAJOR FOOD CROP CALENDAR FOR NORTHERN AND SOUTHERN GHANA	25
FIGURES 5.1: WHITE VOLTA RIVER SHOWING THE EXTENT OF THE RIVER	30
FIGURE 5.2: OUTLINED FLOOD EXTENT MAPS FOR SEPTEMBER.....	30
FIGURE 5.3: EXTRACTED FLOOD EXTENT FOR THE UPPER VOLTA.	31
FIGURE 5.4: OUTLINED FLOOD EXTENT MAPS FOR SEPTEMBER.....	31
FIGURE 5.5: EXTRACTED FLOOD EXTENT FOR THE LOWER VOLTA.....	32
FIGURE: HISTOGRAMS USED FOR SETTING THE THRESHOLD FOR THE UPPER.....	32
TABLE 5.1: INUNDATED AREAS OF THE UPPER AND LOWER VOLTA.....	33
FIGURES5.6A: A CROSS-SECTION OF SENTINEL-1 RADAR IMAGE SHOWING THE MEANDERINGS.	34
FIGURE 5.7B: HIGHLIGHTED AREA FOR THE LOWER VOLTA SHOWING MEANDERINGS	35
FIGURE 5.8: SENTINEL-2 INUNDATED AND PARTIALLY INUNDATED LAND COVERS WITHIN THE FLOOD EXTENTS.....	36
FIGURE 5.9: FALSE COLOUR COMPOSITE OF THE FLOOD EXTENT	36
FIGURE 5.10: INUNDATED LAND USE CLASSES.....	39
FIGURE 5.11: INUNDATED LAND USE CLASSES.....	39
FIGURE 5.12: SENTINEL-2 LAND USE CLASSIFICATION WORKFLOW	39
FIGURE 6.1: DIFFERENCE BETWEEN THE SPOT DEM VALUES AGAINST GCP.....	40
FIGURE 6.2: DIFFERENCE BETWEEN THE SRTM DEM VALUES AGAINST GCP	41
FIGURE 6.3: DIFFERENCE BETWEEN THE PALSAR DEM VALUES AGAINST GCP	41
FIGURE 6.4: SPOT RMSE AND MEAN ERROR FOR DIFFERENT LAND COVER CLASSES.....	42
FIGURE 6.5: SRTM RMSE AND MEAN ERROR FOR DIFFERENT LAND COVER CLASSES	43
FIGURE 6.6: PALSAR RMSE AND MEAN ERROR FOR DIFFERENT LAND COVER CLASSES	43
FIGURE 6.7: MEAN ERRORS OF ALL THREE DEMS COMPARED	44
FIGURE 6.8: COMPARING ROOT RMSE OF ALL THREE DEMS	44
FIGURE 7.1: INTERPOLATED THIRD-ORDER TREND SURFACE	90
FIGURE 7.2A: FLOOD DEPTH AND EXTENT MAP FOR UPPER VOLTA.....	47
FIGURE 7.2B: FLOOD DEPTH AND EXTENT MAP FOR UPPER VOLTA	47
FIGURE 7.3A: FLOOD DEPTH AND EXTENT MAP FOR LOWER VOLTA	48
FIGURE 7.3B: FLOOD DEPTH AND EXTENT MAP FOR UPPER VOLTA	48
FIGURE 7.4 MEANDERS IN THE WHITE VOLTA RIVER. ADOPTED FROM HKV (2012)	49
FIGURE 7.19: CLASSIFIED SENTINEL-2 IMAGE SHOWING VEGETATION IN THE RIVER AND CLOUD COVERAGE	49

FIGURE 7.20: COMPARING FLOODED EXTENT AND DEPTHS FOR ALL THREE DEMS (12 TH UPPER)	51
FIGURE 7.21: COMPARING FLOODED EXTENT AND DEPTHS FOR ALL THREE DEMS (12 TH LOWER)	51
FIGURE 7.22: COMPARING FLOODED EXTENT AND DEPTHS FOR ALL THREE DEMS (18 TH UPPER)	52
FIGURE 7.23: COMPARING FLOODED EXTENT AND DEPTHS FOR ALL THREE DEMS (18 TH LOWER)	52
FIGURE 7.24: COMPARING FLOODED EXTENT AND DEPTHS FOR ALL THREE DEMS	53
FIGURE 7.25: COMPARING FLOODED EXTENT AND DEPTHS FOR ALL THREE DEMS	53
FIGURE 8.1A: FLOOD HAZARD MAP OF THE UPPER VOLTA.	55
FIGURE 8.1B: FLOOD HAZARD MAP OF THE UPPER VOLTA.	55
FIGURE 8.3A: FLOOD HAZARD MAP OF THE LOWER VOLTA.	56
FIGURE 8.3B: FLOOD HAZARD MAP OF THE LOWER VOLTA.	56
FIGURE 8.5: VULNERABILITY INDEX OF CROPS FOR UPPER VOLTA	59
FIGURE 8.6: VULNERABILITY INDEX OF CROPS FOR LOWER VOLTA	60
FIGURE 8.7: ESTIMATED DAMAGES PER CROP FOR UPPER VOLTA	65
FIGURE 8.8: ESTIMATED DAMAGES PER CROP FOR UPPER VOLTA.....	66

List of Tables

TABLE 1.0: SPECIFIC OBJECTIVES AND RESEARCH QUESTIONS 6

TABLE 3.1 DATASETS USED IN THE RESEARCH..... 20

TABLE 3.2: CHARACTERISTICS AND MODE OF ACQUISITION OF SENTINEL-1 86

TABLE 4.1: CROPS GROWN IN GUINEA SAVANNAH OF GHANA 25

TABLE 4.2: CEREAL CROPS AND ESTIMATED YIELDS..... 26

TABLE 5.2: TOTAL INUNDATED LAND USE AND CROPPED AREA FOR THE UPPER VOLTA..... 38

TABLE 6.1: ERROR STATISTICS GENERATED FROM THE VERTICAL ACCURACY ASSESSMENT OF THE THREE DEMs..... 42

TABLE 8.2: FLOOD DEPTHS AND AREA COVERED FOR THE UPPER VOLTA 57

TABLE 8.3: FLOOD DEPTHS AND AREA COVERED FOR THE LOWER VOLTA 57

TABLE 8.4: ANNUAL MAXIMUM DISCHARGES AND THEIR RETURN PERIODS 57

TABLE 8.5: VULNERABILITY INDEX FOR THE UPPER VOLTA 59

TABLE 8.5: VULNERABILITY INDEX FOR THE LOWER VOLTA 60

TABLE 8.6: VULNERABILITY INDEX FOR UPPER VOLTA 61

TABLE 8.7: VULNERABILITY INDEX FOR LOWER VOLTA 62

TABLE 8.8: RISK CATEGORY 62

TABLE 8.9: THE ESTIMATED FINANCIAL VALUE OF RICE FOR THE UPPER AND LOWER VOLTA 63

TABLE 8.10: THE ESTIMATED FINANCIAL VALUE OF SORGHUM FOR THE UPPER AND LOWER VOLTA..... 63

TABLE 8.11: THE ESTIMATED FINANCIAL VALUE OF MAIZE FOR THE UPPER AND LOWER VOLTA 64

TABLE 8.12: THE ESTIMATED FINANCIAL VALUE OF MILLET 64

TABLE 8.13: ESTIMATED DAMAGES PER CROP FOR THE UPPER AND LOWER VOLTA... **ERROR! BOOKMARK NOT DEFINED.**

1.0 INTRODUCTION

Flooding causes significant damages to human life, resulting in massive socio-economic effects in, for instance, coastal and inland areas Globally (Chapi et al., 2015; Komi et al., 2017; Minh et al., 2019). Flooding usually takes place after a torrential downpour of rain, resulting in a build-up and runoff of water often from an upstream towards a downstream depending on the steepness nature of the landscape (Borga et al., 2011). The global incidence of flooding has been up over 40 percent during the last two decades (Hirabayashi et al., 2013). From 1995 to 2015, approximately 109 million people suffered from floods; damage up to 75 billion US dollars annually (Alfieri et al., 2017). Riverine floods, which are the focus of this study, usually occur because of heavy torrential rainfalls occurring in a particular river catchment for a prolonged period (Dhar & Nandargi, 1998), causing the river to overflow its banks and inundate its immediate low-lying surroundings resulting in socio-economic and environmental impacts (Subramanya, 2009) such as loss of human lives, destruction of buildings and other physical infrastructure, croplands and animal farms, and disruption of vital services. River Floods are one of the most reoccurring and devastating natural disasters globally. Determining the extent of river floods is very critical in managing risk associated with floods. Occupants in flood plains gamble with their livelihoods as they weigh the gains and losses associated with living and farming in flood plains and sometimes knowing very well a flood can occur and the magnitude of the flood could be less or great and could last for a long time. Flood plains can, therefore, be considered as both productive and disastrous environments. Farmers find flood plains beneficial as these plains are not only fertile but also wet in times of long droughts or periods without rains.

Climate change in Africa is a threat to agricultural production as it affects production levels and food security (McCusker & Carr, 2006). Agriculture remains an essential source of livelihoods to about 70% of the population of Africa, and agricultural earnings make up about 40% of total exports. About one-third of the African nation income is generated from agriculture (McCusker & Carr, 2006; Yaro, 2004).

Ghana is one of the most vulnerable countries in West Africa in Sub-Saharan Africa in terms of flood. Since 2007, flooding in the White Volta River has occurred frequently because of heavy rainfall in the basin and partly because of upstream Bagre river discharges from neighbouring country Burkina Faso. Throughout Ghana, rain-fed agriculture accounts for about 40% of Gross Domestic Product (GDP), and therefore, floods caused mainly by climate change have a significant impact on the economy. The negative impacts of floods are noticeable in some parts of the country, particularly in the Upper East, Upper West, and Northern regions and reflect on the socio-economic lifestyle of the people. Since 2007, floods have been very erratic and severe in these three northern regions of the country, leading to many deaths, ecological destruction, critical infrastructural damages, farm and other property destroyed as well as socio-economic disruption. In August 2007, flooding in the northern part of the country alone affected around 350,000 residents, with 49 casualties; an overall cost of over 130 million US dollars (US\$), not including long-term damages (Asumadu-Sarkodie et al., 2015)

Floods and the degree of the damage depend on the volume of rains received coupled with spilling of the Bagre dam on the same river course as the White Volta about 30km across the border to the North of Ghana in neighbouring country Burkina Faso. The multipurpose Bagre dam in Bagre, a town in Burkina Faso, is 400km in length, 90km wide with a depth of 40meters and can hold about seven billion cubic meters of water. These dimensions make the dam the largest dam in Burkina Faso with an arable land of about 40,000 to 80,000 hectares, of which only 4000 hectares is currently utilized. The irrigation is geared towards addressing the food security issues locally and on a national scale. The Bagre dam inaugurated in 1994 also serve as a hydro-electric power source and provides about 10% of the nation's electricity requirements. Sapielga, a village in the Upper east region of Ghana located approximately 60km from the Bagre Dam is the point of entry of the

White Volta into Ghana from Burkina Faso (Aloba, 2015; Skinner, 2017). Water is therefore spilled in the months of August and September when the rainfall is at its peak to prevent the dam from breaking. Seasonal torrential rainfalls exacerbated by the spilling of the Bagre dam in Burkina Faso rendered some 161,000 people in Ghana homeless, as reported by Daily Graphic Online in 2015. In 2010, the Volta river submerged a district of the capital and some 55 communities in the Central Gonja district of the Northern region of Ghana. (*Graphic Online*, 2015). Historic notable catastrophic floods that hit the three northern regions of Ghana are the 1999 and 2007 floods affecting 300,000 and 307,127 persons, respectively. Persons affected by floods in the three northern regions are usually only compensated after flood occurrences in the affected areas.

Very little is done in devising rational planning solutions to reduce flood induced disaster. Even though there are advanced plans to construct a multi-purpose dam on the river to reduce the occurrences of flood in the area, nothing tangible has been done yet. The Northern region is characterised by two seasons, dry (November – March) and rainy (April – mid-October) with a total amount of rainfall of about 1000mm (40in) annually that peaks in August (approximately 190mm) and late September (approximately 215mm), sometimes results in flooding. The Bagre Dam in neighbouring Burkina Faso discharges water into the White Volta River in these months, worsening the flood situation in these areas and negatively affects crops and livestock production (Jonkman, 2005). Designing a flood hazard map for the study area will help in identifying areas likely to be at risk of flooding. Outlined Policies can then be applied to such areas to minimize and manage flood risks.

Kasei et al., (2013), observed that from 2003 to 2009, in the year 2007, a discharge of 1306 m³/s at Pwalugu (upstream of the study area), the highest discharge ever recorded in northern Ghana. This discharge resulted in one of the worst flood to ever hit the three northern regions in Ghana. 2008 and 2009 recorded high discharge values similar to that of 2007, which suggest flood years in the Northern Ghana. Again, recently in 2018, floods in northern Ghana killed 34 people and as much as 100,000 locals were displaced because of heavy rainfall and the spillage of the Bagre dam when the water levels increased by about 80% in August 2018 compared to August 2017 when the water levels in the dam rose by 50% (Blašković, 2018; Richard Davies, 2018). The 2018 flood destroyed farms and physical infrastructures such as bridges and buildings, cutting off communities and rendering most of the locals homeless (Richard Davies, 2018). 202 communities in nine districts, totalling about 10,567 people in the northern region, were affected by the floods (IFRC, 2007). The floods also destroyed about 12,000 hectares of farmlands, which threatened food security in the northern region and the country. Nine people were reported dead and twelve others injured (IFRC, 2018). SONABEL, the company responsible for the multi-purpose dam in neighbouring Burkina Faso, started spilling the water on August 25th after the Bagre dam had reached its full capacity. The spillage of the excess water coupled with internal heavy rains in Ghana caused the white Volta to overflow its banks on September 6th (Richard Davies, 2018).

Farmers farming along the White Volta suffer various losses because of frequent flooding that occurs along the river in the northern part of Ghana. These farmers farm along the river because of the readily accessible water from the river for dry season farming, the fertility of the soil along the riverbank, and the moisture condition of the soil, which keeps attracting them despite the risk involved. Surveys and reports reveal that the floods occur frequently and get worse when the Bagre dam in Burkina Faso is opened to spill off some water. (Reliefweb 2018, accessed 25/05/2020). Farmers normally sow hoping to harvest before the floods occur, but mostly, the floods come before the crops are matured enough for harvesting, inundating the farmlands completely in most cases leading to a total loss. There has been an agreement between the two Governments where SONABEL, the electricity company in Burkina Faso is supposed to warn Ghana ahead of spillage but this is not effective as SONABEL is noted for relaying late information and does not allow much time for evacuation of communities along the white Volta river in Ghana. In 2015 as reported

by Joy online; National Disaster Management Organisation, (NADMO) of Ghana only received the warning of the spillage a few hours (Less than a day) prior to the spilling leaving them with very little time to evacuate or warn people along the white Volta river of the impending danger ahead. The information is sometimes not also clear how the spillage would be carried out, either gradually or at once, therefore, compounding the situation. Time, effort, and resources are wasted since these farmers most often cannot recover anything after the flood water recedes, and this weighs heavily on them since most of them are just peasant farmers trying to make a living off the farm produce. There must, therefore, be more appropriate and comprehensive maps and risk assessment for the flood-prone areas of Ghana towards the flood risk reduction and better adaptation to the climate change occurrences. This research, therefore, seeks to carry out a GIS multivariate flood risk and damage assessment of the farms along the white Volta River in the northern part of Ghana.

There are some challenges hindering the successful assessment and modelling of floods in Ghana and developing countries. Barredo et al., (2007) and Kundzewicz et al., (2014) suggested that it is possible that flood-related issues have not yet gained the needed attention and publicity it deserves towards devising solutions to curb the problem. In the absence of effective solutions, impacts of floods have increased and are expected to get worse as the population increases with lots of evolving developments (UN-HABITAT, 2008; Winsemius et al., 2016). The unavailability of high quality and detailed, reliable data to assess and analyze flood risk effectively and the lack of sufficient education and information among the populace is one hindrance to effective control and management endeavours (Merz et al., 2010; Nkwunonwo et al., 2016). For a while now, global freely available datasets in the absence of local data, and approved methods for local conditions have been applied to assess flood risk, with no complete solution to flood hazard (Apel et al., 2006; Brown & Damery, 2002) which at times leads to the over and underestimation of flood risk (Beven, 2016). There is, therefore, a need for high-resolution datasets for the accurate assessment and depiction of flood events (Apel et al., 2009; Wolski et al., 2017).

The lack of meteorological, satellite data and river gauge measurements in some areas of Northern Ghana hampers the proper modelling and simulation of rainfall-runoff events towards better flood prediction and management (Udo et al., 2012). Very accurate detailed measurement of rainfall data can be obtained from a concentrated system of meteorological stations (Goovaerts, 2000). Meteorological stations in Ghana are scattered because of the inability of the country to afford the cost of installations; the result, therefore, is the challenge of obtaining accurate spatiotemporal data (Kebblouti et al., 2012). The malfunctioning of some sparsely located stations compounds the data problem in the country, therefore affecting the availability of continuous data. Installing meteorological ground-based RADAR stations and satellite remote sensing platforms around the country would help to determine the spatial rainfall variability and better estimate rainfall volumes for better calibration of models in Northern Ghana (Udo et al., 2012). Most rivers and streams in Africa are ungauged resulting in the improper management of water resources and lack of accurate river discharge and climatic data (Khalil et al., 2011; Symeonakis et al., 2009) which sometimes leads to a limited understanding of flood occurrences in most tropical regions (Dovie, 2010). In Ghana, the lack or inadequate historical data (rainfall, runoff) related to the management of water resources poses a challenge to hydrological modelling for watersheds (Owusu, 2014). Such data is needed to predict and model time-steps for flood concentration and peak levels. Data such as soil, topographic, climatic, and land use needed for modeling are sometimes inadequate in terms of quality and quantity.

Quality resolution topographic data, long time-series rainfall and river data, demographic data, data on relief and drainage, satellite imagery, among other data essential for flood hazard and vulnerability analysis, are either inadequate or completely lacking in most developing countries (UNISDR, 2004). The quality of data or the total lack of it poses a challenge to flood hazard mapping and flood risk assessment.

Flood hazard mapping is carried out to evaluate the depth, velocity, and duration of floods (Merz et al., 2007) while vulnerability deals with the resilience and sensitivity of the elements at risk (Blaikie et al., 2014). The spatiotemporal analysis of the elements at risk makes up Exposure (Mazzorana et al., 2012). There is, therefore, a need for high-quality data for the modelling and evaluation of current flood events as this would help improve the selection of quality data for a much more efficient outcome.

In this study, Analytical Hierarchical Process (AHP), a multi-criteria analysis was adopted as a decision-making tool in a hierarchical structure to determine the level of flood risk and damage associated with each crop within the flood extents. The AHP as presented by Mastin, (2009) and Masoudian, (2009) as a decision-making tool in resolving complicated decision problems was adopted for this study. The spatial attributes such as the crop fields, flood extent and the different crops and their water tolerance were considered in this analysis to determine the most vulnerable crops

1.1 Application of Radar Satellite and DEM in Flood Monitoring

In recent times, multiple satellite data can be used in particular regions to track the flood condition and the extent (Brivio et al., 2002). In rainy climatic regions, however, large clouds, rain, and haze can be a major constraint on the use of remotely sensed optical data during and after flood events (M. Rahman et al., 2019). The major advantage of using SAR data is that, besides the penetration ability of SAR data, land and water are easy to distinguish (Dewan et al., 2006). Sentinel-1 SAR sensors can detect the flood as levelled surfaces, reflect a signal away from the sensor (acting as a hypothetical reflector) and lower the amount of radiation received (Gan et al., 2012). It leads to relatively dark pixels for water areas contrasting with non-water regions in radar data. There has been a proliferation in using SAR remote sensing data for monitoring and mapping of floods and other water-related activities (Voigt et al., 2009). The temporal resolution of SAR data for most sensors may not be sufficient for short duration agricultural flood monitoring. Most SAR systems have a revisit time of about ten days except for Sentinel-1 with a revisit of six days, making it more useful compared to the others. The low temporal resolution of SAR images shows that flood-damaged crops in a short period of less than a week are likely not to be detected by SAR data. There is, therefore, a need for very high temporal resolution data for remote sensing flood crop monitoring and loss assessment applications (Di et al., 2017; M. Rahman et al., 2019). This study seeks to monitor the duration of riverine floods using Sentinel-1 data.

A wide range of techniques are used in the generation of Digital Elevation Model (DEM), some of which are through differential GPS measurements, LiDAR, InSAR, photogrammetry (digital), digitizing contours from existing geography maps, geography levelling and EDM (Electronic Distance Measurement). DEMs are used in determining the elevation of water surfaces, delineate the extent of the flood, and also flood base elevations (FEMA 2009). Technologies such as using Global Positioning Systems (GPS), radar, laser altimetry, and SAR are new technologies that have attempted to solve the problems of lack of high-resolution elevation data.

RADAR imagery can be combined with DEMs in flood depth and volume analysis to assess land elevation relative to water levels, thus the difference between the water level and surface level (Matgen et al., 2007; Puech & Raclot, 2002). Very coarse DEMs of approximately 30m Spatial resolution can be used to extract water depths (Kiel et al., 2006), but DEMs at such resolution are not vertically accurate enough for hydrological and terrain modelling (Jing Li & Wong, 2010). High-resolution elevation data such as aerial photogrammetry and LIDAR are much more accurate in predicting and estimating flood depth and extent (Coveney & Roberts, 2017).

In Ghana, most of the data used in flood studies are free open DEMs at coarse resolutions and therefore do not give accurate estimations (Forkuo, 2010, 2011; Kwang & Osei, 2017; Nyarko, 2007; Udo et al., 2012). This study also seeks to compare DEMs to determine the accurate one for flood risk analysis in the study area.

1.2 Research Identification

Flood risk assessment is important in predicting the occurrences of flood and to set up strategies, coping mechanisms, and proper management structures to deal with floods. Meteorological, topographic, satellite, and other geophysical data serve as sources of data for carrying out hydrological modelling, flood hazard, and risk assessment, but the quality of such data is usually poor for local assessments or even lacking altogether. Such is the case of Ghana, where freely open-source data are mostly used for flood analysis, and the few national climatic, meteorological, and river gauge stations are insufficient or malfunctioning, resulting in insufficient historical and up-to-date data. This research seeks to gain information on datasets by exploring and testing the potential of the data and tools to improve the quality of flood risk assessment in data scarcity regions.

1.3 Research objective

This research seeks to determine the best quality data for a flood risk damage analysis and crop loss assessment along the white Volta river in the northern region of Ghana. The loss analysis aims to investigate the possibility of carrying out this investigation in a region with inadequate data; in terms of quality and quantity and without carrying out extensive flood modelling.

The size of the basin and the influence of the dam water management upstream of the study area makes it impossible to do a full flood hazard modelling for different return periods. Only one year (2018) is being studied and there is no sufficient continuous discharge data to estimate the water inflows within and from the Bagre dam to carry out a comprehensive modelling. Gauges along the white Volta river are either malfunctioned or absent.

Amidst the challenges, HKV consultants in 2012 carried out a flood risk analysis in the area and most of their results and findings would be referred to in this study to carry out a loss assessment.

1.3.1 Specific objectives and research questions.

Table 1.0: Specific objectives and research questions

Specific objectives	Research questions
1. To investigate how well Sentinel-1 imagery can be used in delineating the extent of riverine floods in an agricultural area.	I. Can the progress, in time of flooding along a large section of the White Volta river, be extracted from sentinel-1 images. II. How challenging is it to differentiate and delineate flooded extent from the surrounding non-flooded areas as observed from the Sentinel-1 images?
2. Determine the flood extent and depth using Sentinel-1 images and different sources of DEMs (SRTM 30m, ALOS PALSAR 30m, and a SPOT DEM 30m)	I. What are the differences between the three DEMs in terms of quality? II. To compare and investigate how the three different DEMs influence flood analysis in terms of depths and flood extent. III. Which trend surface as formed from the DEMs best fits or represents the earth and flood surface.
3. To Investigate the relationship between the different crop cycles and the occurrence of flooding in crop fields along the White Volta river.	I. How well can we classify and differentiate farmland from other land cover classes in the area using Sentinel-2 images? II. What is the relationship between the crop cycle and the incidence of flood in the area? III. How do the floods affect the different crops in the area in terms of flood extent and depth? IV. Is it possible that the farmers can harvest their mature crops before the occurrence of a flood considering the start of floods and the growth cycle of the crops?
4. To assess the agricultural economic losses of the various crops in the area within the flood extents.	I. Which crops at risk are more vulnerable, taking into consideration the type and economic value? II. How much financial loss is suffered by the farmers in the event of a flood?

1.4 Benefit of the study

This research seeks to reconstruct the 2018 flood event that occurred in the northern region of Ghana, and also to assess and estimate the agricultural loss associated with the floods that occurred along the white Volta river. This research assessed the hazard, vulnerability, risk, and economic losses of crops. This research studies the timing of floods and how the floods affected crops in the study area and also assessed the quality and accuracy of selected DEMs.

2.0 LITERATURE REVIEW

2.1 Impacts of floods

The severe impacts of floods include loss of human life, disruption to buildings, degradation of crops, loss of livestock, and worsening of health conditions related to waterborne diseases. Conversely, industrial instability will lead to loss of livelihoods. (Asenso-Okyere et al., 2012; Karley, 2009). Flooding in key agricultural production areas may trigger significant crop damage and livestock destruction. As food prices rise due to shortages in supply, the flow-on effects of reduced agricultural production can often have an impact well outside the production area. (Sanyal & Lu, 2005). The scale, study objective, and available data determine the flood estimation methods to be applied (Brémond & Grelot, 2013; V. Meyer et al., 2013), which can also translate into the tangible and intangible cost (Changnon, 2003; Smith & Ward, 1998). Damage to crops and livestock constitute direct flood costs while the indirect flood costs make up the effects resulting from the lack of crops and livestock resulting in the increase in food prices due to scarcity, disruption of economic and trading activities and job losses (Okuyama, 2007). Agriculture is prone to groundwater and surface flooding (Joe Morris & Wheeler, 2007). Depending on the growth stage, the crops can be very sensitive to excess water, which can affect the quality, yield, and value of the crops and seeds. Floodwaters over an agricultural field affect the crops differently depending on the water tolerance of the crop, the soil type, land use characteristics, and the peculiar nature of the flood such as the duration, depth, and frequency of the flood event (J Morris & Hess, 1988).

J Morris & Brewin, (2013) conducted a study in Somerset, England, where they collected data on the impact of the flood on farming activities to understand the coping strategies of the farmers in the event of a flood and to measure the effects of seasonal flooding on the farming businesses. Their findings indicated that the cost of flood damages compared to the agricultural production was appreciable and also depended very much on the adaptive and coping strategies of the farmer to flooding.

Kotera & Nawata, (2007), in a simulation experiment, established a relation between flooding of rice crops and yield reduction at the different developmental stages. The results showed the development stage of the crop, together with the flood characteristics such as the duration and depth, determine the level of yield losses likely to be incurred by the farmer. Higher losses were expected at the vegetative stages as compared to the reproductive stage of the rice crops.

2.1.1 Damage Function

The crop, inundation depth, duration of the flood and the growth stage of the crop are factors considered in agricultural flood damage assessment (Peltonen-Sainio, et al., 2010; van Aalst et al., 2008). In the absence of historical data, depth-damage functions based on previous flood behaviours can predict or mimic behaviour of floods based on land use and flood data. The damage-function method uses depth duration crop development stages to estimate agricultural damages (Messner, 2007; Penning-Rowsell et al., 2013). Figures 2.1 and 2.2 shows examples of flood damage functions.

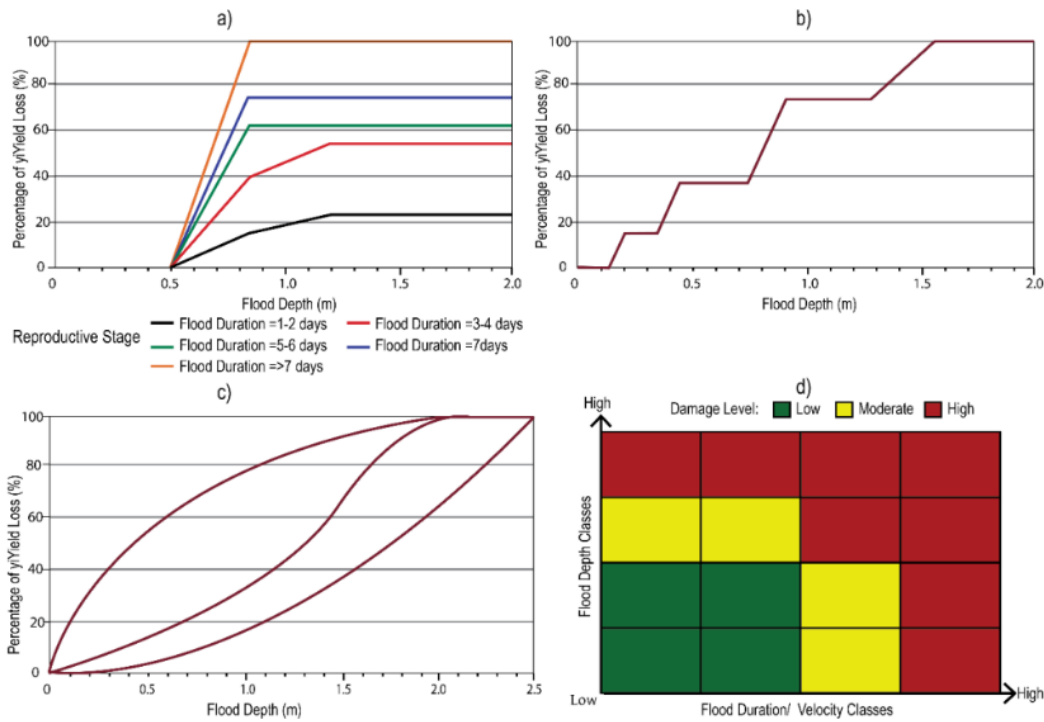


Figure 2.1a: Schematic stage–damage function for flood crop loss assessment. (a) Depth–duration–damage curve; Shrestha et al. 2015. (b) illustration of a linear piecewise depth–damage curve as adapted from Amadio et al. 2016 (c) Exponential, quadratic, and S-shape depth–damage curves adapted from Dutta et al. 2003 (d) Tabular format of stage–damage function of loss assessment Samantaray et al. 2015

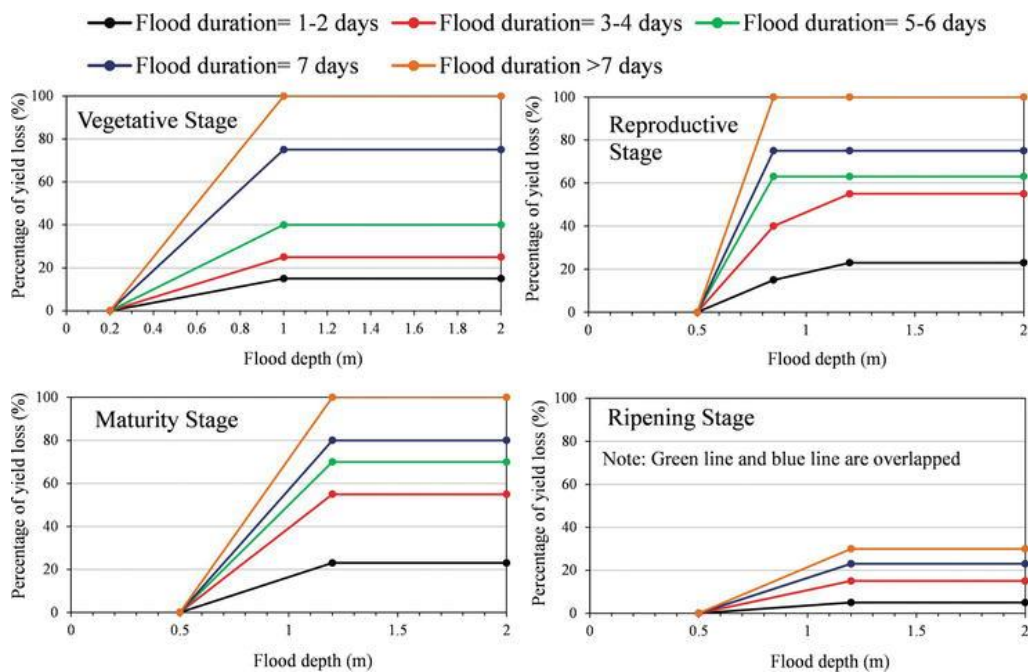


Figure 2.1b: Rice crop Depth-duration–damage function curves adopted from Shrestha et al. 2018

2.2 Risk and Hazard

Disaster risk is expressed as the likelihood of loss of life, injury or destruction, and damage from a disaster in a period (UNISDR & others, 2015). Population, property, economic activity, including public services, or any other defined values exposed to hazards in an area are often referred to as the elements at risk (UNISDR, 2004). These elements are also called assets. Elements at risk also possess spatial and non-spatial features. The manner in which the quantity of elements-at-risk is defined, such as the number of buildings, the number of people, the economic value, or the region of significant qualitative groups, often determines how the risk is portrayed. The relationship between hazards and elements at risk demonstrates how exposed the elements-at-risk are (Westen, 2009).

While some hazards can be considered being exclusively natural, the spatial and temporal patterns of hazard occurrence are increasingly correlated with patterns of human behaviour and relationship with their natural environment. Human practices such as the alteration of natural drainage, the creation of landfills, or the destruction of the natural environments and increased groundwater extraction may radically alter the pattern of the hazard behaviour (Otieno, 2004). In this research, river flood is considered as both natural hazards, and a human-made hazard since dam management practices upstream of the flooded area also contribute to flooding in the area.

2.3 Flood Vulnerability

Vulnerability encompasses exposure, susceptibility, and the inability to cope with the consequences and impact of the flood as a hazard. Spatial, social, economic, geographic, and economic methodologies have all been adopted to assess vulnerability (Sahana et al., 2018). United Nations Educational, Scientific, and Cultural Organization is one of such and defines vulnerability using an equation; $Vulnerability = Exposure + susceptibility - resilience$ (Rehman et al., 2019; Scheuer et al., 2011).

Various methodologies have been adopted to assess vulnerability, such as the use of remote sensing data dating as far back as the early 2000s compared to the physical, socioeconomic methods that involved fieldwork in the 90s. The development and improvements in methods and methodologies led to the utilization of three-dimensional GIS hydrological modelling in 2010 (Rehman et al., 2019). Ever since then, there has been a proliferation of very high-resolution images such as Radar, LIDAR, and SAR images; notable among these are the sentinel-1 and sentinel-2 images with high quality and short revisit times producing timely images that are used in flood vulnerability analysis (Rahman & Thakur, 2018). Sometimes due to the uncertainties involved in flood vulnerability assessments, indices are combined with vulnerability assessment methods in a multi-criteria analysis to better estimate and quantify the vulnerability and risk involved (G. Lee et al., 2014). Volker Meyer et al., (2009) developed a multi-criteria approach that encompasses ecological, economic, and social vulnerabilities in flood risk analysis, which was also adopted by Kubal et al., (2009) in a multi-criteria flood risk mapping. Multi-criteria analysis involves the assigning of weights to diverse indicators, which are together evaluated in a single criterion component (Scheuer et al., 2011). The integration of GIS and multi-criteria analysis for flood risk analysis has proven to be reliable and efficient (Zelevnáková et al., 2015).

2.4 Methodologies used in flood risk mapping analysis

The integration of Remote sensing and GIS in delineating flood extents and modelling of the risk and hazard is on the increase globally (WMO, 2013). Flood hazard and risk maps can be developed through flood modelling, the use of historical data, and the use of geomorphological data.

The historic method mostly involves gathering reports from news, articles, and publications regarding flood occurrences, the extents, damages to both life and properties as reported by the media. The other way is also through the use of images from the flood events, satellite images, maps can be used to assess the extent of the flood and to estimate the damages within a particular

area. Such information is, however, not fully reliable as they may not cover the whole affected area and therefore provide insufficient information and sometimes not so reliable information (Sayers et al., 2013). A similar study involving the use of historical data was carried out in Uganda by Wagemaker and Jjemba, (2015) for the period between 2001 and 2015 where newspaper reports were used as a source of data to map out flood-prone areas and assess the preparedness put in place over the period leading to the creation of flood hazard maps for some selected districts in Uganda.

The geological approach involves using flood extents and water height markings of the past flood to gather information on floods. This approach is usually data and time-intensive and requires a long-term series of data regarding flooding and change patterns in the river bed and surrounding flood plains. In El Salvador, Fernández-Lavado et al., (2007) used information collected from sedimentation and erosion, alluvial fans, and stream channel characteristics in the mapping of floods in Jucuaran. The information gathered was used together with images and local knowledge. Modelling involves simulating diverse magnitudes of floods through the integration of GIS and remote sensing together with hydraulic and hydrology data. Physical data such as the soil, geology, land use land cover, hydrological data such as discharge, rainfall, water velocity, rainfall, among others, are all parameters used by the models to simulate and predict as accurately as possible the behaviour and characteristics of flood in an area (WMO, 2013). A DEM is used in hydraulic and hydrological models to delineate watershed, streams, and river networks and basin.

2.5 Basic Operating Principles of Synthetic Aperture Radar (SAR)

The SAR technology is currently commonly used in radars (Curlander & McDonough, 1991). Synthetic aperture techniques evolved from the ability to control the amplitude and phase of microwave emissions using antennas (Cafforio et al., 1991). SAR are active sensors, and so operate day and night irrespective of the weather conditions as compared to optical sensors that are passive and easily affected by the weather conditions (Campbell & Wynne, 2011). The ability of SAR to penetrate through clouds and night conditions gives it an advantage over optical sensors (Jawak et al., 2015; Moreira et al., 2013). Spaceborne SAR remote sensors are side-looking radars.

SAR sensors operate using L-band, C-band and X-band frequencies (Figure 1.0 and Table 1.0 in appendix A) For Sentinel-1 (monostatic SAR system), the emitted pulse is sent and received by the same antenna

2.6 Radar Back Scattering Effect

Surfaces of calm waters, paved runways, and roads are visible in radar images as dark areas with rough surfaces appear bright. Smooth surfaces behave like mirrors and therefore act based on the principle of specular reflection where most of the incident radar is reflected away from the surface in a uniform direction so that the angle of incidence is equal to the reflected angle. Figure 2.2 and 2.3 below are illustrations of specular and diffuse reflections on surfaces respectively (Liew, 2001)

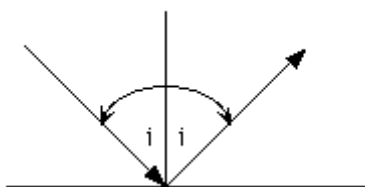


Figure 2.2: Specular reflection

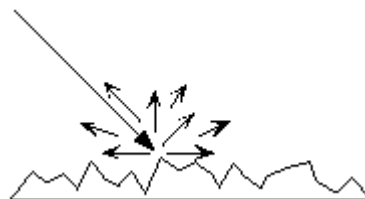


Figure 2.3: Diffuse reflection

The disturbed water surface and the vegetation in the water do not behave as a smooth surface and therefore are seen as white surfaces which are not mostly accurate in the case of flooded areas. The structures may also cause a double bounce of the reflected rays causing an increase in the reflected

ray which is recorded by the sensor as dry instead of flooded areas resulting in errors (Martí-Cardona et al., 2010; O’Grady et al., 2014). It is a major challenge when attempting to detect flood in croplands and Urban areas from images due to the inference such as the wind and double bouncing effect from the buildings and vegetation resulting in much-emitted reflections regarding the dry areas. Figures 2.4 to 2.6 shows reflections in soil; thus the behaviour and interaction of the incident ray with soil.

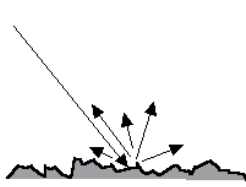


Figure 2.4: dry soil reflection

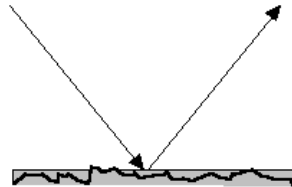


Figure 2.5: Wet soil reflection

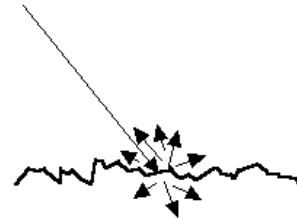


Figure 2.6: Flooded soil

2.7 Flood Inundation mapping with radar and optical remote sensing image

The thresholding approach based on the Histogram backscatter is used to derive flood extents from SAR images. The thresholding is global and may not be appropriate for all areas in the image (Martinis & Twele, 2011; B. Wang & LinHo, 2002). A refined classification method that included the use of multi-resolution segmentation was proposed as a solution to deal with roughened water surfaces caused by wind or rain. A 99.05% accuracy was realized from the classification, therefore, emphasizing the credibility of the method Han et al., (2019)

Radarsat-1 and ASTER images in a study to map flood and wetlands were used by Maillard et al., (2008) to delineate flood extents and to classify palm swamps. It was concluded that SAR classified images obtained during the rainy season or afterwards had a low incidence angle, therefore, resulting in many accurate results, but the ASTER images produced better results in the classification of the types of vegetation. The study also acknowledges the limitation of optical images in the delineation of the flood extent and the water cycle within the wetlands due to cloud coverage.

Honda et al., (1997) used JERS-1 together with Landsat TM data to map and extract flood extent. In this study, Both Radar and optical images were overlaid to classify and map the affected regions in a 1995 flood event that occurred in the plains of Thailand. They concluded that JERS-1 had the potential to monitor and map floods.

Duy, (2016) in a paper titled “Automatic detection of surface water bodies from Sentinel-1 SAR images using the Valley-Emphasis method,” used the automated Otsu method to extract surface water bodies at different landscapes and land covers from Sentinel-1A IW images using Landsat 7 and 8 as reference data. Comparing the results to other results obtained using the Otsu method, the writer concluded that the method used in this study was simple to execute and could be implemented in other regions at local and global scales. The method produced an overall accuracy of 89.7 per cent.

Marechal et al., (2012), in a related study using a supervised Segmentation process involving the use of RADARSAT-2 data, proved that radar data could monitor periodic changes or occurrences in wetlands and could also provide detailed information on water features and flood extents.

In a flooded forest in Brazil, Y. Wang et al., (1995), during a study, concluded that the proportion of C-band backscatter between non-flooded and flooded forests was estimated at 1.8 and 1.0 at an incident angle of 200 and 600, respectively.

Pultz et al., (1991) in a study to monitor the Red river flood using RADARSAT in Manitoba and North Dakota, proposed that shorter revisit times and wider incidence angles of the ERS-1 produce much accurate flood information. The difference between flooded regions (dark) and the non-

flooded agricultural regions was realized through the use of images produced by beams modes at diverse incident angles.

Adam et al., (1998), during a flood study in 1996 and 1997 of May in Peace-Athabasca Delta, Canada successfully used RADARSAT data together with segmentation methods, identified, mapped, and classified the images into diverse classes namely; flooded willows, open water bodies, and Non-flooded regions.

2.8 Related research in Northern Ghana

In a regional level flood hazard mapping, Forkuo, (2011) using an ASTER image, generated contours and elevation data together with a 1: 50000 scale generated topographic map for the whole region in a GIS suit, and created a flood hazard map for the districts in the Northern region high lightening and categorizing the area into flood-prone zones based on the level of identified hazard. The study was geared towards developing an adequate and practical method for generating flood hazard maps for flood-prone regions in the country. Variables such as the distance from the river banks, farmlands in the area, population density, among others, were utilized in a composite index additive model to create the flood hazard map.

Musah et al., (2013) studied the effect of the flood on livelihood systems in the Tolon and Kumbugu District of the northern region of Ghana. Six out of twenty-two initially selected communities in the districts were considered for this study. The selected communities are known for periodic floods that occur in August and September, mostly as a result of the opening of the Bagre dam. The floods are said to destroy farmlands and therefore affected the livelihood and food security of the district. The floods also caused erosion in the communities, which therefore affects yields production in the district.

Udo et al., (2012) was contracted by the world bank to conduct a flood hazard assessment for the White Volta River and its tributaries. The study involved flood hazard modeling starting from the Burkina Faso – Ghana border upstream and ending at the Volta lake in Ghana downstream. The study also included a flood risk assessment using the determined vulnerability of the communities to flood and land use in those areas. The study also assessed the resilience of the flood management and coping system that were in place at the time of the study. Duration, flood extent, and depth maps were prepared for the period of 2007 – 2010 in this study.

3.0 STUDY AREA AND DATA DESCRIPTION

3.1 Case Study Area description

3.1.1 Physical features and climate

The then northern region of Ghana, is the largest region in terms of the land area, and was estimated at 70,384 square kilometres. It is bordered by Upper East and Upper West Regions to the north and shares southern boundaries with the then Brong Ahafo and Volta Region. It is also bordered to the east and west by neighbouring countries such as Togo and Cote d'Ivoire, respectively. Except for some high elevated areas such as the Gambaga Escarpment within the north-eastern edges and also areas near the western corridor, the landscape can be largely described as a low-lying area. The White and Black Volta rivers, together with their many tributaries, serve as main drainages for the region (Ghana Statistical Service, 2010).

The study is conducted along the White Volta in the Northern region of Ghana. This study considered the White Volta River due to its shattering effect on the study area whenever it rains excessively or when the Bagre Dam in neighbouring Burkina Faso releases water into it. The study site's climate is semi-arid, with two major seasons: dry and rainy. In the dry season, the winds of Harmattan are dusty and warm, usually from the ending of November to mid-March. During the dry season, the Harmattan wind carries a lot of dust, and is sometimes cold at night, often between December and early part of February, with temperatures between 14°C at night to 40°C during the day (Ghana Statistical Service, 2010). The average annual rainfall in the northern region is between 750mm and 1050mm.

Rainfall in the Northern Part of Ghana is characterized by mono modal rainfall, which starts from May/June to September. Heavy rainfalls in the area are as a result of the interaction between the Monsoon and Harmattan winds in the Inter-Tropical convergence zone of the Volta basin. The resultant high potency of the two winds results in heavy rainfall and thunderstorms (Barry et al., 2005; Zwet, 2012). Approximately 60% of the rain is recorded within the periods of July to September. The rainfall peaks within this period. The heavy rainfalls usually result in large volumes of runoff, since the rainfall intensity is higher than the soils' absorptive capacity.

The possible annual evaporation is estimated to be more than annual precipitation in this semi-arid climate (Zwet, 2012). Between November and April, high evaporative values are reported. Figure 3.1 shows the location of Ghana, its bordering neighbours, and the White Volta catchment

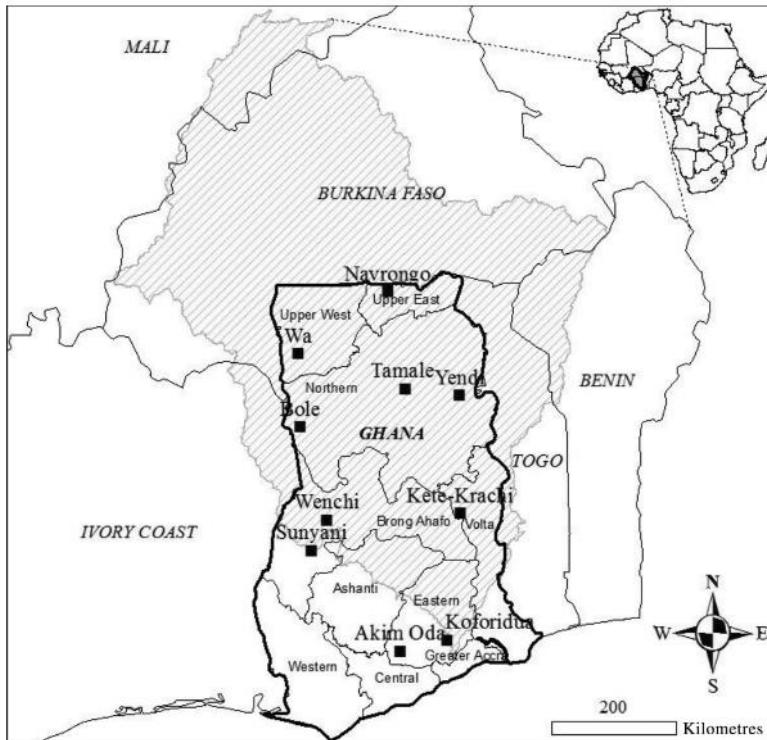


Figure 3.1: Ghana outlined in thick dark lines with interior administrative divisions, and the hatched area is the Volta River basin. Areas outside the thick dark lines outline borders of neighbouring countries. Source: Anayah et al., 2013)

The area of the Volta basin is about 400,000km² of which 42% (165,830km²) lies in Ghana and 43 (171,105km²) in Burkina Faso (F. Anayah & Kaluarachchi, 2009). The Volta basin has four affluents: Black Volta, which has a surface area of 147,000 km², white Volta, also about 106,000 km², 72,000 km² for Oti, and lower Volta and Lake Volta together with a surface area of 73,000 km². The running coefficients for these affluents are 4.9%, 7.1%, and 13.5% for Black Volta, White Volta, and Oti, respectively (Van de Giesen et al., 2001). Figure 3.2 illustrates the general overview of the Volta basin in Ghana and neighbouring countries.

Average rainfall within the white basin is about 1025 mm per year (140 - 190 days of rain), out of which 9% (36 km³) translates into river flow (Van de Giesen et al., 2001) with evaporation of 2000mm/annum (Siaw & others, 2001). Figure 3.3 shows average annual rainfall and temperature for northern Ghana, as obtained from climate-data.org. The data is collected by a climate model from several weather stations globally. The data is collected from the period of 1982 to 2012 at a resolution of 30 arc seconds. The model uses data points from over 220 million locations globally based on the OpenStreet Map project, which is constantly refreshed to keep it updated.

The elevation in the Volta basin is between 42m and 537m(Zwet, 2012). In Ghana, the channel slopes of the white Volta are about 16cm/km to 34 cm/km (Zwet, 2012). Given the two massive reservoirs Bagre (Burkina Faso) and Akosombo (Ghana), the White Volta catchment in Ghana is still a fairly natural river. When the wet season begins, the soil absorbs most of the rain first. When precipitation exceeds evapotranspiration, and storage is filled, the discharge of the river begins to build. Once flood plains continue to flood, old river arms tend to transport water or retain it. In the White Volta Region, the aggregation of rainfall events during the wet season is the main cause of the flooding. The water rise usually starts in August and takes at least one month to hit its height (Udo et al., 2012).

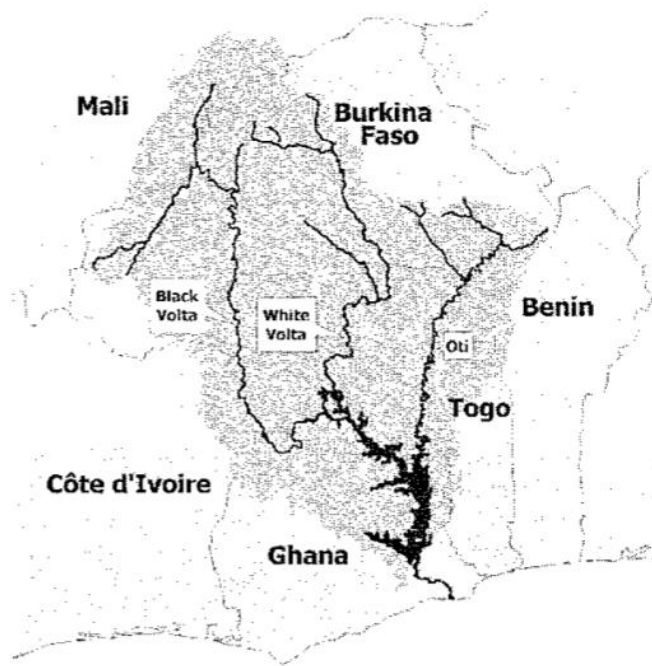


Figure 3.2: General overview of the Volta basin in Ghana and neighbouring countries. The dark region is the Volta basin, while the very dark lines are the river bodies as labelled. Adapted from Andreini et al., 2002

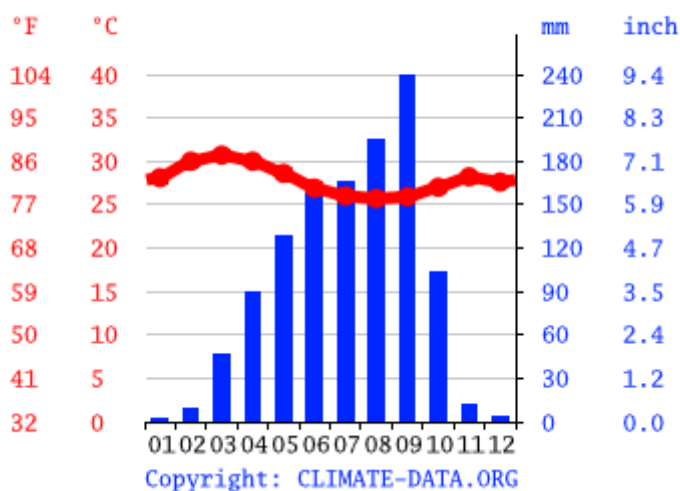


Figure 3.3: Annual average rainfall and temperature in the northern region. Source: [Climate-data](#)

The study area covers approximately 8410 square kilometres and is in the Volta River Basin region of Ghana. This area has been chosen because of the recurrent floods in the area during the rainy and growing season. Farmers carry out agricultural activities in the floodplains, which are often flooded in the event of heavy rains coupled with the opening of the Bagre dam upstream.

Figure 3.4a shows the location of the study area. It is a district map of Ghana highlighting the affected districts along the White Volta river (left) in the event of a flood. The study is based on the former or the then ten regions and associated districts of Ghana. Figure 3.4b is a Sentinel-1 change detection image of Ghana, highlighting the study area. Currently, Ghana has sixteen new regions that were carved out of the existing ten (10) regions through a referendum held on the 27th of December 2018. For this study, the white Volta River within the Northern region of Ghana was

zoned into two areas, as indicated by the red squares into zone A, hereby referred to as the Upper Volta and zone B, as lower Volta.

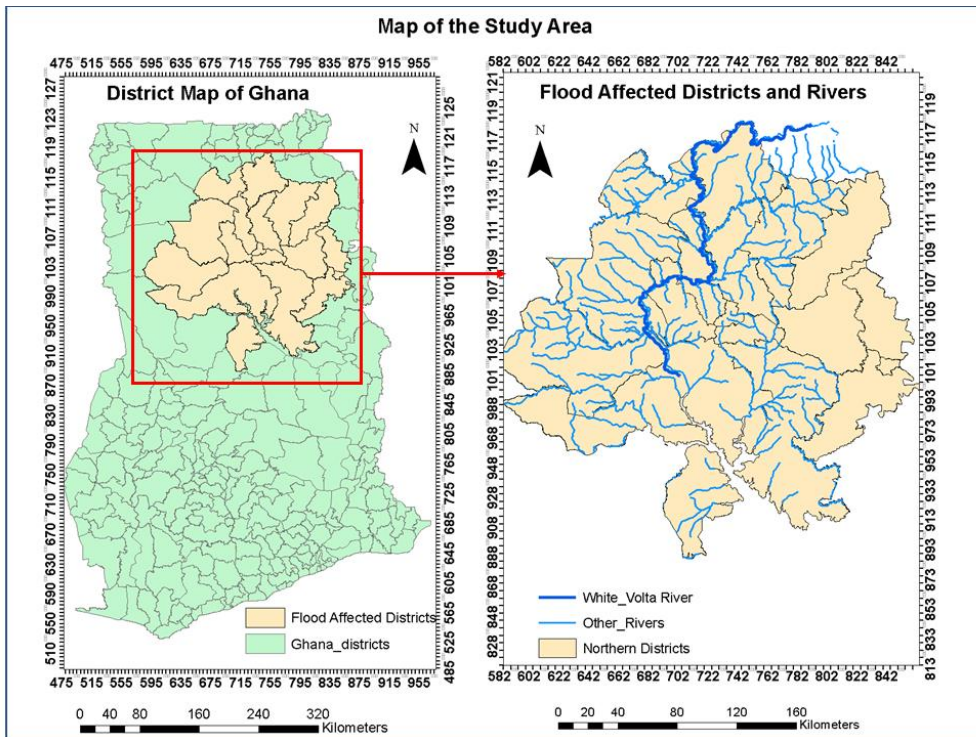


Figure 3.4a Map of the Study area. This is a district map of northern Ghana highlighting the flood-affected districts (left in the box) and also the white Volta river and its many tributaries that serve as drains of the district.

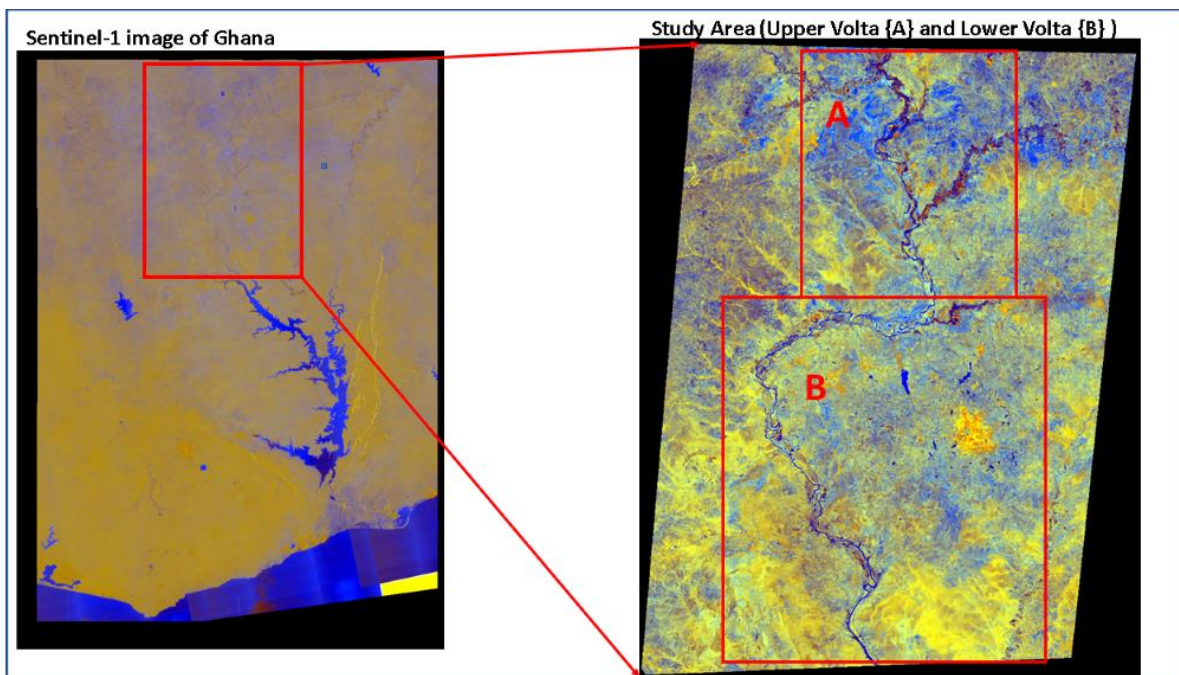


Figure 3.4b Sentinel-1 land-cover Map Highlighting the study area in the bound box; the area is divided in two: the northern part (upper Volta) denoted by box "A" and the Southern part (lower Volta) denoted by box "B".
 Source: Jorg Haarpaintner, (2019) ArcGIS hub.

3.2 Soil types

In the White Volta catchment, a sharp difference can be distinguished when looking at the geology. There are two main types to consider (Carrier et al., 2008): regions with a soil composed of Voltonian deposits (sandstone and/or mudstone) and regions with granitoid rocky soil (Carrier et al., 2008). Voltarian series and Birimian granitoids form the underlying bedrock in the area (Kesse & O, 1985). As far as soil is concerned, Eutric fluvisol, gleyic lixisols, eutric gleysols, and lithic leptosols amongst others can be found in the floodplain of the Volta river. Figure 3.5 shows the types of soil in the area. The contributions to surface water vary from season to season, and the water volume across the entire wetland represents inflows of 6 mm per day from the real surface and groundwater refill (Nyarko, 2007).

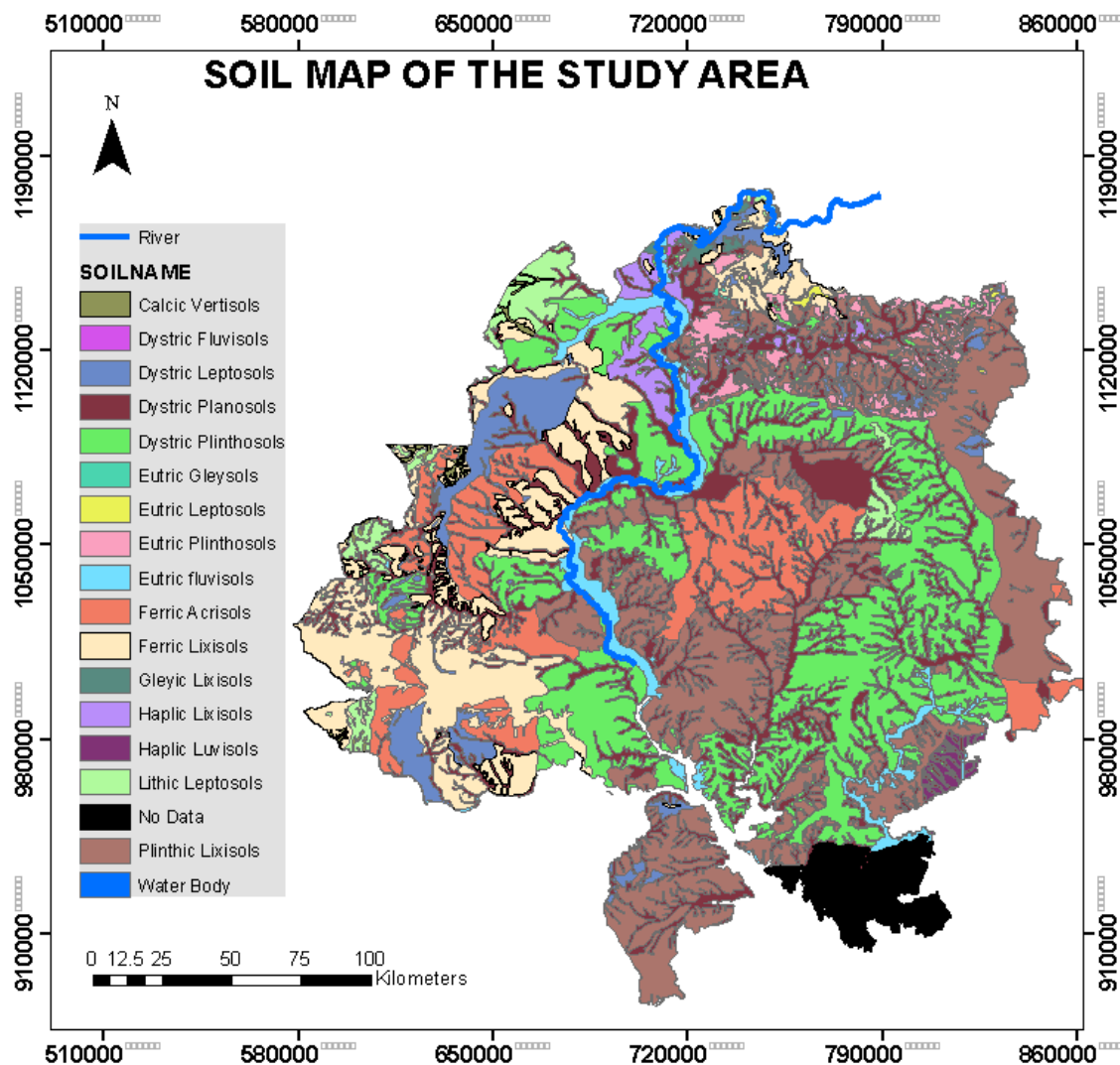


Figure 3.5: soil map of study area

3.3 Vegetation

The vegetation pattern in northern Ghana is grassland characterized by dispersed trees and shrubs resistant to bushfires and drought. The savanna zone is characterized by scattered woody and guinea savanna tree species mostly as a result of the frequent bushfires in the region (Andersen et al., 1998; Bagamsah, 2005). The woodland in the savannah makes up about 65.5% of the total landmass of Ghana. *Azēlia africana* and *Diospyros mespilliformis* are common tree species in the zone. The bushfires burn the continuous vegetation, forcing only adaptive resistant species to grow in

the area. The vegetation has transitions from south to north. Southmost part of northern Ghana within the savanna zone is characterized by densely thick wood trees and very strong grass species such as *Andropogon, spp*, the density of the trees is reduced and somewhat scattered; dominated by the woody grassland species further north within the Sudan and Guinea Savanna regions (Ekekpi et al. 2000). Further, into the arid regions within the zone, the shrubs and trees are scattered or completely missing but mostly dominated by grasslands. Some other common tree species with economic values found in the region are mango (*Mangifera*), shea nut (*Vitellaria paradoxa*), neem (*Azadirachta indica*), and baobab (*Adansonia digitata Linn*). The bushfires in the area impact soil fertility and also influence erosion of the topsoil by both running water and wind since it is often bare. Figure 3.6 shows a landcover map illustrating the various land cover types in the area.

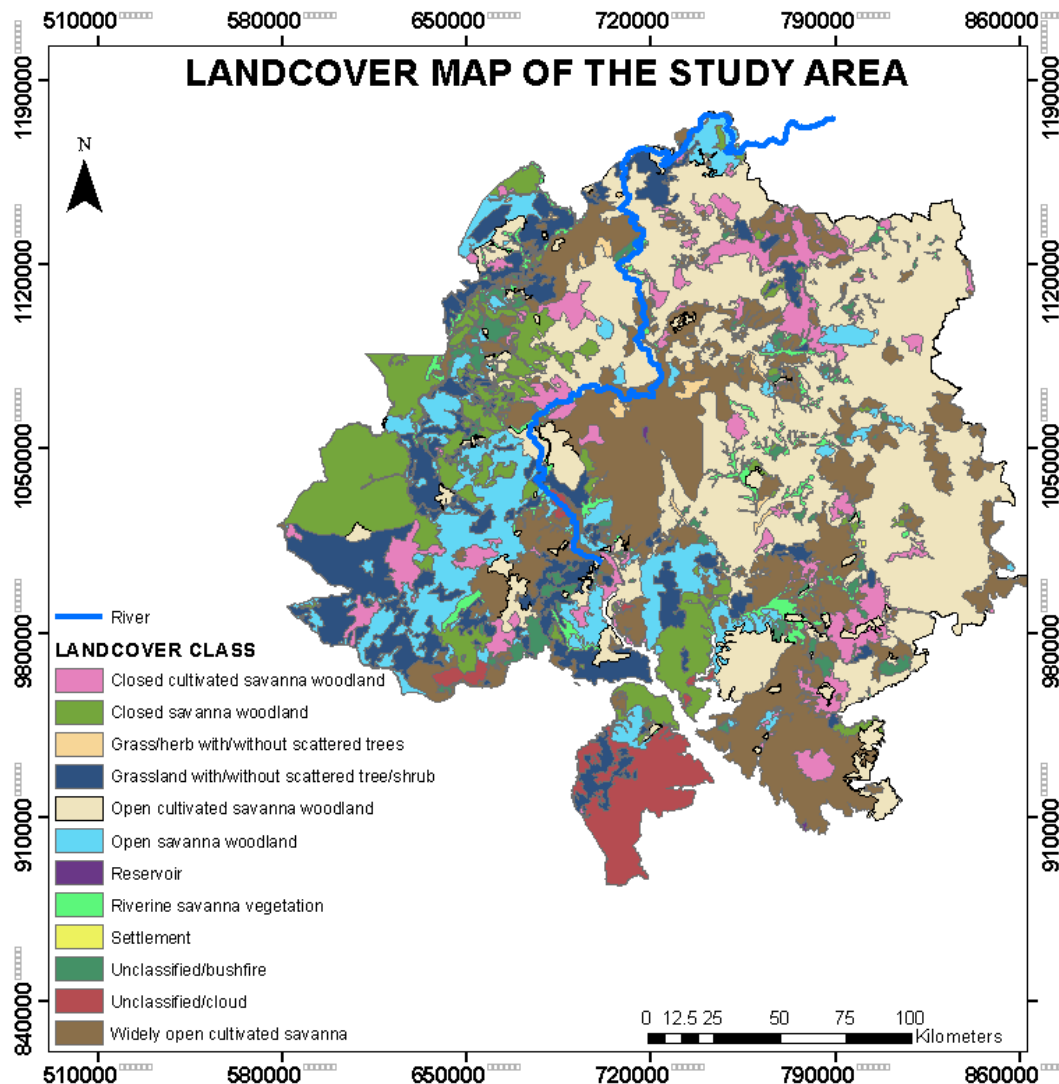


Figure: 3.6: Land cover map of the study area

3.4 Data and Method

The following section describes the available data and methods used in this study to achieve the intended results. This study does not involve fieldwork and, therefore, only makes use of secondary data. SNAP software was used to process all the Sentinel-1 data, including extraction of the flood extent. ERDAS Imagine software was used to process and carry a supervised classification using Sentinel-2 imagery from 2018. ArcGIS 10.6 software package was used for data processing and

preparation of final maps. The spatial analyst package tool was used to develop the trend surfaces through the interpolation method. The general methodology for this study is shown in figure 3.7. Figure 3.7 briefly explains and outlines the data, steps, and process used to achieve the objectives of this research. Sentinel-1 data downloaded from archives repository of ALASKA was used to extract the flood extents in the study area. The images were first corrected geometrically, radiometrically, and speckle filtering carried out to reduce the noise in the images before applying thresholding to extract flood extent. Sentinel-2 images using maximum likelihood supervised classification was used to detect and outline crop areas and other land use within the flood extents. Ground Control Points (GCP) from the study area as obtained from a different study, were used to assess the accuracy of three DEMs to determine the best quality one among the three which would then be used in a trend surface interpolation to assess flood depths within the flood extents extracted earlier from the Sentinel-1. The flood depth map is overlaid with the cropped area from the classification process to determine the flood the vulnerability of the crops through an economic loss assessment. The final risk associated with crop farming in the area based on the 2018 flood is assessed by combining the determined vulnerability and hazard.

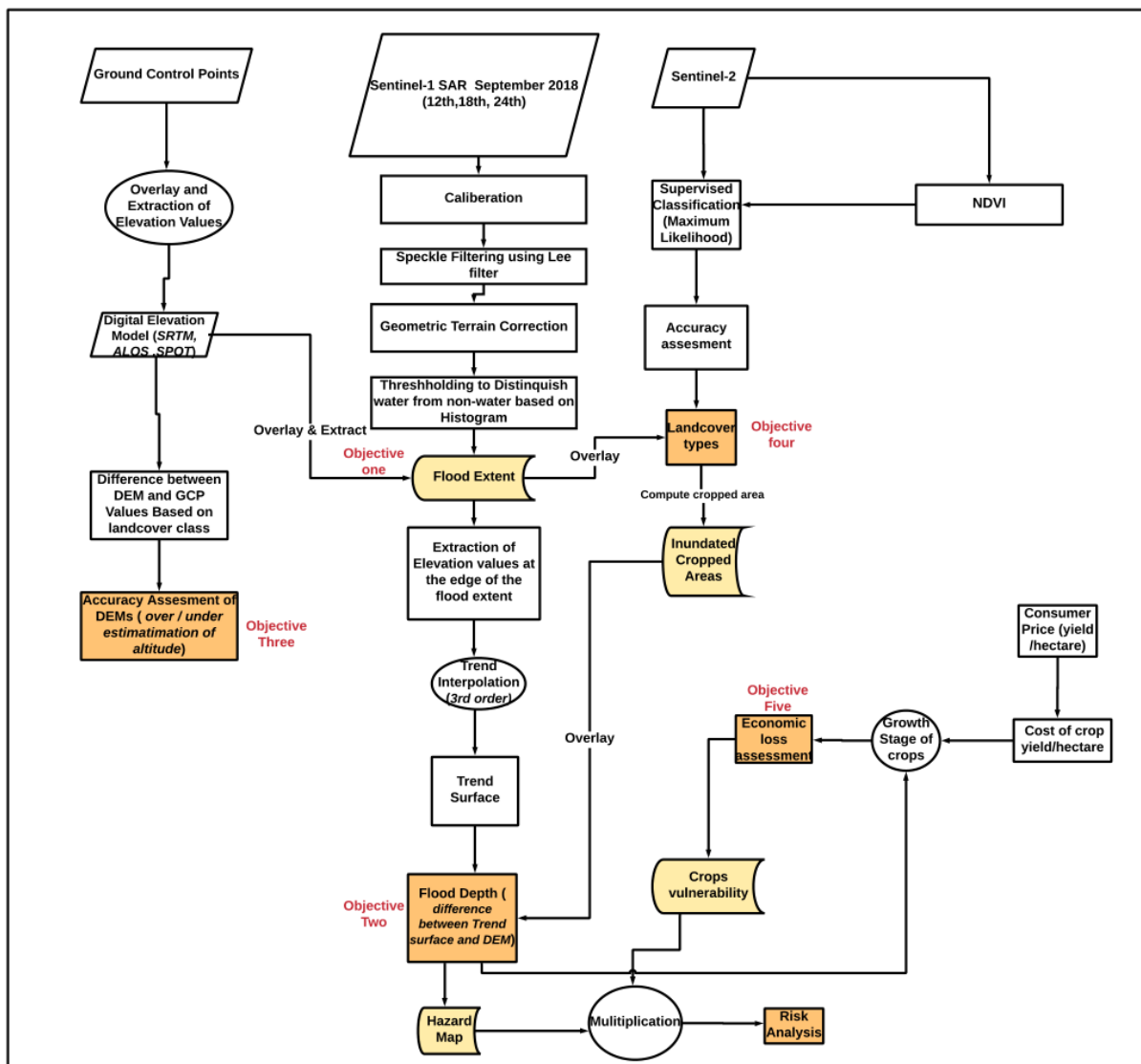


Figure 3.7: General flowchart outlining the methodology of the research process

3.4.1 Available Data

The data used for this study was mostly secondary data obtained from departments or downloaded from website data sources such as Global Land Cover Facility (Sentinel-2), Alaska data sites (Sentinel-1), and river discharge data from the ministry of water resources in Ghana. Listed in Table 3.1 are the data used for this study.

Table 3.1 Table 3.1: Datasets used in the research are summarized

Data	Data source	Format	Software / Tool	Application
Sentinel-1 Ground Range Detected (GRD-IW) Level 1	Alaska Data (https://search.asf.alaska.edu/#/)	GeoTIFF	SNAP	Delineation and extraction of flood extent
Sentinel-2 (10m)	Global Land Cover Facility (https://glovis.usgs.gov/)	GeoTIFF	ERDAS IMAGINE package®	Supervised Land cover classification
Digital Elevation Model (DEM) (30m)	SRTM - Global Data Explorer (https://earthexplorer.usgs.gov/) ALOS PALSAR - ALASKA Earth Data Vertex (https://search.asf.alaska.edu/#/) SPOT – HKV Consultants Ltd.	GeoTIFF	ARCGIS package® (Spatial analyst tool)	Mapping of flood extent and extraction of elevation values.
River discharge data	Hydrological Services department of Ghana	Excel sheet	ARCGIS package®	Plotting and Studying the trend in the river levels
Ground Control Points (GCPs)	HKV Consultants Ltd.	Data Points	ARCGIS package®	Accuracy Assessment of DEMs
Study Area Boundaries	CERSGIS -Ghana (https://cersgis.org/)	Shapefile	ARCGIS package®	Outlining the boundaries of the Study Area.

3.5 Data, Tools/ Software Description, and Processing

This section briefly describes the data, tools, and software used in this study.

3.5.1 Sentinel-1 Data

Sentinel-1 SAR images were used for this study. Sentinel-1 is a near-polar sun-synchronous orbit satellite with a repeat cycle of 12 days and 175 orbits per cycle of each satellite (Sentinel-1A and Sentinel-1B) at an altitude of 693 km. Sentinel-1 satellites were launched on 3rd April 2014 and 22nd April 2016, respectively. The SAR instrument operates in one of the four modulation modes within the C-band (5.407 GHz) frequencies: strip map (SM), interferometry-wide swath (IW), and wave (WV). IW is the land-based default mode, operating under the concept of TOPSAR (Terrain Observation with Progressive Scans: SAR) (Geudtner et al., 2014). The SAR instrument comprises

an interferometric swath width of 250km, three sub-swaths (IW1, IW2, and IW3), an incidence angle between 29.1° to 46.0° , and an Azimuth angle of $\pm 0.6^{\circ}$ (De Zan & Guarnieri, 2006). Level-1 Sentinel-1 Ground Range Detected (GRD) C-band Interferometric Wide Swath (IW) mode data with a swath width of 250km and a 10m geometric resolution was used for this study. SAR images polarisation refers to the geometric plane that transmits and absorbs the radar wavelength. In the majority of systems, polarization is horizontal (H) or vertical (V), producing four specific polarisations in relation to the satellite antenna: HH, HV, VH, and VV. Although-polarization can be used for flood delineation; the radar signal backscatter features differ, which affects the accuracy of the flood maps generated (Clement et al., 2017). By using Sentinel-1 for flood forecasting and mapping, it is important to understand the shortcomings of either polarisation because environmental conditions vary. Earlier work has already shown that VV provides a marginal advantage in Sentinel-1 flood detection (Twele et al., 2016). This is because the medium incident angle of the VV polarisation makes it well suited for flood detection as compared to the HH polarization. Therefore, VV polarisation is considered in this study. In all, seven Sentinel-1 images were downloaded from Alaska Data (<https://search.asf.alaska.edu/#/>) With an acquisition interval of six days. The mode of Acquisition and characteristics of Sentinel-1 data are listed in table 1.1 in appendix A.

The Sentinel-1 images obtained from Alaska data search vertex were radiometrically calibrated, and terrain corrected using the Sentinel Application Platform (SNAP) tool. Images from September 2018 depicting floods in the study area, as observed from the Sentinel-1 images, were selected for the study. In all three-date imagery, 12th, 18th, and 24th were selected for this study, referred to as the crisis image. These images are six days apart because of the revisit time of the sentinel-1 satellite. The selected images were compared to the period of no rain and flood to examine the extents of the flood from the river banks better. The mapping of the extents also aids in understanding the duration and receding period of the flood over the surfaces of the Earth. There are two images for each recorded date because of the swath and coverage. The area is wide, and the satellite cannot cover it all in a swath.

3.6 Pre-processing of Sentinel-1 images and extraction of flood extent

The techniques used in this analysis are seen in Figure 3.8. The Sentinel-1 Image is initially pre-processed, to minimize the SAR-typical noise in the images. Throughout the pre-processing period, radiometric and spatial anomalies attributable to the image characteristics and the image parameters were resolved, and radiometric adjustments were made to increase the representation and understanding of flood imagery. Pre-processing steps included data entry and subsetting to the area of interest.

In the pre-processing period, the Graph Processing Tool (GPT) of ESA's sentinel-1 toolbox (S1TBX), which is embedded in the sentinel application framework (SNAP), conducts a field correction Range-doppler of Sentinel-1 data and radiometric calibration to sigma naught (dB). The GPT allows all individual pre-processing modules to be performed consecutively in a completely integrated production line. For the purposes of quantitative analysis, it is eminent to initially calibrate SAR images to ensure the pixel values are a direct representation of the backscatter from the reflecting surfaces (Meenakshi & Punitham, 2011).

SAR images are known to have speckle noise, which interferes with the accurate interpretation of images. The speckle is caused by the backscatter effect when radar pulses hit a surface. In order to enhance cognition and backscatter detection, the SAR image was tuned to a linear scale and screened using a sophisticated lee filter to remove speckle noises. At this point, Lee Sigma's single product filter approach was used to eliminate Speckle noise since several research have shown that Lee and Lee Sigma filters are most useful (Jaybhay & Shastri, 2015; J. S. Lee & Pottier, 2009). The Sigma filter uses the statistical distribution of the DN (digital number) values inside the moving

median 3 by 3 kernel to estimate the pixel value. Multi-look processing has been carried out to minimize speckle further and enhance the interpretability of the image.

Unprocessed digital SAR images most of the time are geometrically distorted and therefore need to be corrected before they can be used for further analysis. Level-1 Ground Range Detected (GRD) items consist of oriented, multi-looked, and projected SAR data that has been observed in the Earth utilizing Earth Ellipsoid models. Including the satellite details, the processor utilizes many other sets of data: such as the Scope Doppler Terrain Correction (Schreier, 1993), and Radiometric Sentinel-1 data are used to perform arcsecond shuttle radar topography missions (SRT Mission). In addition to pre-processing SAR data, data from SRTM is used to collect slope data as well as the mean and standard deviation from the automated thresholding method for all water bodies. Using the SRTM 3sec digital elevation model, after pre-processing the Sentinel-1 image, the image was sub-set to the region of interest, and geometrical data correction was applied.

In GRD images produced by the ESA, geometrical distortions induced by ground effects of the region of interest are not regarded. The ground range detected (GRD) images would then be updated in the field to enhance the geolocation of the imagery. The toolbox can automatically download SRTM tiles, which correspond to the specific Sentinel-1 scene. (<https://sentinel.esa.int/web>, accessed 01/01/2020). The GRD imagery of Sentinel-1 is ground-based and mapped to Geographical Coordinates of the SRTM DEM (Lat / Lon, WGS84). The calibrated data are filtered after the pre-processing with the S1TBX to reduce the noise inherent in SAR and to cut it to azimuth and range to eliminate noise in the resulting image. A projected, radiometrically corrected, and resized normalized radar cross-section (NRCS) image is the product of this pre-processing.

To map and extract flooded areas in SAR images, the image is classified into water and Non-water. Dark tones representing flooded areas are used to distinguish flooded from non-flooded areas (land) based on the smooth properties between land and water surfaces, as described earlier in chapter two. The linear-to-backscatter curve decibel scaling (dB) transition was applied to convert the image bands to a decibel. The DN values of the SAR image were converted to an 8-Bit image with a radiometric resolution, thus with values between 0 and 255. An ideal threshold, centred on the histogram of the image, was employed, to identify flooded areas and distinguish water areas and non-water areas (Gong et al., 2001). Determining the threshold for distinguishing between inundated and non-inundated areas involves an iterative process. In thresholding, a set of low digital number (DN) values are allocated to the “Flood Zone” class through an iterative process. Therefore, the threshold value of the DN that distinguishes the “Flood Zone” from the “Non-Flood Zone” is determined in this manner. The water surfaces are reasonably and consistently defined as low-return areas in the SAR results. Nonetheless, a flooded field can be difficult to achieve, depending on the image advantage and field interactions.

To set the threshold values, $DN \leq T_W$ Was set to extract the inundated areas while $DN \geq T_L$ was set to extract the inundated (land) area, where T_W and T_L represent threshold value for water and land, respectively and DN is the Digital Number (Rahman & Thakur, 2018). Images from periods without flood were used as a reference guide together in trial method based on the histogram to best determine the flood extent from the banks of the river based on an ideal threshold value. This was necessary to differentiate the actual flood caused by the overflow of the river, from the surrounding wet areas that might have been caused by rain. The thresholding was carried out using band math tool in the SNAP toolbox. All the aforementioned processes were implemented using the ESA Sentinel Application Platform (SNAP). The open-access SNAP toolbox is capable of downloading, pre-processing, and displaying Sentinel-1 SAR files. The workflow described above was implemented using the graph builder model in SNAP. This is an automated process that saves time and limits the possibility of human errors once the model is correctly calibrated.

The images from the period without flood also aided in identifying and differentiating permanent water bodies from the actual flood within the flood extents. The above-described procedure was used to process three images from the time of the flood in September 2018 (12th, 18th and 24th). The extracted flood extent was super-imposed with supervised classified Sentinel-2 Image to determine the area and level of crop inundation. The three images also show the duration and propagation of the flood through time. The extracted flood extents superimposed with three different DEMs are used to estimate the flood depths within the extracted flood extents.

3.7 Digital Elevation Model (DEM)

Many techniques exist that can be employed in developing high-resolution DEMs that are capable of capturing topographic information from the Earth's surface. ASTER, SRTM, and LiDAR are often used to generate very fine DEMs with less noise and environmental effects in the DEMs. There exist many software algorithms and methods adopted by researchers to correct and extract interesting variables or data from DEMs for various analyses. The entire process of cleaning up the DEM is mostly to minimize or eliminate outliers where possible, minimize terraces, and outlining water bodies in DEMs. Advanced filtering techniques are employed to locate and possibly eliminate undesired noise while preserving the relevant terrain information either embedded or covered by the noise in the DEM. The Lee filter creates grids in all directions of the band cells and calculates the standard deviation of the individual elevation bands in all directions. The newly created elevation values devoid of noise for each grid cell are formed using the initial elevation cell values and the lowest standard deviation of the bands with mean elevation values. In recent times, the proliferation of satellite-based images with high spatial and temporal resolutions and also increased stereo capabilities has resulted in the rise in production and use of remote sensed DEM as compared to the use of directly measured techniques. DEMs are models that represent the Earth's elevation surface, but often than not, the DEM is treated and recognized as an actual rendition of the Earth's surface (Wechsler, 1999).

3.7.1 SRTM DEM

In September 2014, NASA released the Shuttle Radar Topography Mission (SRTM) DEM 30M (1 arc-second) resolution and made it publicly accessible. It covered almost the whole Earth. The 30m resolution is said to be an enhancement of the 90m (3 arc-seconds) resolution that was released earlier in 2003 (Boncori, 2016). The SRTM is said to have an absolute vertical height of about 16m, less than 10m vertical relative height error, a location error of less than 20m and a relative circular geolocation error of 20m in terms of accuracy Globally (Farr et al., 2007; Santillan & Makinano, 2016). The SRTM DEM is produced from SAR images. The base to height ratio interferometric principles of SAR is used in the processing of DSMs (Merryman Boncori, 2016). The SRTM for this study was downloaded from Global Data Explorer (<https://earthexplorer.usgs.gov/>) with a Universal Transverse Mercator Zone (UTM 30N) projection in a GeoTIFF file format.

3.7.2 ALOS Global Digital Surface Model “ALOS World 3D – 30m (AW3D30)”

AW3D30 is a global DSM with about a 30m horizontal resolution (1-arcsecond). An optical sensor, the Panchromatic Remote-sensing Instrument for Stereo Mapping (PRISM) that was on the Advanced Land Observing Satellite (ALOS) was used to capture the DSM using the stereo matching method. The AW3D-30 was resampled from the five-meter resolution W3D topographic data considered as a precise global elevation data. (JAXA,2015). The AW3D30 was downloaded from the NASA ALASKA Earth Data Vertex (<https://search.asf.alaska.edu/#/>) with a Universal Transverse Mercator Zone (UTM 30N) projection in a GeoTIFF file format.

There are many studies that have been carried out to compare and test the accuracy and quality of these SRTM-30m and AW3D30 (Gesch et al., 2012; Suwandana et al., 2012). Statistical computation is mostly carried out to determine the Root Mean Square Error (RMSE) values, and

comparing the RMSE values gives a measure of accuracy. In this study, a statistical accuracy assessment was carried out to determine the quality DEM amongst three DEMs.

3.7.3 SPOT DEM

The SPOT DEM was generated from high-resolution photogram metric imagery. The absolute vertical and horizontal accuracy of SPOT depends on the characteristics of the landscape and the region of interest. Block Interpolation method can be used to fill SPOT DEMs either locally or it can be filled by the use of other data sources such as SRTM 90m and GTOP30. Usually, the bigger the area, the better the accuracy that can be expected using the block interpolation method. The DEM is based on SPOT, and the vertical accuracy was improved using Ground Control Points (GCP) from the area of interest. It originally had 200m resolution but was resampled to 30m resolution, to make it comparable with the SRTM and AW3D30 DEMs and projected to Universal Transverse Mercator Zone (UTM 30N) projection in a GeoTIFF file format. The GCP points were sampled from areas with sudden changes in elevation, levelled plain surfaces, cultivated fields, open meadow areas, and at about 20m from structures and trees. In all, about 23 pair GCP points evenly spaced were collected across the study area. The GCP points were collected using a dual-frequency survey-grade GPS receiving device. The observation time was varied from about 40 to 100 minutes. Figure 3.9 shows the three DEMs used in this study. Figure 20 in Appendix D show the SPOT DEM in detail and the location of GCPs.

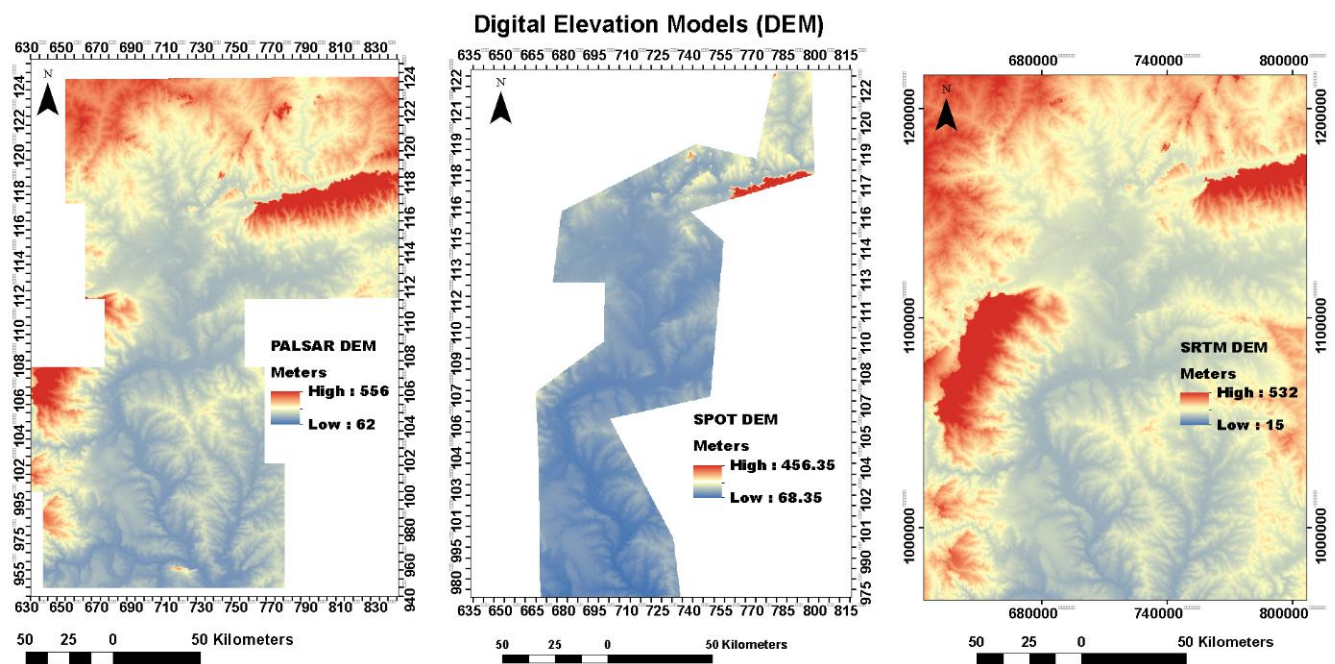


Figure 3.9: The three different Digital Elevation Models of the Study Area

3.8 Ground Control Points (GCP)

Ground Control Points (GCP) as measured and collected by Udo et al., (2012) during a flood risk assessment in the study area was used in this study to assess the accuracy of DEMs since fieldwork was not carried out in this study. Figure 19 in appendix D shows the locations of the GCPs. The control points were measured and collected in areas such as farmlands (four points), open lands (16 points), meadows (3 points), cultivated fields (6 points), football ground (11 points) and tarmac slabs (3 points) as land cover types within the study area. These areas are relatively constant and have not changed over the years.

4.0 Description of Crops considered in this study

Rainfed agriculture is a common farming practice in Ghana. This is mostly a result of the high cost of irrigational farming, which most of the poor and vulnerable communities in the northern sector cannot afford (Namara et al., 2011). The region is also blessed with a lot of fertile river flood plains from the many Volta river tributaries that favour the cultivation of maize, rice, millet, sorghum, potatoes, yams, melons among others (Motsumi et al., 2012). Figure 4.1 shows some crops and their growing season in Ghana. Northern Ghana heavily depends on rainfed agriculture, with a few irrigational farming activities mostly carried out by institutions. Farming activities in the north commence in the latter part of May when the rains start and last till October when the crops are harvested. Among the several crops grown in the region, most are staple foods, and so the majority of the farmers are subsistence farmers. Farming in the north is not without problems, as there are recurrent floods that occur in the area. The floods usually damage crops on farms along or close to river banks partially or wholly, resulting in various degrees of losses. The occurrence of flood and the subsequent damage meted to some crops (maize, millet, sorghum, and rice) considered as important in Ghana in terms of food security and fight against hunger are discussed in this section. The growth stages, timing, and extent of the floods are considered in this section. Crops grown in Guinea savanna are listed in table 4.1.

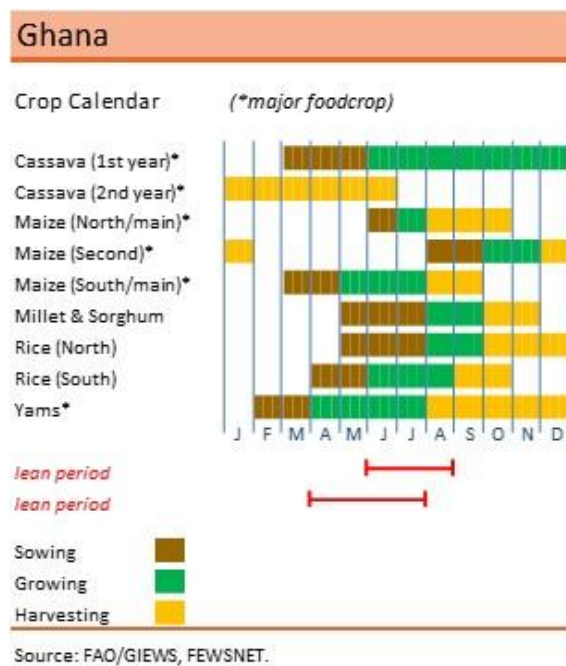


Figure 4.1: Major food Crop calendar for Northern and Southern Ghana

Table 4.1: Crops grown in Guinea Savannah of Ghana

Zone	Cereal	Legumes	Starchy foods	Tree crops	Vegetables
Guinea Savannah	Maize, millet, sorghum, rice	Groundnut, Bambara beans, cowpea, and soybeans	Yam and Cassava	Cashew and shea fruits	Pepper and Tomato

Source: FAO 2005 and MOFA 2011

Table 4.2 shows the cereal crops, their estimated mean yields, the month of harvest, average weight yields among others in the Northern region.

Table 4.2: cereal crops and estimated yields

Crops	Average yield (t/ha)	Months of Harvest	Months of Stock Depletion	Months of food insecurity	Total Outputs (MT)	Average weight yields (Kg/Ha)
Maize	0.76	September	June	3	158.27	763
Millet	0.49	November	June	5	28.74	487
Sorghum	0.58	November	June	5	17.08	576
Rice	0.49	October	May	5	2.80	492

Source: Quaye (2006)

Ever since this research was carried out in the early 2000s, there have been improvements in the quality of seeds by government agencies and scientific communities to develop hybrid seeds with better yields and improved resistant varieties. These newly improved varieties, their maturity period, and yields for maize, rice, millet, and sorghum are discussed below.

4.1 Maize crop

Maize (*Zea mays* L.) is a versatile annual staple crop cultivated in many agro-ecological zones globally. In Ghana, maize is cultivated across the country but mostly in the upper west, upper east, North East, Savannah, Northern, transition, forest, and southern regions, making it the largest staple crop in the country. In developing countries especially, maize serves as both food and a source of income for local farmers, the poor and vulnerable in society. Aside from its economic importance, flour from maize can also prepare a variety of dishes worldwide. Maize offers a lot of nutritious benefits to humans as food and animals' livestock as feed (Ranum et al., 2014). As the largest cultivated crop in Ghana, about 1,000,000 hectares of land representing a 50-60% of cereal production. Smallholder farmers produce about 70% of the total maize in the country. Registered maize yield in 2013 by the Ministry of Food and Agriculture was estimated at 1.7 t/ha with the potential of producing about 6 Mt/ha (MOFA, 2013). The potential yield of maize grains depends on the genetic variety of the maize plant in a particular environment amidst the fertility and soil conditions.

Due to the variations in the fertility of the soil, amount of rainfall, porosity of the soil, and the crop pest and diseases, there are different maize adapted to the different environmental conditions. There are genetically modified maize varieties that ensure early maturity and higher yields. In appendix B table 1.6 is some recommended maize varieties and their characteristics in Ghana. Table 1.6 in appendix B outlines the varieties, maturity days, average yield potential, drought resistance, among other characteristics of recommended maize varieties in Ghana currently. Generally, from the table 1.6, it can be concluded with these new varieties that maize has a maturity period of between 90 to 120 days, depending on the variety as against the earlier varieties that took 120 – 180 days. These current varieties are also high yielding. This stage of reproduction of the crops takes place between 65 days to 100 days. Assuming the planting was carried out in the last week of June, it implies that the crops would have been about 75 days old and in their reproductive stage towards maturity. Thus around September when the floods set in and most of the time destroys the crops. Maize crops usually are about 70 to 220cm long, depending on the variety.

4.2 Sorghum Crop

Sorghum grain [*Sorghum bicolor* (L.) Moench] native to Africa and adapted to the climate (Taylor, 2011) is considered as an essential food crop together with maize and millet in Northern Ghana.

Subsistence farmers mostly cultivate it on small landholdings of not over two hectares of land (Kudadjie et al., 2004; Premachandra et al., 1995). Sorghum solves the problem of food security, serves as a source of income, and also used in the local and industrial breweries to produce local pito and alcoholic beverages, respectively.

Sorghum is ranked third after maize and rice in Ghana. Sorghum constitutes about 12% of the overall cereal production value. The availability of early maturing white maize crops shifted the focus of local farmers from sorghum cultivation to maize cultivation and hence the reduction in the area for sorghum production. Farmers appreciated this shift because it favoured the lean periods and food security in Northern Ghana, where Sorghum is largely cultivated. There has been a general increase in yields of sorghum per variety from 0.9mt/h to about 1.28 mt /ha (Atokple, 1995; SRID, 2004). Some newly introduced varieties produce up to 3.5mt/ha (NASTAG, 2017). Sorghum, just like the maize crop, is cultivated under rainfed conditions in Sudan and Guinea savannah zones of Ghana with a 990mm and 1000mm annual average rainfall, respectively. (OECD, 2010). Sorghum is highly resistant to drought and high temperatures, which therefore makes it suitable and well adapted to the conditions in these regions (Kudadjie et al., 2004). Sorghum grows well in fertile and deep, well-drained soils. Sorghum is much more tolerant to water-logging conditions within a short period compared to maize. Sorghum is planted latest by June in Northern Ghana. Sorghum grows taller than maize and so can be able to withstand flood depths as high as 1m at the reproductive stage of development for a short period. Flood depths higher than 1m are likely to submerge the crops completely. In general, the sorghum crops could survive higher flood heights compared to maize, but only for a short period. Considering the flood in the area, it, therefore, implies that the survival of sorghum within 0 to 1m flood depths depends on the duration of the water in that location. A more extended period would consequently suggest a complete loss, even though the crops may not have been completely submerged. In appendix B table 1.7 are genetically improved high yielding sorghum varieties.

4.3 Millet Crop

Millet [*Pennisetum glaucum* (L.) R. Br.] from the family of grass is cultivated under rain-fed conditions in the northern part of Ghana (FAO, 1996). Annually, about 14 million hectares of Pearl millet is cultivated in Africa and Asia. Millet is adapted to areas with low soil fertility dry conditions in some parts of Africa and India. There are varieties of millet such as Foxtail millet *Setaria italic*, Finger millet, Proso millet, Foxtail millet *Setaria italic*, among others. Pearl millet was first brought to Ghana as far back as 1250 BC by invaders from the north and cultivated at Ntereso located in Northern Ghana (Davies, 1968) and is therefore considered as one of the oldest domestic cereal crops. Millet has maturity days from 80 days to 180 days. Millet aside, being used for food also serve other purposes such as leaves and stems for fodder, stalk for fencing and roofing of local houses, and as saltpetre for cooking.

Table 1.8 in appendix B shows a list of improved millet varieties developed in 2015 by the Council for Scientific and Industrial Research- Ghana. Millet is better adapted to dry conditions and so does not do well in wet areas. About 0.5m water height can easily inundate millet crops.

4.4 Rice Crop

Rice is regarded as the second significant staple cereal crop after maize in Ghana (MoFA, 2009). Averagely about 300,000 metric tons of rice produced in Ghana, represents about 30% of the total demand, this, therefore, results in the importation of the remaining 70% to meet the demand (Darfour & Rosentrater, 2016). Rice is also the most imported cereal crop in the country, representing 58% of imported cereals (Osei-Asare, 2010). *Oryza Glaberima* and *Oryza Sativa* are the major rice types cultivated in Ghana (Blench et al., 2003). Rice production has been on the rise, especially after 2007. In 2010, it was observed that rice production recorded an increase in area from 0.09 to 0.16 million hectares, and the recorded yields were between 1.7 tonnes to 2.7 tonnes

a hectare. The year 2010 recorded a double of the quantity recorded in 2007, thus from 185,300 to 491,600 tonnes (FAO, 2013). Rice is mostly cultivated in three regions in Ghana, namely the upper East, Volta, and Northern, which together produce about 45000 to 60000 tonnes annually, of which the Northern region is the largest contributor producing about 63,000 tonnes in 2009(USAID, 2009).

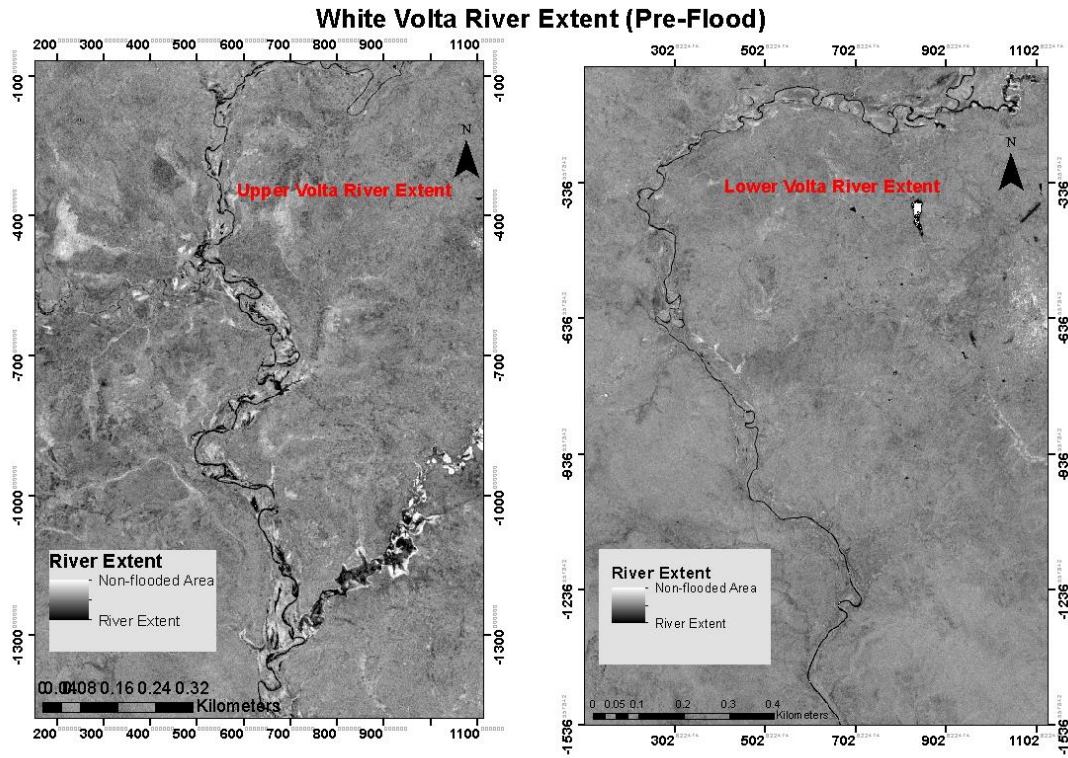
There are three principal methods of producing rice in Ghana, namely, Valley- bottom rice, Upland, and controlled flooding. Valley bottom and Upland methods are considered as traditional and make use of an African rice variety called *O. glaberrima*. The cultivation is done on small scales by individuals, but its widespread mostly in rural and remote areas. Valley-bottom rice is so-called because it is planted in valley bottoms close to rivers. Upland rice is rain-fed and cultivated in the mountainous areas of Ghana, while the controlled flooding method involves the deliberate channeling or pumping of water from dams and rivers into rice fields in a controlled mechanical manner. Along the white Volta river in the Northern region Of Ghana, the Valley-bottom method is mostly used in rice cultivation. Aside from consumption, the straw is also beneficial as feed to livestock, especially in the dry season. Rice is a water-loving crop and so can stay in water up to particular depths and periods of flooding as compared to the other crops discussed above. This is an advantage of rice in a flood situation, and so rice has a greater chance of surviving underwater for an extended period. Rice can also withstand flood heights between 0.5 and 1m without being submerged. Table 1.9 in appendix B shows some rice varieties developed by Council for Scientific and Industrial Research - Savanna Agricultural Research Institute (CSIR-SARI) of Ghana.

5.0 SENTINEL-1 FLOOD ANALYSIS AND RESULTS

Sentinel 1 and 2 data, together with SNAP toolbox, and GIS suite were used in the extraction and study of the spatial and temporal phenomenon of the flood within the study area. Figure 5.1 shows the actual extent of the river before the occurrence of the flood (Pre-flood). Figure 5.2 and 5.3 shows a geometrically and radiometrically processed images showing the extent of the flood for the Upper and Lower Volta in the study area, respectively. The images shown represent flood from the 12th, 18th and 24th of September 2018. The dark pixels depict the flood extents, mostly as a result of the specular reflection as explained earlier in chapter two. From the analysis, as observed from the images, it was realized that there are river flow dynamic disparities between the upper and lower Volta. The two areas do not get flooded at the same time. For instance, on the 12th while high volumes of water and larger flood extents could be observed in the upper Volta (figure 5.2), the Lower Volta (figure 5.4) suggested less flooding in the area. On the 18th, a reduction in flood extent was observed in the upper Volta while there was an increase in and flood extents of the images from the Lower Volta. There was a further reduction in the flood extent for the Upper Volta on 24th resulting in a slight increase in the flood extent in the Lower Volta. The extent can be estimated visually from the very dark appearance of the pixel reflection as opposed to the bright appearance of the surrounding region or Land. The dates and progression of the flood for the Upper and Lower Volta are shown in figures 5.2 and 5.4.

The next stage was to extract the flood extent from the processed images based on the grouped backscatter pixel effect. Binarization by choosing two threshold values for the identification of water and non-water areas based on a band math equation algorithm to detect flooded and non-flooded pixels according to the set histogram-based threshold. The resultant image is a grayscale image composed of a continuous single data band. The equation used was; {single band (in dB) > set a histogram threshold value of -15 (upper) and -20 (lower)}. The set threshold was based on dB values of the histogram, as shown in figure 5.3 (upper Volta) and 5.5 (lower Volta). The values for water or the flood extent were the least values (below zero), and the histogram showed that most of the pixel values were between -15 and 0 (Upper) and -20 and 0 (lower) as indicated by the peak within this region, hence setting of -15 and -20 as the threshold value. The pre-flood images also guided the setting of the threshold values. The threshold values were calculated from the study of pre-flood event datasets together with the histogram.

The extracted flood extent (figure 5.3 and 5.5) was overlaid with the land use data to determine the artefacts at risk of flooding and the estimation of the damages and risk associated with the flood. Table 5.1 shows the total inundated areas of the Upper and Lower Volta for the three observed dates.



Figures 5.1: White Volta river showing the extent of the river for the upper and lower Volta. Date: 20th/08/2018

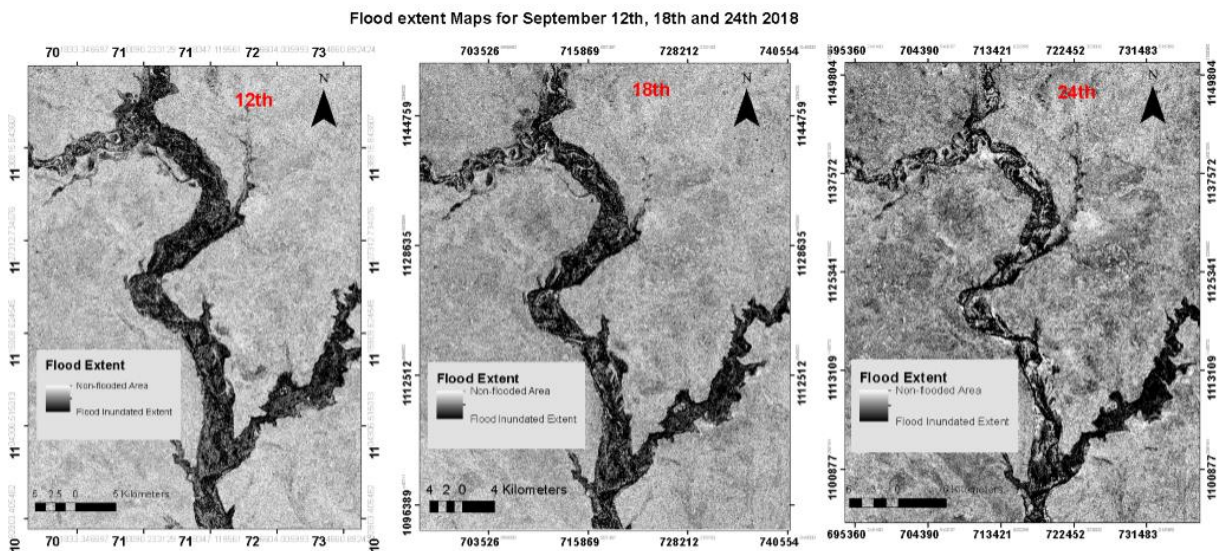


Figure 5.2: Outlined Flood Extent maps for September 12th, 18th and 24th of 2018. (Upper Volta). Darker pixels as a result of the specular reflection and the white background rough reflection of the land and non-inundated areas.

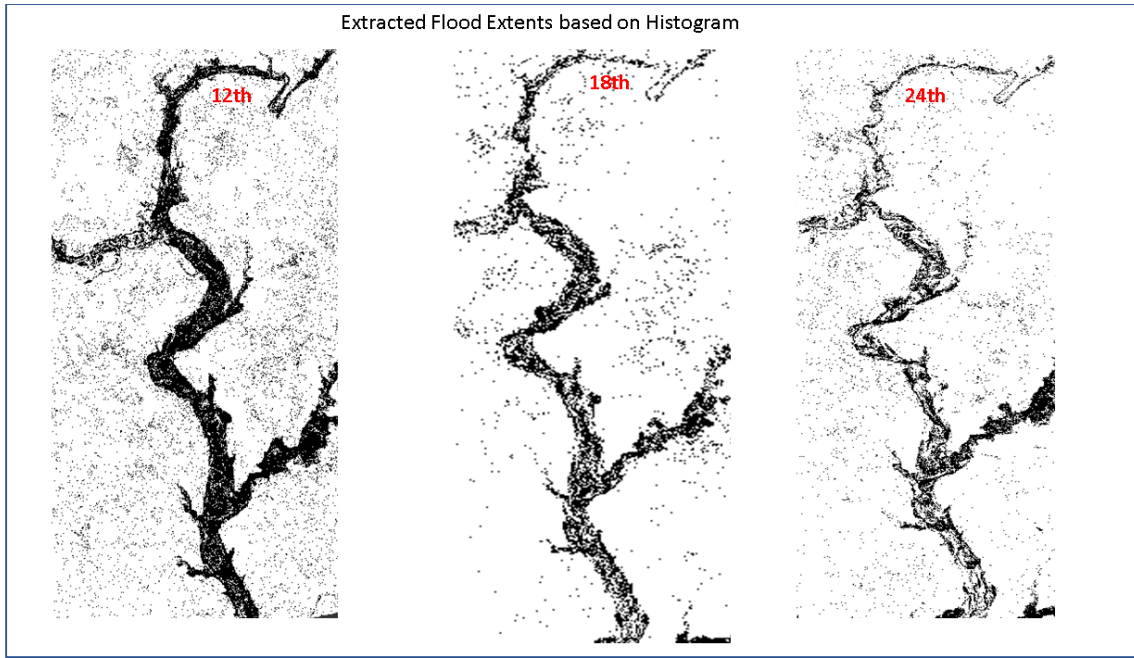


Figure 5.3: Extracted flood extent for the Upper Volta (12th, 18th, and 24th). The darker areas (pixels) are the flood extents while the white background represents un-inundated areas (excluded dry pixels). The extracted flood extents were based on the histogram to set a threshold. The floods were high on the 12th, but receded on the 18th and further on the 24th.

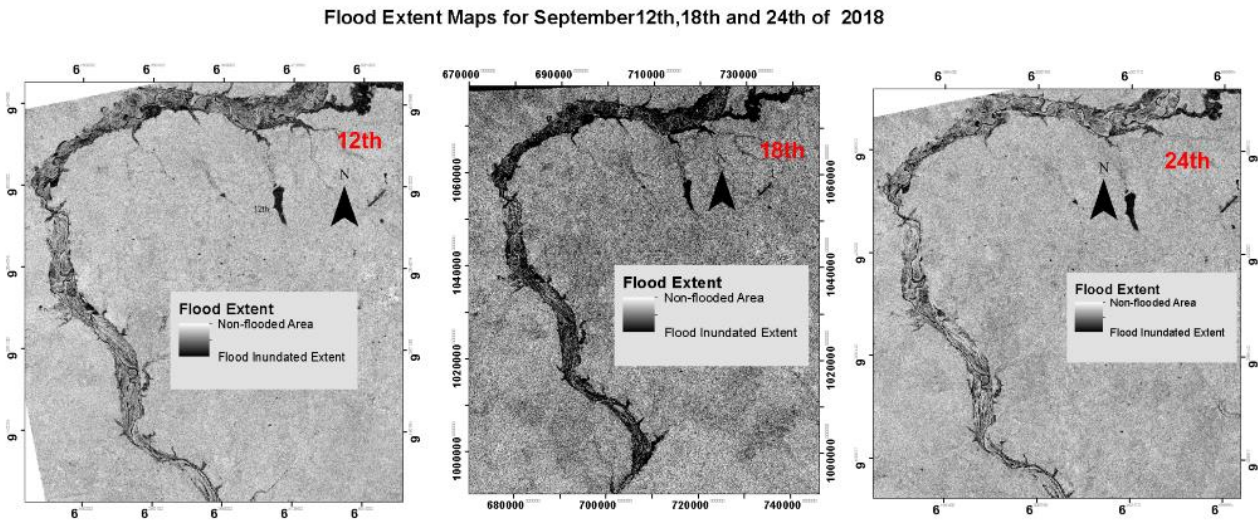


Figure 5.4: Outlined Flood Extent maps for September 12th, 18th and 24th of 2018. (Lower Volta). Darker pixels as a result of the specular reflection and the white background rough reflection of the land and non-inundated areas.

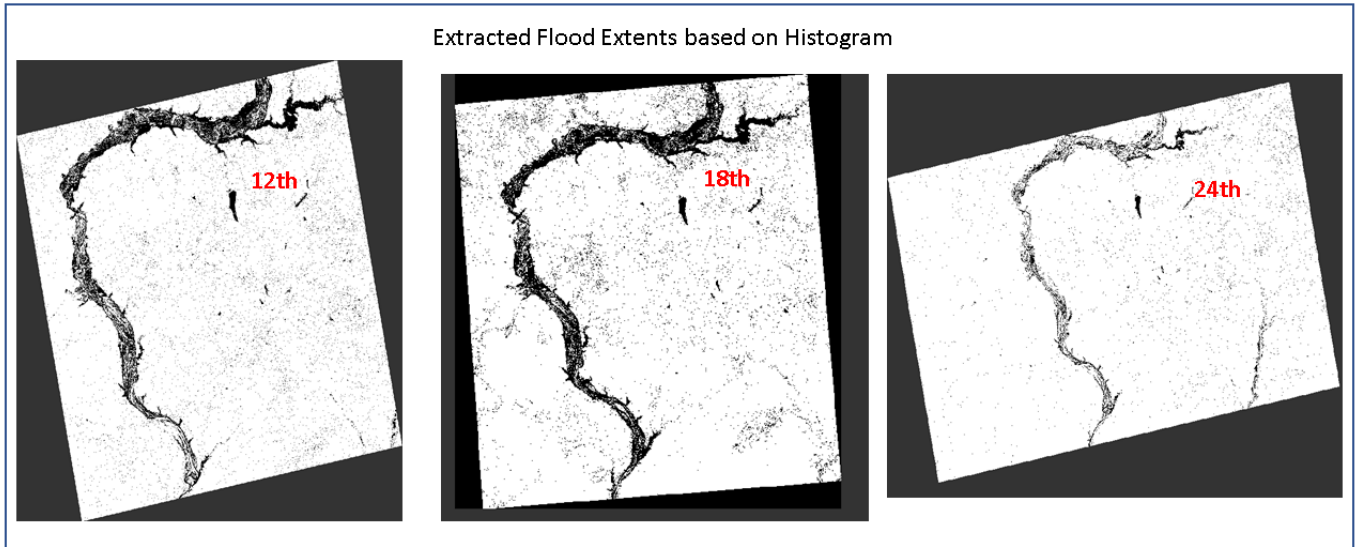


Figure 5.5: Extracted flood extent for the Lower Volta (12th, 18th, and 24th). The darker areas (pixels) are the flood extents while the white background represents un-inundated areas (excluded dry pixels). The extracted flood extents were based on the histogram to set a threshold. The floods were high on the 12th, higher on the 18th but receded on the 24th.

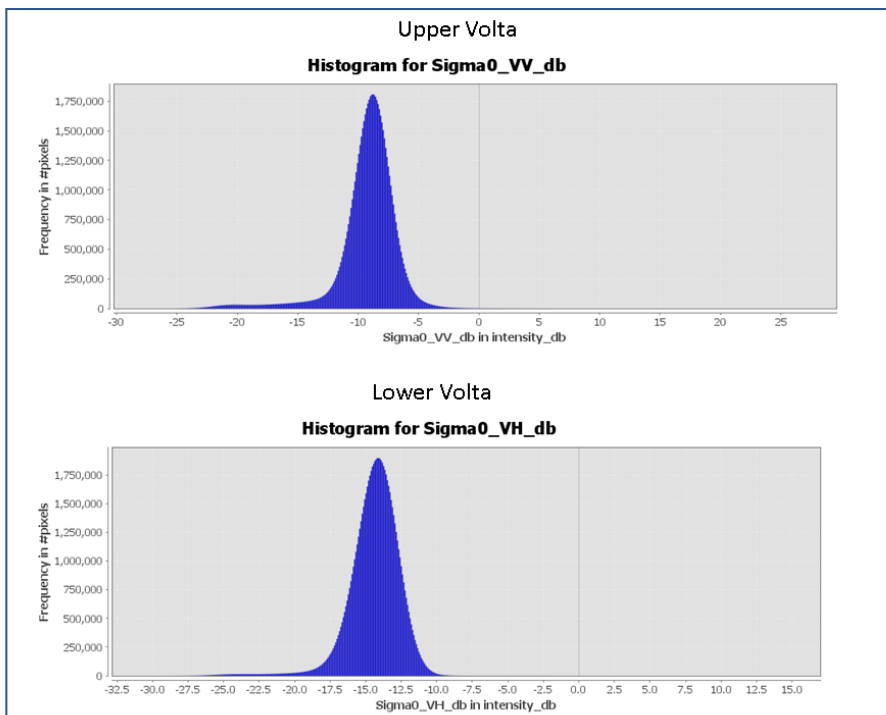


Figure 5.6 : Histograms used for setting the threshold for the upper ($db > -15$) and for the lower ($db > -20$)

Table 5.1: Inundated areas of the upper and lower Volta

Date	Inundated area (ha) Upper Volta	Inundated area (ha) Lower Volta
12th September	34,017	11,075
18th September	26,215	8,570
24th September	20,709	10,738

5.1 Characteristics of the extracted flood Extent

A closer look at the images of the flood extent revealed that the images were so speckled. ‘Dry’ pixels were sometimes observed within the flood extent, and this is because of the geomorphology or river basin characteristics of the study area. The Volta river is a meandering river and flood plains are characterised by meanderings, oxbows, and oxbows lakes (figure 5.7 – 5.8), point bars, natural levees, vegetation, and shrubs sticking out of the water in some parts of the river. The radar backscatter of these regions is, therefore, different from the surrounding water. The differences and variations in the image result from the backscattering effect of radar as explained earlier in chapter two for the soil, water, and moisture content and vegetation all interacting with the incident rays hitting the surface and the reflection of the incident rays. The vegetation and point bars, for instance, are interpreted as dry land since they have the same backscatter effect as the non-flooded areas as opposed to the water or fully submerged regions that are interpreted as smooth surfaces (specular reflection) and therefore appear as dark pixels. The different backscatter returns within the flood extents result in different pixel values between adjacent pixels. Applying a threshold value to extract the flood extents also results in the elimination of dry pixels within the flood extents, therefore, resulting in the gaps and scattered pixels within the flood extents, as observed in figure 5.8. Since the river characteristics and land cover are not readily visible in the radar images, Sentinel-2 optical images were therefore used to highlight the river characteristics and land cover types within the flood extents as illustrated in figure 5.9. Figures 5.7 and 5.8 shows the flood extents and highlighted sections showing the meanderings. In the riverbed, the darker blue areas within the swale and between the point bars and the oxbow lakes are the areas where we have specular reflection and that is mostly the point where the tributaries flow into the major river resulting in complete flooding of those areas. This is because of the absence or complete inundation of the vegetation. The lighter blue areas are partially inundated vegetation that causes a diffuse reflection in the image due to the rough scattering effect.

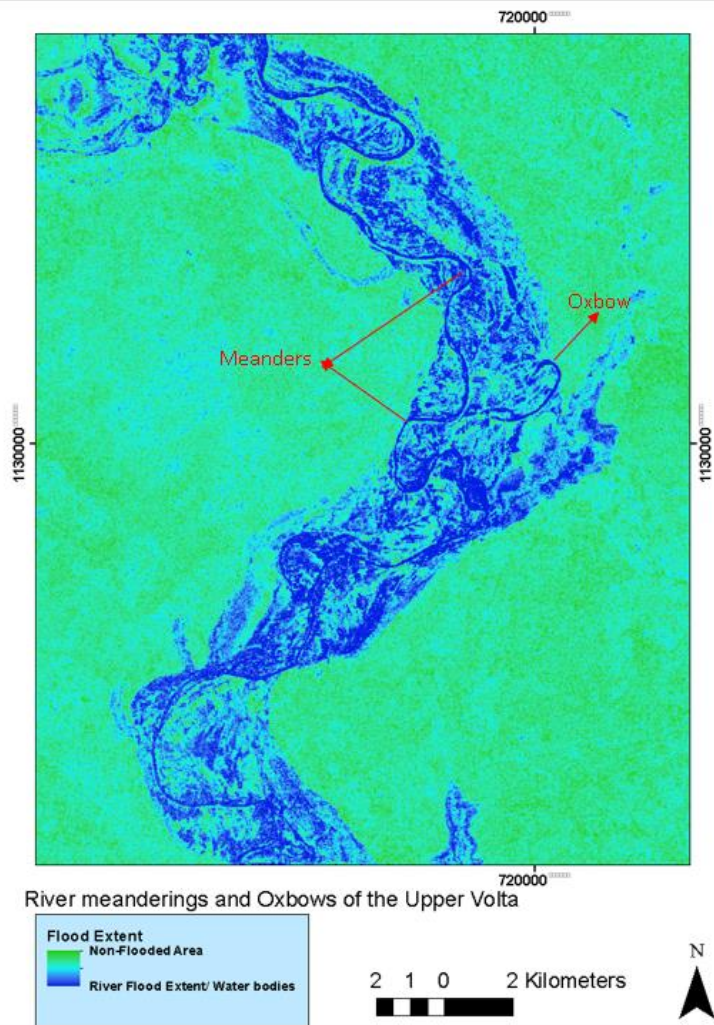


Figure 5.7a: A cross-section of Sentinel-1 radar image showing the meanderings, oxbows, and “dry regions” within the river flood extents in the upper volta. Deep blue areas have high water levels compared to the lighter blue areas

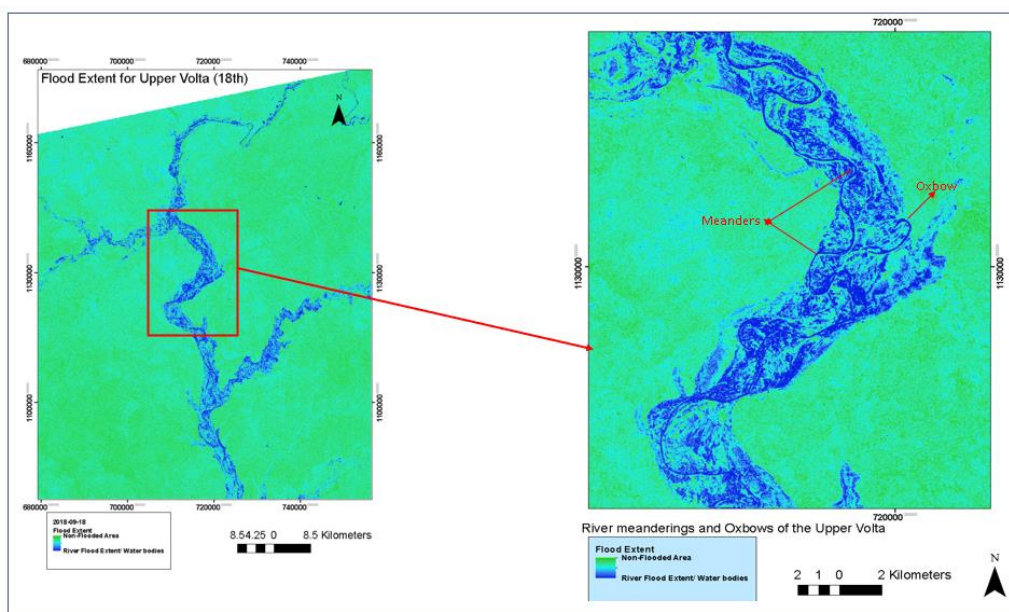


Figure 5.7b: Location of the highlighted area

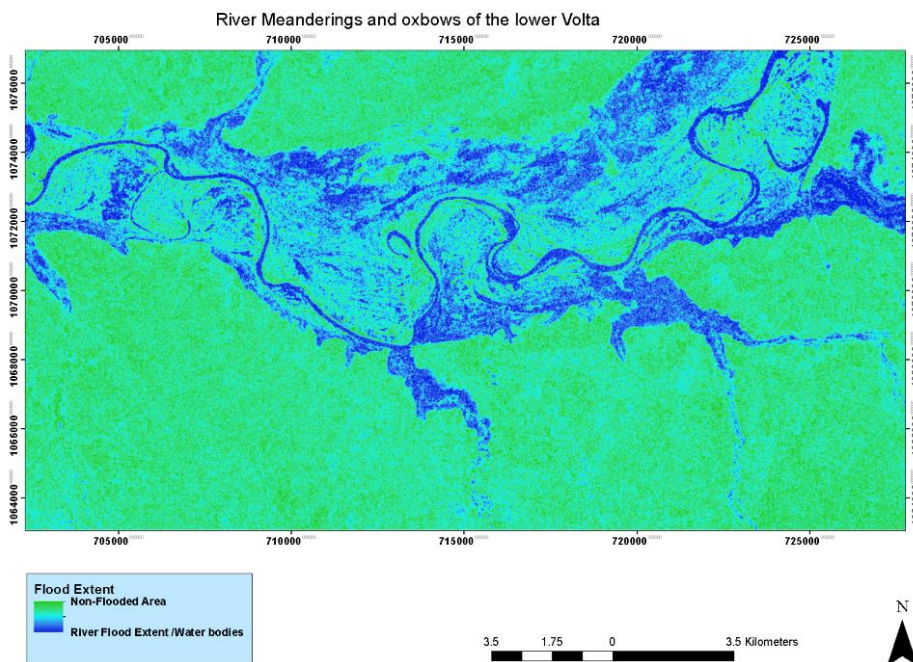


Figure 5.8a: A cross-section of Sentinel-1 radar image showing the meanderings, oxbows and “dry regions” within the river flood extents in the Lower Volta. The point at which the tributaries joins the river can be seen to be more flooded(deep blue) compared to the less blue areas (diffuse reflection). 12/09/2018

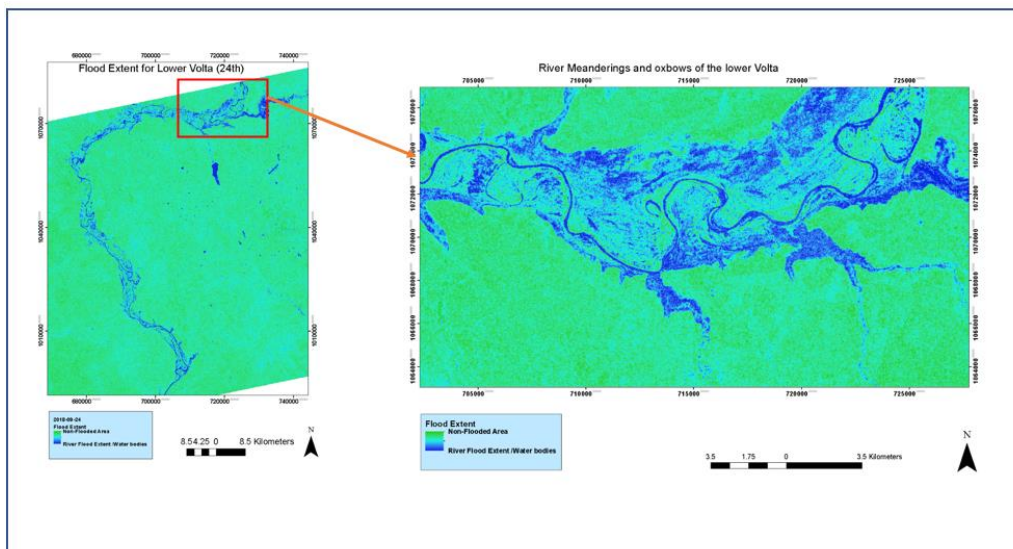


Figure 5.8b: Location of the highlighted area for the lower Volta showing meanderings

Despite the high spatial resolution of the radar images, it's challenging to distinguish land cover features (roads, buildings, forest vegetation, and water bodies) in the image as they appear similar when reflected. In the absence of additional ground data or optical data, it can be difficult to visually identify and distinguish ground features within the extracted flood extents. Optical remote sensing data acquired around the same time as that of the radar images during the flood period can be very beneficial in masking out land cover features from radar images. In this study, Sentinel-2 optical NDVI image detailing the characteristics of the river and inundated vegetated and field areas, as shown in Figure 5.9, was used to mask out the land-cover features within the flood extent. It shows

the meanders, oxbow, and curvatures within the river floodplains and the fields. It also outlines the grass fields, crop fields, and bare lands. The cyan to yellow areas are partially inundated fields and bare areas within the flooded area, while the reddish areas are vegetation. The blue areas are clear water that has either fully submerged the vegetation or without vegetation. Using both extracted flood extent from SAR and optical Sentinel-2 images were very beneficial in delineating and identifying inundated land-cover features within the flood extents. The NDVI image in figure 5.9 was used in the supervised classification to determine bare crop and grass fields.

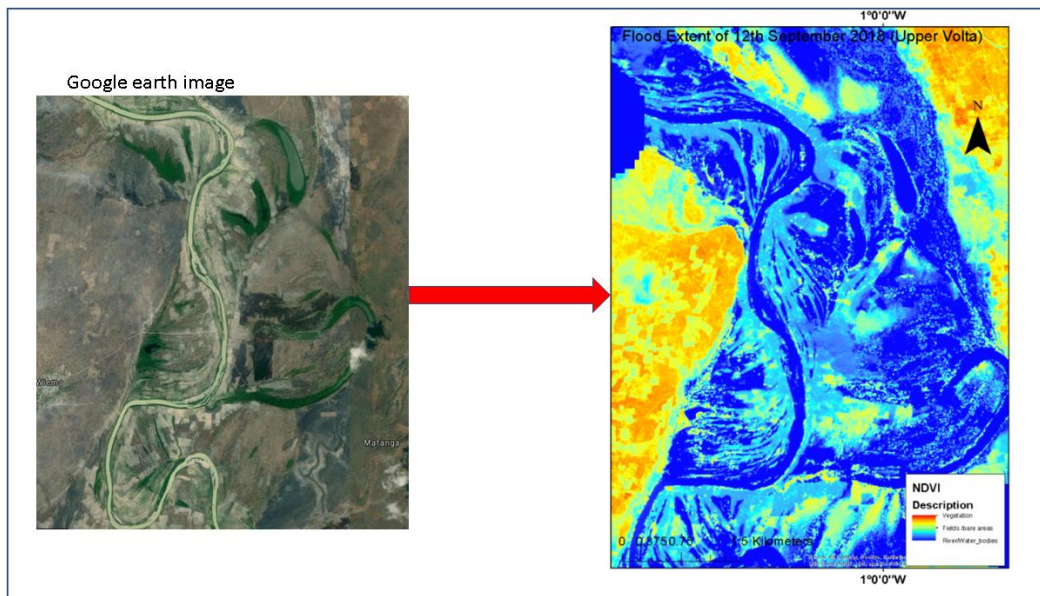


Figure 5.9: Sentinel-2 image (right) showing inundated and partially inundated land covers within the flood extents the image on the left is a google earth image showing the highlighted cross section of the Upper Volta (12th September)

Figure 5.10 shows a false colour composite showing vegetation in red; green areas are floodwaters, and white is cloud cover in the image. The clouds in the images during flood periods also influenced the decision to use Radar instead of optical images for monitoring flood in this study.

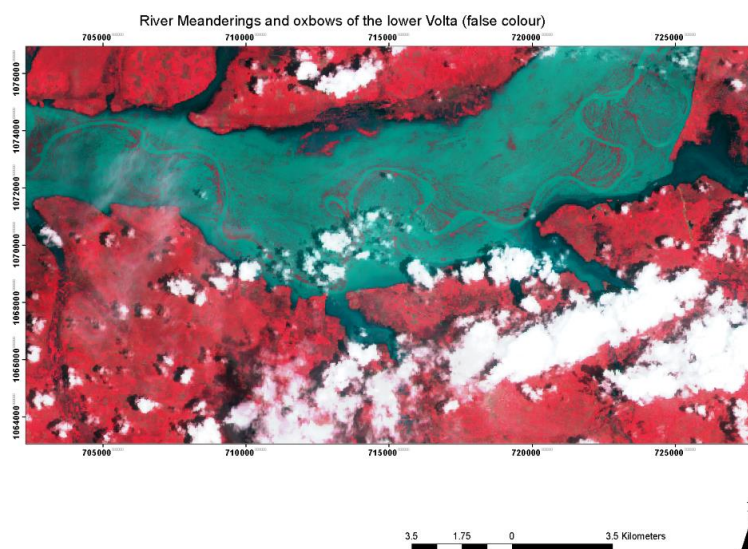


Figure 5.10: False colour composite of the flood extent showing vegetation (red) on the levees and point bars sticking out of the water (green) and clouds (white)

5.2 Sentinel-2 Processing

Geometrically and radiometrically corrected cloud-free images of sentinel-2 downloaded from Global Land Cover Facility (<https://glovis.usgs.gov/>) were used in a Supervised classification to classify the image into four land use classes, namely water, grassland, crop fields, and bare land areas. The classification technique employed in this case was the maximum likelihood algorithm in ERDAS software. According to Dewan & Yamaguchi, (2009) and Jia et al., (2019), the maximum likelihood classifier is great and beneficial for land-use land cover classification into distinct classes. Bands 8 (842nm,10m), band 4(665nm,10m), and band 3(560nm,10m) of Sentinel-2 optical images in a composite band were used in the classification to produce the desired land use and land cover classes. The selected band combination is the infrared colour range and can distinguish between healthy and unhealthy vegetation through the use of chlorophyll reflection. This would help in distinguishing between crop and vegetation fields in the field. The classification process is outlined in figure 5.14. The flooded areas, as observed from the Radar image, differed for both the upper and lower Volta for the three dates. The overall accuracy of the classification was about 70%. The land use map (figure 5.11) was overlaid with the flood extents to determine the elements at risk, and crop fields were identified as the elements at risk in this study. The other land cover classes were not considered as vulnerable as far as flood risk is concerned. The total inundated areas varied according to the flood extents for the different dates observed; the extent also differed for the upper and lower Volta. The total inundated area and cropped areas in hectares for the upper and lower Volta are shown in tables 5.2 and 5.3, respectively. The tables also show the difference in inundated areas for the three dates. Figures 5.12 and 5.13 show the inundated land use classes, and the area covered for each date of the flood for the upper and lower Volta, respectively.

From the tables (5.2 and 5.3) and figures (5.12 and 5.13), for some dates, the upper and the lower regions experience different extents and levels of flooding. This is because the water in the river channel travels from the north (upper elevation) down to the south with lower elevations coupled with varying rainfalls and water from connecting tributaries. The travel time for the water from upper to lower Volta takes about seven to eight days (HKV consultants 2012). For instance, both upper and lower Volta show large extents of flood on the 12th and receding floods on the 18th. On the 24th there was an increase in flood extent for the lower Volta (+4254ha) and a reduction in flood extents for the upper region (-1531 ha). There is also a relationship between the increasing and decreasing of cropped area in the upper and lower Volta due to flood extents.

The area also has many tributaries that contribute volumes of water into the white Volta river, especially the lower Volta has many tributaries with shorter arriving time compared to the upper with fewer tributaries and longer arriving time of seven to eight days.

The recorded difference in inundated areas gives a sense of the duration of the flood. There was a wide and sharp decline in the inundated area for the upper region in the first week, but it slowed down between the second and third weeks. This can be attributed to the fact that the water was close to the bank of the river at this point, which already contained high volumes of water, hence the slow movement of the water. Meanwhile, this flow resulted in an increase downstream, which continued to increase in the subsequent weeks. The build-up of the water contributed to the second increase in the flood extents for the lower Volta on the 24th. The increasing and decreasing relationship between the land cover classes due to flood extents can be observed in the graphs (Figures 5.12 and 5.13). The total inundated land-use area for the three observed dates are listed in tables 5.2 and 5.3.

Land Use / Land Cover Classification for Lower and Upper Volta

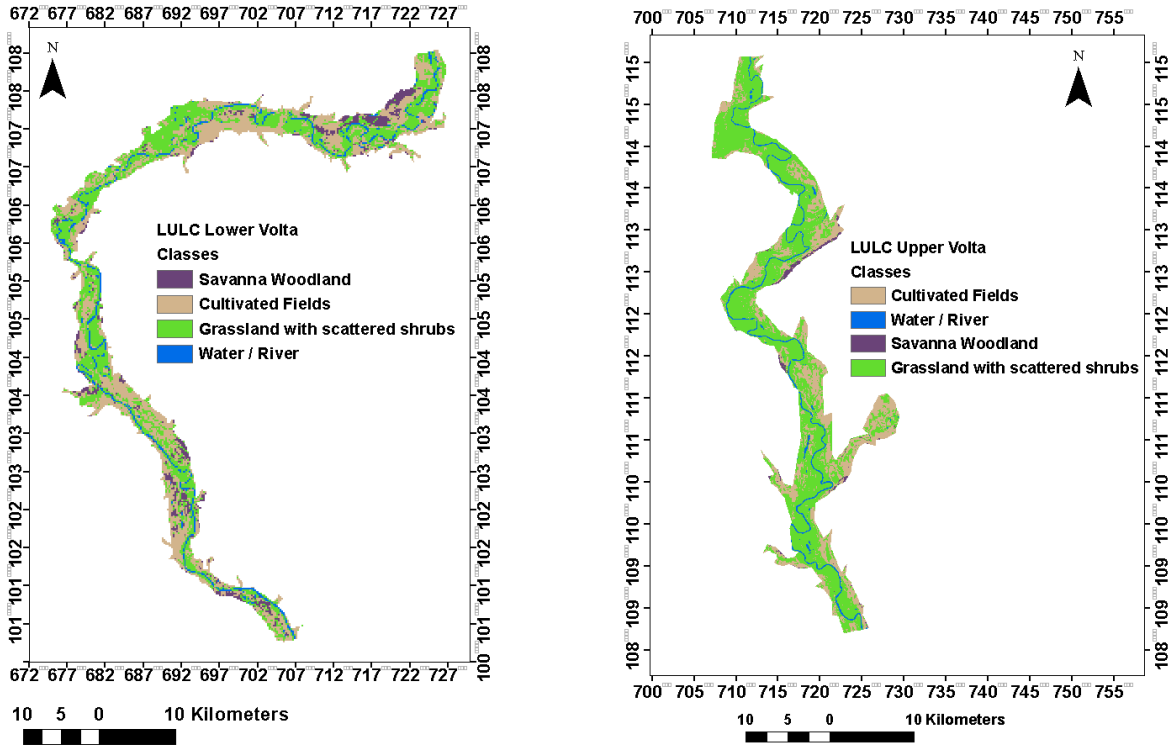


Figure 5.11: Supervised Land use /Land cover classification for the lower and upper Volta. Sentinel-2 classified image was clipped to the extracted flood extents from Sentinel-1

Table 5.2: Total inundated land use and cropped area for the Upper Volta

Date	Inundated area (ha)	Crop area affected (ha)	The difference in the inundated cropped area
12 th September	34017	9536	-
18 th September	26215	5050	4486.00
24 th September	20709	3519	1531

Table 5.3: Total inundated land use and cropped area for the Lower Volta

Date	Inundated area (ha)	Crop area affected (ha)	The difference in the cropped area
12 th September	11075	4644	-
18 th September	8570	14800	10156
24 th September	10738	19054	4254

The graphs below show the area of all inundated land-use types within the flood extents.

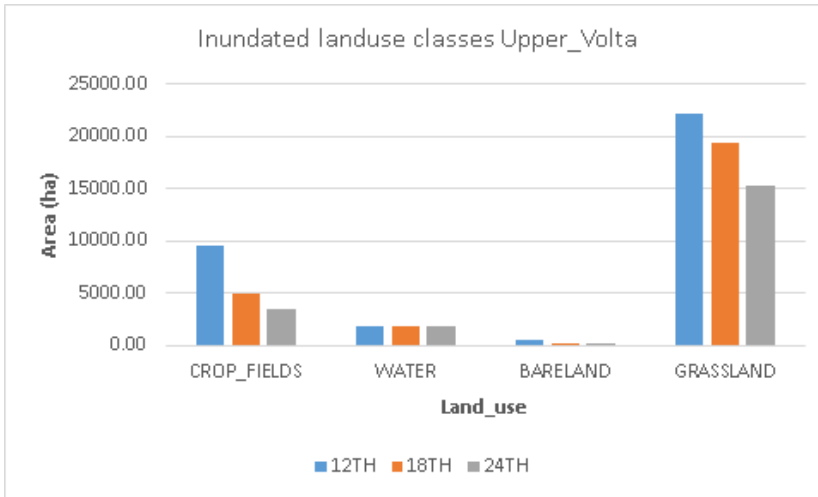


Figure 5.12: Inundated Land use classes and the area (hectare) covered by each class for the three dates (12th, 18th, 24th) of the upper Volta.

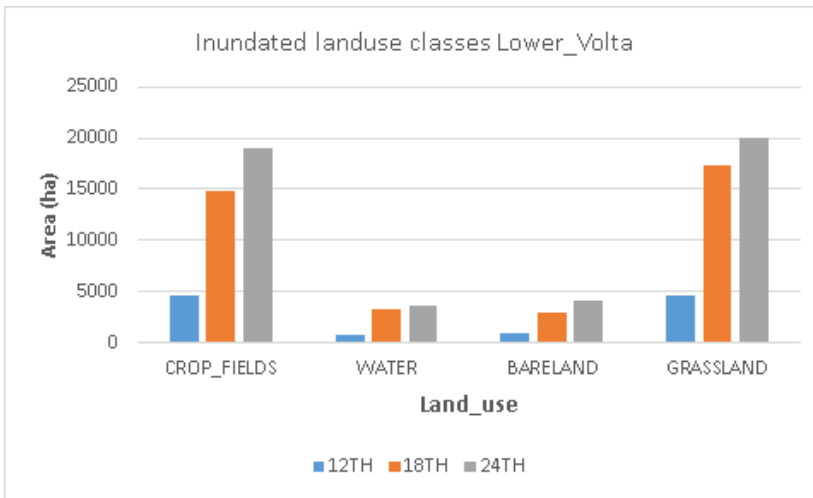


Figure 5.13: Inundated Land use classes and the area (hectare) covered by each class for the three dates (12th, 18th, 24th) of the lower Volta.

Workflow for land use classification is shown below;

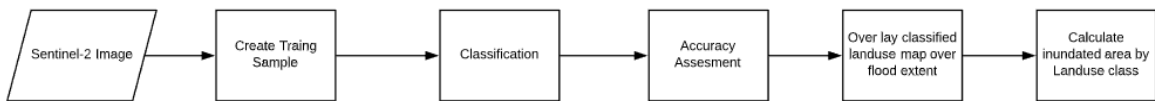


Figure 5.14: Sentinel-2 Land use classification workflow

6.0 Accuracy Assessment of DEMs

To assess the accuracy of the three DEMs, extracted DEM values from the individual DEMs (SPOT, ALOS, SRTM) were compared to the GCP values (Gesch et al., 2012). The spatial analyst tool of ArcGIS desktop software 10.8.0 was used to extract the elevation point values from the DEMs based on the position of the GCPs. The measured errors for each DEM were calculated by finding the difference between the GCP and its correlated DEM value. The results from this computation merely show the places at which the DEM points overestimated or underestimated the elevation when compared to the GCP elevation points. Thus, DEM points above the GCP are the positive errors, and point values below the GCP are negative errors. Using the DEM error values computed from the previous steps, the mean errors, Standard deviations, and Root Mean Square Error (RMSE) were calculated for each DEM. The mean error is a measure of the vertical offset of the DEM from the actual ground level. The offset can be negative or positive (Gesch et al., 2012). An accuracy assessment was carried out to test for variations in DEM values between the different land cover classes where the GCP were measured.

6.1 Results and Discussion of DEM Accuracy Assessment

As observed in the error plotting in figures 6.1 - 6.3 for all the three DEMs, a direct relationship of increasing or decreasing errors in relation to the DEM elevations cannot be established. In the meantime, For the SPOT (figure 6.1) and SRTM (figure 6.2) DEMs, the computed errors are unevenly dispersed on the two sides (positive and negative) of the error axis. While the ALOS DEM (figure 6.3) error points are dispersed only in the positive quadrant of the graph. It can be inferred from the plottings that all three DEMs overestimated the actual ground elevation as most of the mean errors are positive values with a few negative values in the case of SPOT and SRTM and none for PALSAR DEM. The closer the value is to zero, the higher the accuracy and vice versa.

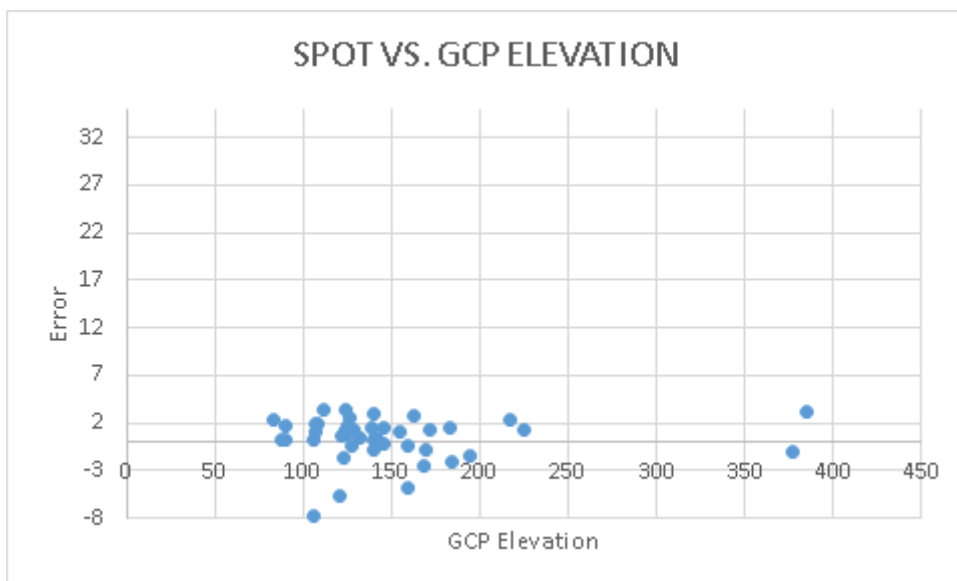


Figure 6.1: Difference between the SPOT DEM values against GCP.

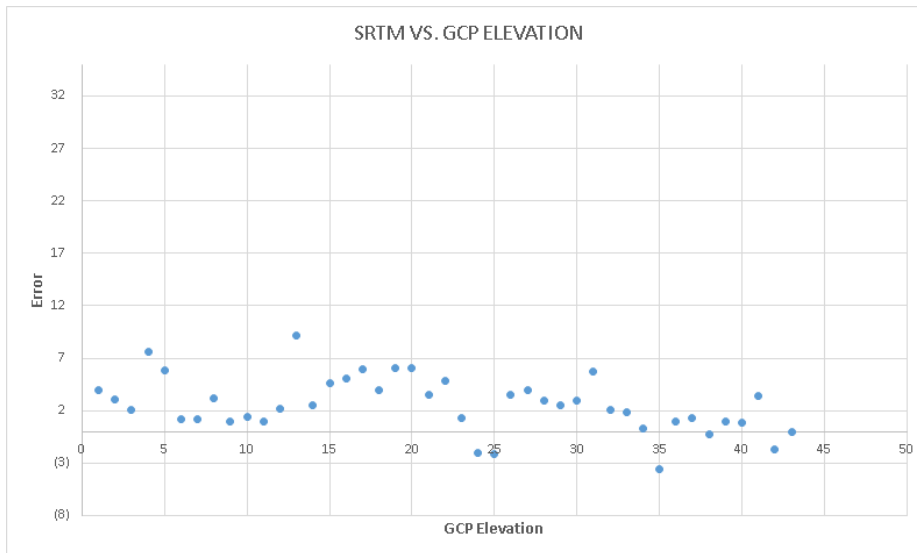


Figure 6.2: Difference between the SRTM DEM values against GCP

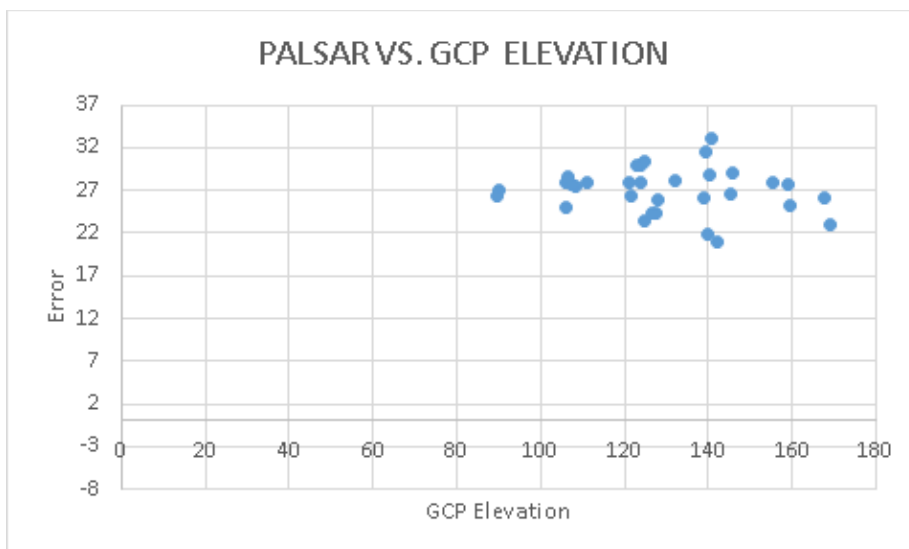


Figure 6.3: Difference between the PALSAR DEM values against GCP

In table 6.1 is the summary of error statistics computed from the vertical accuracy assessment of all three DEMs using the 43 GCP values. The SPOT DEM recorded the lowest mean error of 0.39m, the lowest RMSE of 2.32m, and a standard deviation of 2.32m with error values between -7.70 - 3.38m.

SRTM DEM followed closely with a mean error of 2.62m, RMSE of 3.67, and a standard deviation of 2.60m, making it the next accurate DEM to the SPOT DEM. The error values range from a minimum of -3.56m to a maximum of 9.13m.

ALOS PALSAR DEM was the worst of the three DEMs as it overestimated all the elevation points with a mean error of 27.17m, RMSE of 27.28m, and a standard deviation of 2.38m. A range of minimum and maximum values between 20.87 and 33.13m, respectively.

SRTM and SPOT DEM have a near similar distribution of errors, except for the wide range distribution of positive error values of the SRTM DEM between 0 – 10m compared to the 0 -4m range of SPOT DEM. Similarly, SPOT DEM has a wide range of negative values from 0 to -8m compared to SRTM with fewer negative error values from 0 to -3.56m.

Table 6.1: Error statistics (in meters) generated from the vertical accuracy assessment of the three DEMs using 43 ground control points.

DEM	Minimum	Maximum	Mean	Standard Deviation	RMSE
SPOT	-7.70	3.38	0.39	2.32	2.32
SRTM	-3.56	9.13	2.62	2.60	3.67
ALOS PALSAR	20.87	33.13	27.17	2.38	27.28

6.2 Landcover Accuracy assessment of DEMs.

After the General assessment of the DEMs, there was the need to assess the errors according to Land cover classes. This was carried out to determine any variation within the Land cover classes and the accuracy of the DEMs in different Land cover classes. The GCP points were collected within different land cover classes. The GCP points were overlaid on the Three DEMs to determine the elevation, mean error, and RMSE errors of the points at those Land-cover locations of the DEMs. Below are the plottings of the mean error and RMSE according to Land cover classes for the three DEMs. Comparing the results of the DEMs, there are obviously variations within the Land cover classes of each DEM, and the class error values also vary for the different DEMs. For the SPOT DEM, except for the cultivated areas that recorded a high mean error, the mean errors for the other classes were below 1m. Meadows, football grounds, and Open land had very low mean error values (-0.52, 0.09 and 0.11), respectively. It, however, recorded very high RMSE values for all the Land cover classes, as observed in figure 6.4.

SRTM, on the other hand, recorded very high mean errors and RMSE error values for all classes (figure 6.5). The root mean errors and RMSE values were closely Matched with a difference of about 2m between the values as compared to the SPOT DEM that had wide margins between the mean errors and RMSE. PALSAR clearly overestimated all the elevation in all the classes with almost equal extreme values for both RMSE and mean error (just a appoint or less difference) in all land cover classes (figure 6.6). Figure 6.7 and 6.8 compares the mean error and RMSE plottings respectively, for all three DEMs.

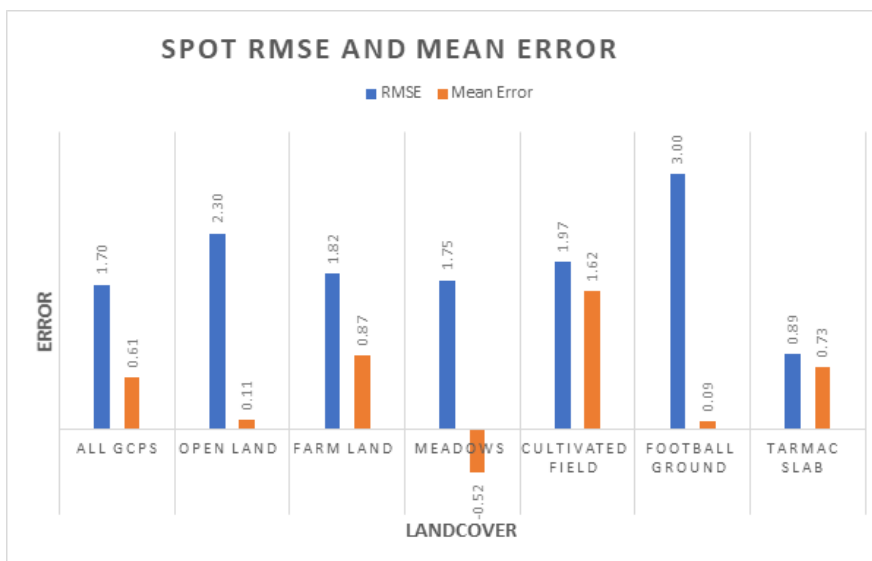


Figure 6.4: SPOT RMSE and mean error for different land cover classes

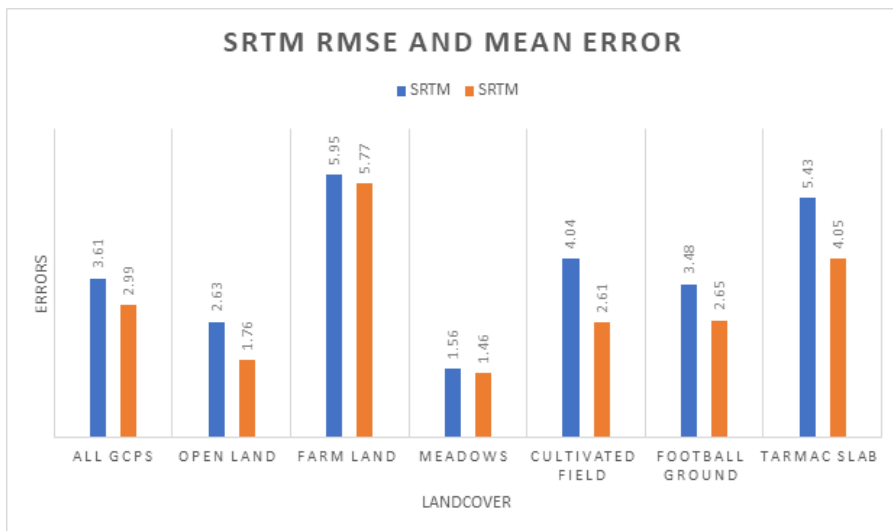


Figure 6.5: SRTM RMSE and mean error for different land cover classes

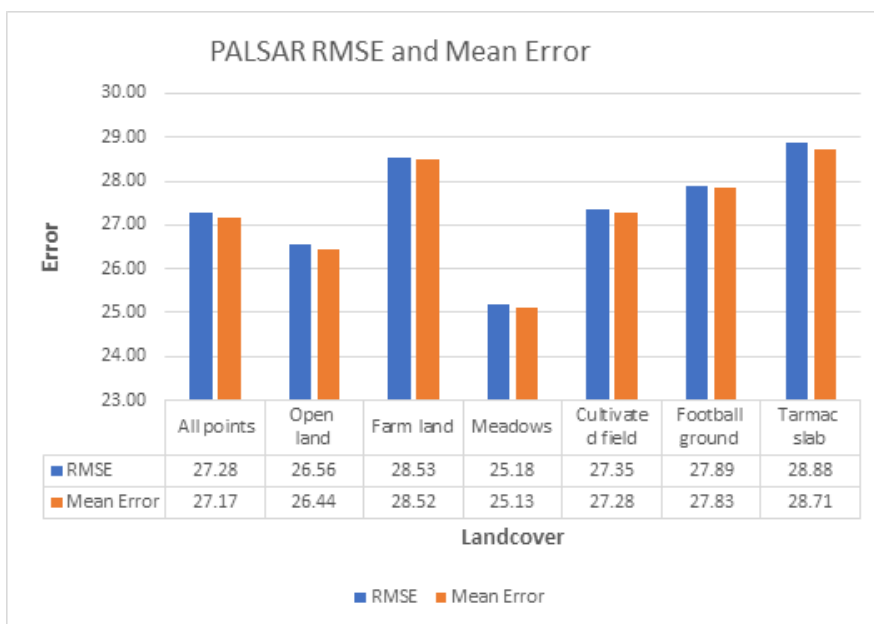


Figure 6.6: PALSAR RMSE and mean error for different land cover classes

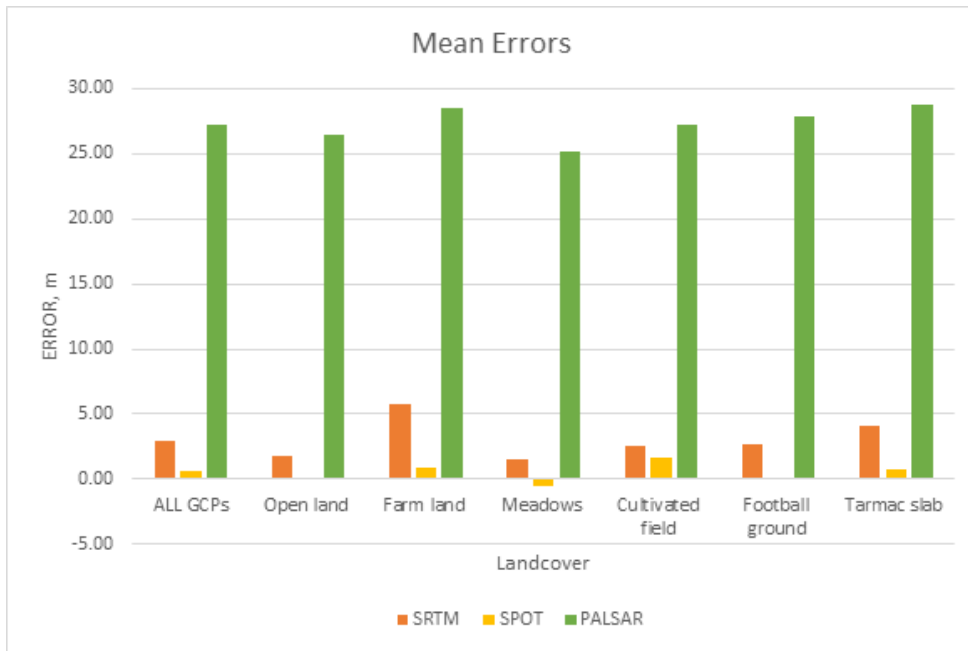


Figure 6.7: Mean errors of all three DEMs compared

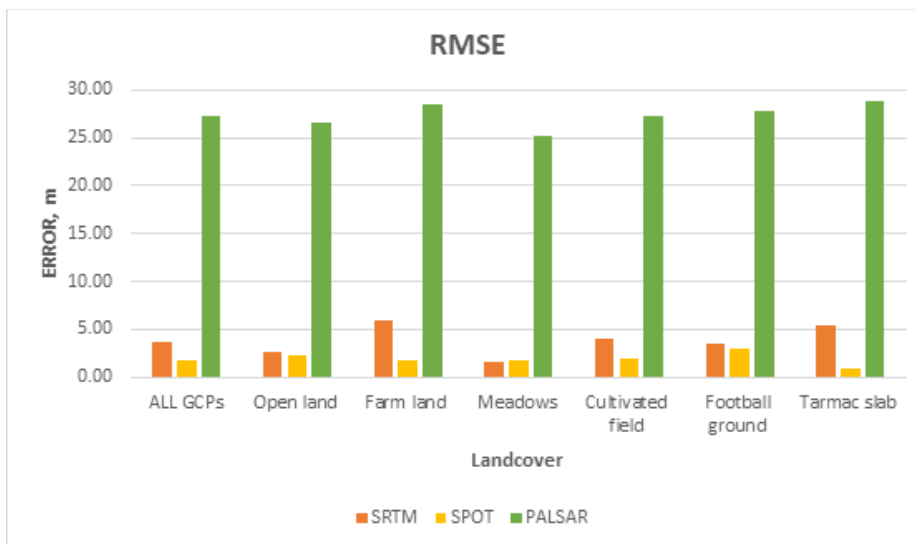


Figure 6.8: comparing root RMSE of all three DEMs

Generally, all the DEMs mostly overestimated the elevations. Based on the RMSE and mean error values of the three DEMs, it is clear that the SPOT DEM has the lowest values of 2.32m and 0.39m, respectively, and therefore can be considered as the most accurate DEM amongst the three. The SRTM also outperformed the PALSAR DEM with RMSE and mean error values of 3.67m and 2.62m, respectively, while PALSAR performed very poorly.

7.0 Flood Depth Analysis and Digital Elevation Model (DEM) Interpolation Processing

7.1 Flood Depth Analysis

To calculate for the flood depths in the study area, a method was adopted that involved the use of interpolation methods. Elevation values extracted from the flood extent were used to form a trend surface through a third-order trend interpolation method to form an elevation surface that represented the surface of the river at this point. The interpolated surface was then subtracted from the various DEMs to determine the flood depths within the flood extents of the river. Brief definitions and descriptions of the methodologies are discussed below.

7.2 DEM Interpolation

A DEM can be formed through the interpolation method by using sampled elevation data points. Interpolation is a method that uses a few sampled data points to predict raster cell values. Unknown elevation and rainfall values, among others, can be predicted using the interpolation method. A disadvantage of this method is that the raster cell values produced are degraded to some extent and are likely not to be the same value as the sampled point. Interpolation assumes that there is a spatial correlation between distributed objects within a spatial domain. That is to say, the closer the objects are to each other, the greater the chance of these objects sharing the same characteristics. Jin Li & Heap, (2008) identified three groups of spatial interpolation methods, namely; Geostatistical methods, non-Geo statistical methods, and the combined statistical methods. The grouping was based on the level of statistical computation involved with each method listed above. This study would be focused on the use of the Geostatistical interpolation method, namely Trend surface interpolation. The surface of the study area has gradual trends, which are better represented by using trend interpolation. There are several statistical methods such as Kriging, Nearest neighbourhood, Regression models, Natural neighbours, Fourier series, etc. which are not considered in this study.

7.3 Trend surface Interpolation

The trend surface uses sampled inputs points through a mathematical polynomial interpolation function to form a smooth surface. The formed trend surface varies moderately across while attempting to encapsulate the coarse-scale samples in the data. The trend surface polynomial has twelve orders that can be explored in the ArcGIS Spatial Analyst tool. The first-order polynomial is linear and results in a tilted looking flat plane. The second-order is a quadratic polynomial and results in a parabolic surface. The third-order is cubic in nature. The higher the order, the lower the Root Mean Square (RMS) errors, and the higher the accuracy. Interpolated surfaces with lower RMS errors represent the input points correctly as much as possible. Orders one through to three are the most commonly used. In principle, the main concept of trend surface concerns fitting a surface (mostly flat or U-shaped) between two elevated points. The bending surface should as much as possible fit the surface or space between the elevated points. Depending on the surface, whether a flat surface or a depression, a mathematical formula can generate an interpolated surface that fits the intended surface as best as possible. The interpolated surface hardly captures all the intended points used for creating the surface, therefore, making the trend method an inexact estimator.

In this study, to determine the flood depths, the extracted flood extents from Sentinel-1 were overlaid with the three DEMs to mask out the DEM according to the flood extents. Points were digitized along the edges of the flood extents at a 10m interval using the create points tool in ArcMap toolbox. Based on the generated points, the elevation values at the edge of the masked DEMs were extracted. The extracted elevation points values were then used in a Trend

interpolation to form a trend surface. The spatial analyst trend surface tool was used to create the trend surface. The third-order linear interpolation was used since it recorded the least RMS error compared to orders one and two, and also showed a better representation of the surface when compared to the DEMs. The interpolated trend surface was then subtracted from DEMs to determine the flood depths within the flood extents. Figures 2.0 – 4.0 in appendix C shows the results from the first, second and third trend interpolation analysis, while figures 5.0 to 9.0 also in appendix C shows the results of the trend surface analysis for the upper and lower Volta clipped to the extracted flood extents, respectively.

7.4 Flood depth analysis

Flood damages to agricultural fields in this study encapsulate the function of the depth of the flood, the extents, span of the flood, and the development stage of the crops. Flood damages here refer to the flooding and destruction of crops. This research seeks to assess the effects of the flood on the crops in the fields along the white Volta to determine to what extent floods affect the crops in terms of the flood extent, depth and duration. Crops considered in the area are maize, millet, sorghum, and rice (mostly lowland). The flood depths were computed by subtracting the interpolated surfaces from the DEMs, thus (Trend surface – DEM) as described above. All three DEMs were resampled through the nearest neighbour technique to a 30m resolution cell sizes for fair and accurate comparison of results. Figures 7.1 and 7.2 shows excerpts of the flood depth in details for the upper and lower Volta, respectively. Also observed in figures 10 – 12 (upper Volta), and figures 13 – 15 (lower Volta) in appendix C; the largest flood occurred on 12th September (upper and Lower Volta) and also on the 24th (only lower). From the Legend, high flood depths can be observed on these dates for both the upper and lower Volta. The flood receded a bit on the 18th. This resulted in a reduction in flood extent and depth, as seen in the images and the legend for both the upper and lower Volta. The reduction was, however, more evident in the upper as compared to the lower Volta due to receding waters travelling down to the Lower Volta. For the 24th, there was a bit of disparity between the upper and lower Volta. The flood continued to recede in the upper Volta but rather increased in the lower. The increase resulted in higher flood depths and extent for the lower Volta. The increase can be attributed to the many tributaries of the lower Volta arriving later to increase the volume. Flood depths ranging between 0 and 4+ meters were considered for this study since crops are the objects of interest in this case, and flood and higher flood heights are irrelevant. Flood depths farthest away from the river channel were much shallower compared to those closest to the river.

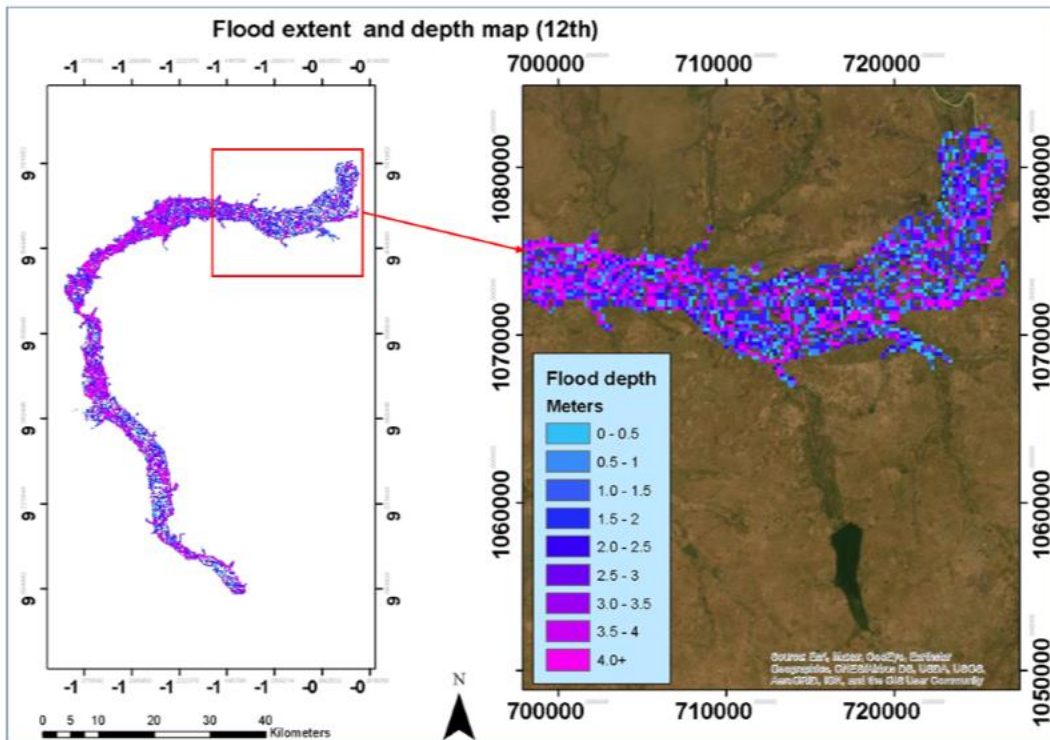


Figure 7.2a: Flood depth and extent map for Lower Volta highlighting a detailed portion of the full extent (12th)

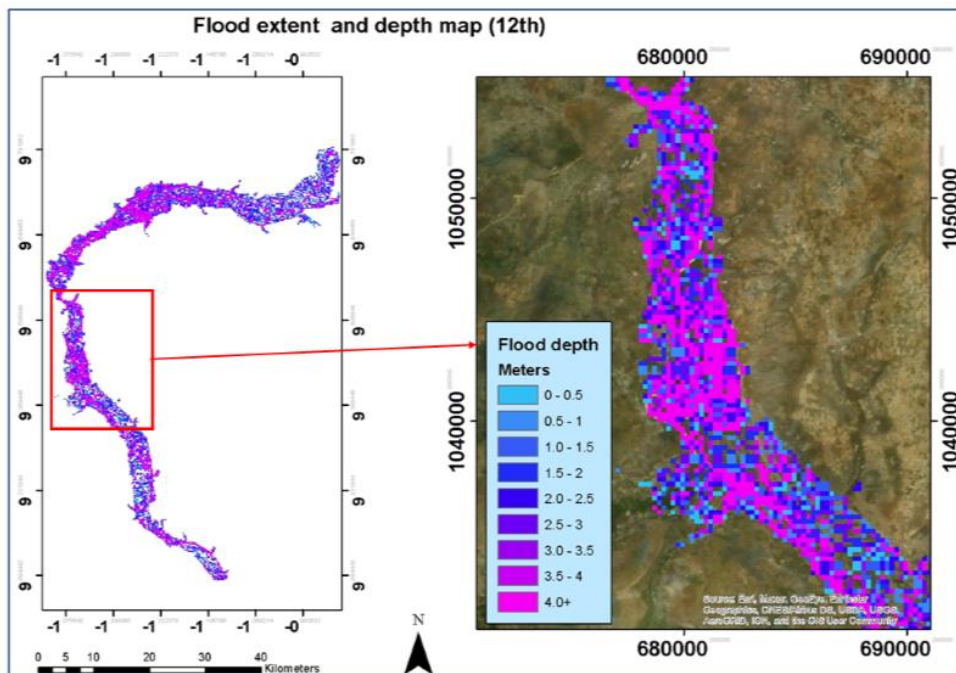


Figure 7.2b: Flood depth and extent map for Upper Volta highlighting a detailed portion of the full extent (12th)

Deeper flood depths are more pronounced in periods of high floods and scattered across the flood extents. This is because of the complex natural dynamic meandering and braided pattern of the river channels, sand point bars caused by the deposition and erosion of sand and the presence of vegetation (shrubs) growing in the middle and close to the edges of the river banks. There are some old river branches that still hold and transfer water to the main channel. The river is also

characterized by natural levees and back swamps. The meandering effect also caused the creation of naturally occurring oxbows in river plains. At the lower Volta, the meanderings are intensive with very wide flood plains. Below is an image (figure 7.3) depicting meanders in the Lower Volta. It also shows the distances between the meanders and the wide flood plains. Figure 7.4 is a classified image of the land-use/land cover of the area. Shrubs and grasses can be seen sticking out on the surface of the river.

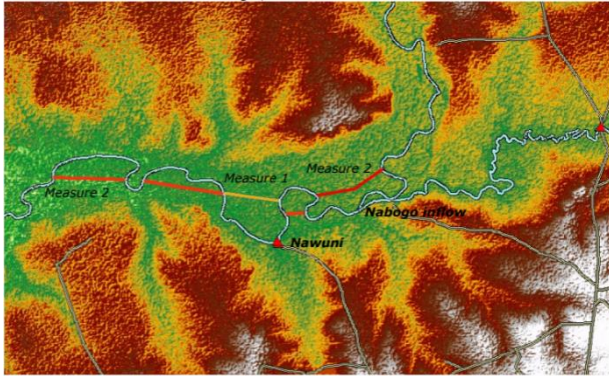


Figure 7.3: meanders in the white Volta river. Adopted from HKV (2012)

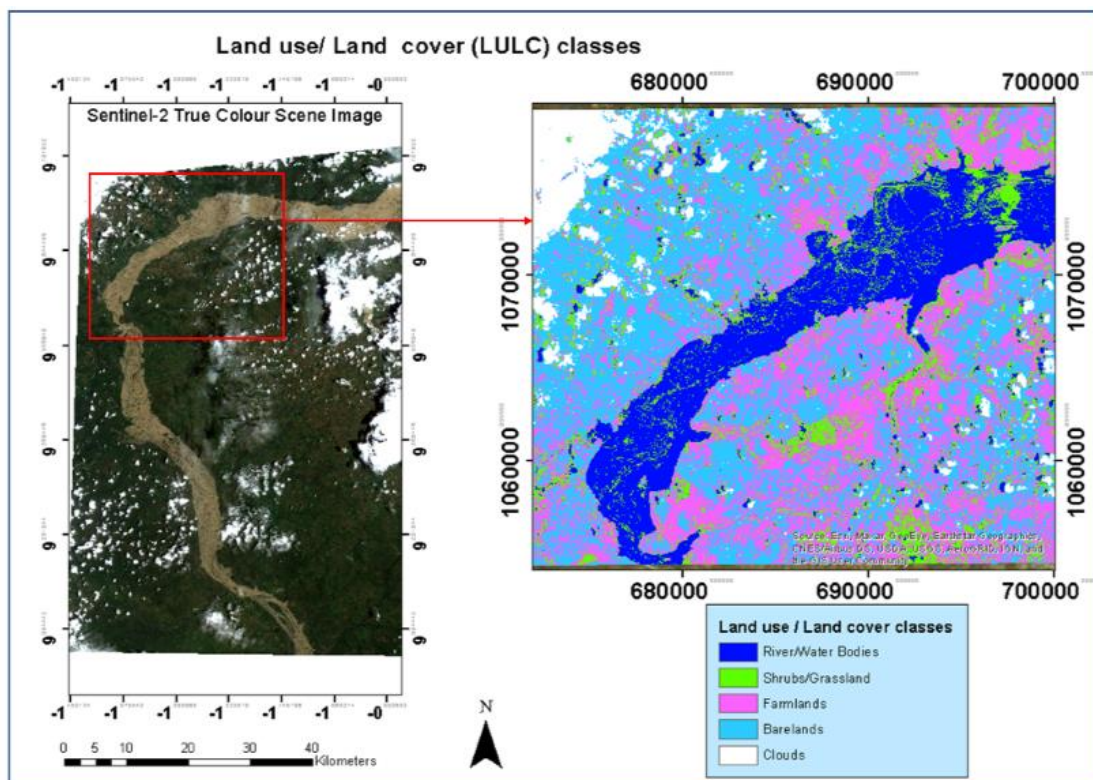


Figure 7.4: Classified Sentinel-2 image showing vegetation in the river and cloud coverage

The shrubs, vegetation, sandbars, and meanderings affected the results of the flood depths. Areas or cells where these above-mentioned were located resulted in negative values since their elevations were above the surface or level of the river. The interpolated surface could not represent the surface as uniformly as possible due to the uneven nature of the surface. The negative values were therefore treated as anomalies and omitted from the results of the calculations, hence the empty spaces and scattered nature of the pixels as observed in figures 7.1 and 7.2.

7.5 Flood Depths of Inundated Area

To quantify the area covered by the flood depths, the area of each cell was converted to a hectare. The area covered by the flood depths in hectares was calculated using the formula below: **Cell count within each flood depth * Area of cell size / (10,000)**. The formula was adopted and modified from (Masood & Takeuchi, 2012a)

The formula basically counts the cells within a depth value, multiplies it by the area of the cell in meters square (m^2) and then divides the result by 10000 hectors to convert the area to hectors instead of meters square. This was necessary since the focus was agricultural land and hectors seem more appropriate for easy comprehension. Comparing the three DEMs in terms of the covered area, the SPOT (HKV) DEM, in most cases, recorded higher values when compared to the PALSAR and SRTM. PALSAR, in most cases, was also slightly above the SRTM in terms of the estimated inundated areas. The SPOT DEM, however, recorded lower area coverage at higher flood depths of 5m to 6m compared to the other two DEMs in all cases. As observed from the radar Sentinel-1 images, the flood receded over the weeks for the upper region and fluctuated in the lower region. This trend is clear in the graphs figures 7.20 – 7.25, as there is a general decrease in inundated areas for the upper; thus, a shift from, especially in the shallow region towards the deeper areas. This trend is most evident in the PALSAR and SRTM. The SPOT (HKV) DEM sometimes deviates from this trend and suggest higher values for some areas where lower values are expected according to the receding trend.

This study would mostly focus on flood depths between 0m to 2m since depths above this range suggest total and permanent inundation and are not relevant for the study of the crops in this area. Also, the heights of the crops throughout their growth stages are between 0 and 2m. From the graphs in figures 7.20 – 7.25, it is evident that a greater portion of the flooded area was mostly within the regions with lower flood depths between zero to about three meters depths. The largest flood occurred on 12th September, and all three DEMs show that flood depths between 0 and 1 meter covered about eight thousand (8000) hectares of land for the upper Volta region and close to nine thousand (9000) hectares for the Lower Volta representing about 29% and 30% of the inundated area, respectively. About five thousand hectares (18%) of land were under flood depths between one and two meters for the upper Volta and about seven thousand hectares (18%) for the Lower Volta. About five thousand and six thousand hectares of land were flooded at depths between 2m to 3m for the upper and lower Volta, respectively. Flood depths between 3m to 6m are either very close to the bank or are depths within the river itself. The total inundated area of the upper Volta and lower Volta was 26642 and 36746 hectares, respectively. The lower Volta has wider flood plains compared to the upper, hence the larger areas in the lower portion. Elevation wise too the upper Volta has higher elevations compared to the lower Volta regions. Inundated areas within the flood depths for all three DEMs are compared in the following graphs (figures 7.20 – 7.25).

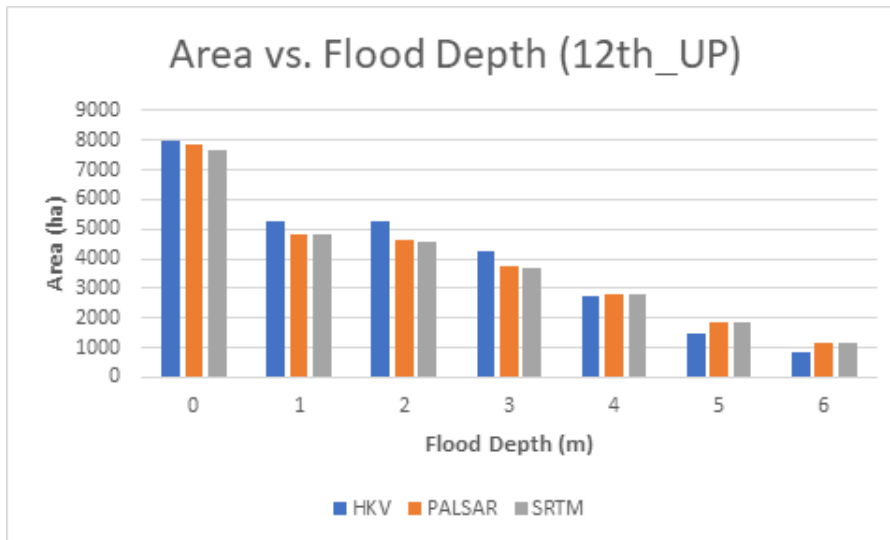


Figure 7.20: : Comparing Flooded area (hectares) and depths (meters) for all three DEMs (12th upper Volta). Blue colour (HKV or SPOT DEM), orange colour is (PALSAR) and grey colour (SRTM)

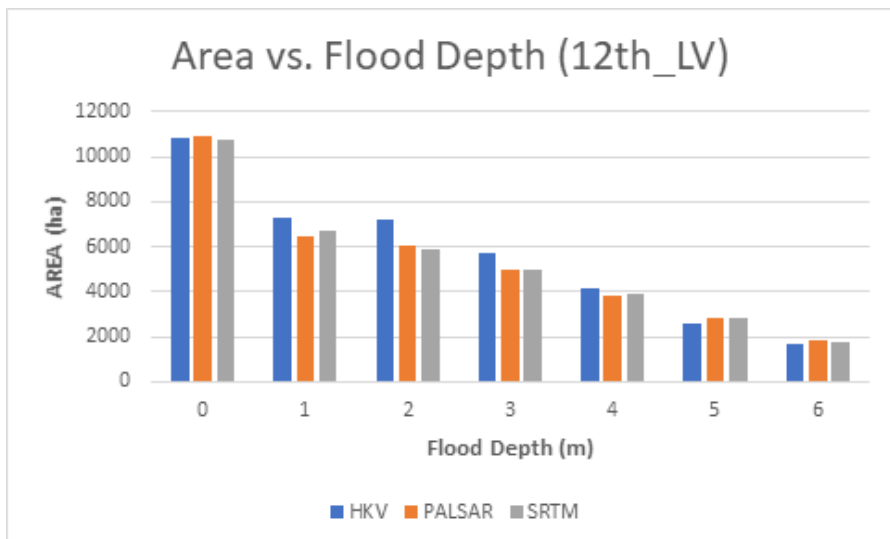


Figure 7.21: Comparing Flooded area (hectares) and depths (meters) for all three DEMs (12th Lower Volta). Blue colour (HKV or SPOT DEM), orange colour is (PALSAR) and grey colour (SRTM)

On the 18th, the floods were observed to have receded within the inundated area. The flood had receded a bit, as observed from the graph (figure 7.22) and the sentinel-1 images showing the flood extents. The receding floods lead to a decrease in the pixels or area with higher flood depths and an increase in the areas with lower flood depths. This is as a result of the reduction in the volumes of water and also because of the fewer higher depth pixels included in the depth range of 0 to 6m. The SPOT DEM showed an increase in the area of flood depths between 0m and 1m. On the 12th, about 8000 hectares were flooded, but on the 18th, the area increased to about 8664 hectares while SRTM and PALSAR suggest a slight decrease in the area within this depth from 7843 on the 12th to 7702 hectares on the 18th. There was, however, an apparent reduction in areas with flood depths between 1m to 2m. The coverage reduced from around 5000 to about 3000 hectares of land. There was also a general reduction in flood depth areas between 2 to 6m. The situation was different for the lower Volta as the flood depths between 0 to 1m increased in the area for all three DEMs but showed the same receding trend as the upper Volta for the other depth ranges. This, again, can be attributed to the water from the upper region travelling downstream. The area with flood depths between 0 and 1m increased from about 10000 hectares to 12133(SPOT) and about 11000 (SRTM

and PALSAR) hectares. Flood depths between 1 and 2m also decreased accordingly from around 7000 to about 4500 hectares. The flooded areas between 2m to 6m decreased accordingly as observed in the figures 7.22 and 7.23

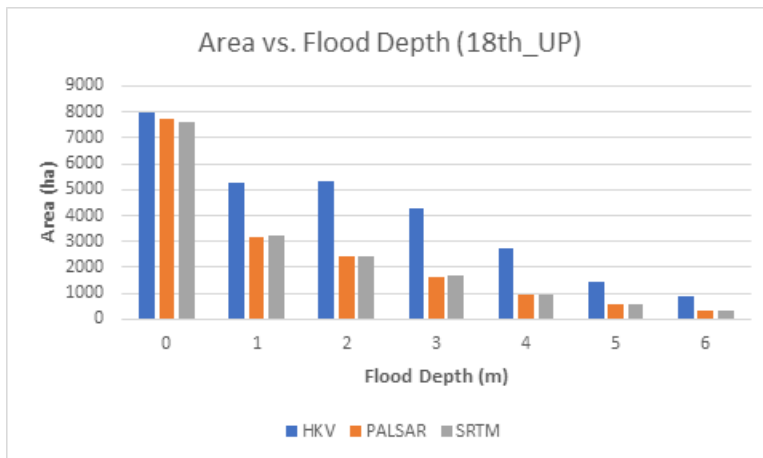


Figure 7.22: Comparing Flooded area (hectares) and depths (meters) for all three DEMS (18th upper Volta). Blue colour (HKV or SPOT DEM), orange colour is (PALSAR) and grey colour (SRTM)

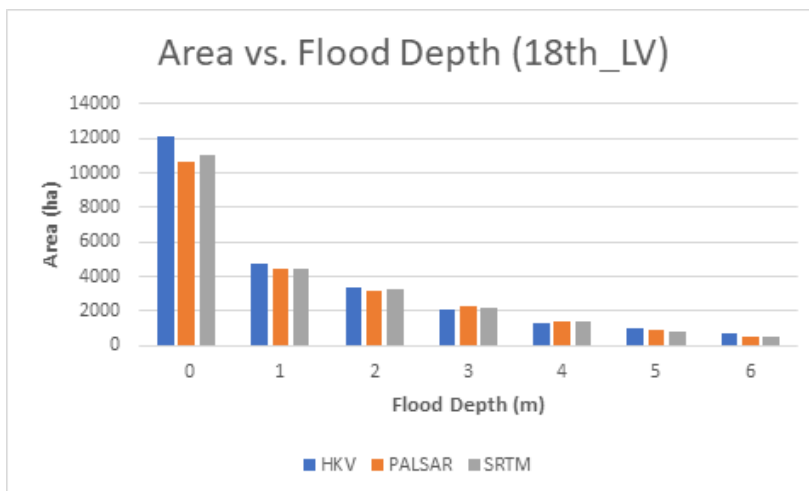


Figure 7.23: Comparing Flooded area (hectares) and depths (meters) for all three DEMS (18th Lower Volta). Blue colour (HKV or SPOT DEM), orange colour is (PALSAR) and grey colour (SRTM)

For the 24th, the flood continued to recede from 8664 (SPOT) and about 7702 (PALSAR and SRTM) to 6477 (SPOT) and about 5925 (SRTM and PALSAR) hectares for the upper Volta for floods depth of 0 to 1m. For flood depth between 1m to 2m, the reduction in the area was not as much as compared to the 12th and 18th. Flooded area reduced from 3570 (SPOT) and about 3248 (PALSAR and SRTM) hectares to 3185 (SPOT) and 2675 (SRTM and PALSAR) hectares. Again, for the lower Volta, the trend changed a bit. There was rather a decrease in the flooded area with flood depth of 0m to 1m and an increase instead in the areas 1m to 2m and above.

The increase was about 4745 to 6771 hectares (SPOT) and about 4420 to 6937 (PALSAR and SRTM) hectares for flood depths within 1 to 2m. There was a general increase in flood depths between 2 to 6m.

The increase in area and flood depths for the 24th can be attributed to the many tributaries of the lower Volta that may have added volumes of water to the water in the white Volta river and also the receding water from the upper Volta. These tributaries take about four to eight days to arrive at the white Volta river from the source. Considering the revisit time of the satellite (six days), that was enough time between the last image taken on the 18th and the current 24th image to cause a difference in volume. It can be observed from the figures 7.21 and 7.25 that the flooded areas and depths of the lower Volta for the 12th and 24th are almost equal. For example, the SPOT DEM estimated flooded area for depths between 0 to 1m as 10878 hectares for the 12th and 10329 hectares for the 24th. The general increase in flood depths and the corresponding increase in extent is almost the same for depths 1 to 6m for both images. Rainfall can easily be ruled out because the increase only affected the lower Volta, excluding the upper Volta on the 24th. The 12th, however, can easily be attributed to rainfall since the flood showed the same behaviour throughout the area for both the upper and lower.

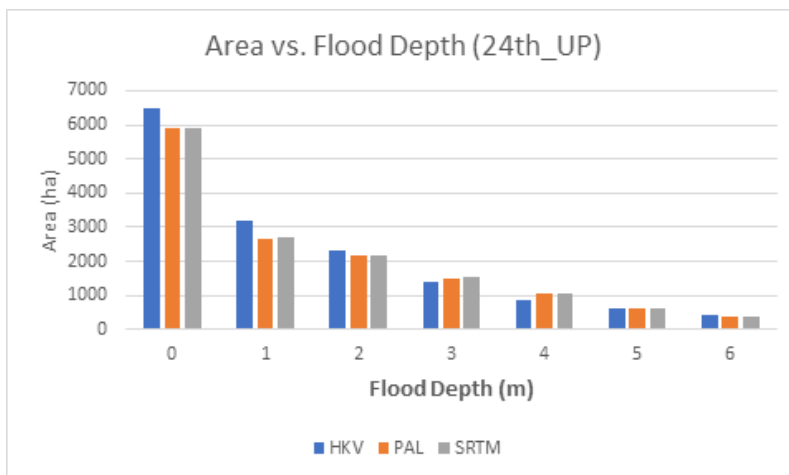


Figure 7.24: Comparing Flooded extent (hectares) and depths (meters) for all three DEMS (24th upper). The SPOT (HKV) DEM is denoted by blue, PALSAR (orange) and SRTM (grey) colour

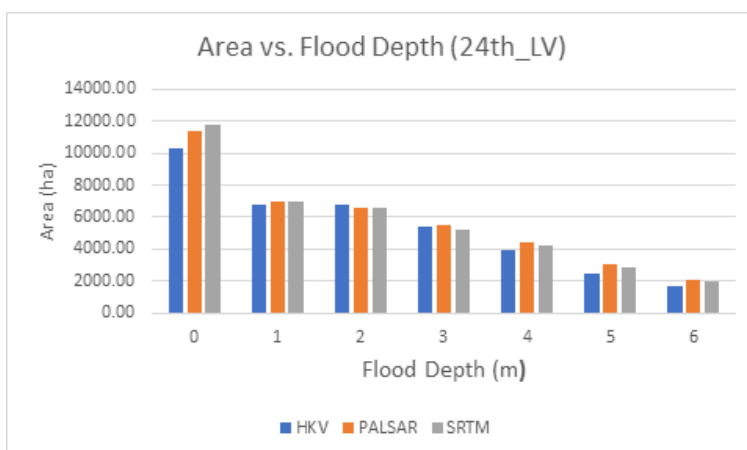


Figure 7.25: Comparing Flooded extent (hectares) and depths (meters) for all three DEMS (24th lower). The SPOT (HKV) DEM is denoted by blue, PALSAR (orange) and SRTM (grey) colour

From the vertical accuracy assessment of the DEMs carried out earlier in this study, using ground truth points it is only fair to consider the flood depths and extents of the SPOT DEM as accurate since it was more accurate compared to the other two DEMs; Followed by the SRTM and the worse as PALSAR, even though in terms of the flood depths, the SRTM and the PALSAR values were very close.

8.0 Vulnerability, Hazard and Risk Assessment

Risk is a combination of vulnerability and hazard (Wisner, 2004). All three can be summarized in the formula $R = H * V$ (Wisner, 2004). To develop a risk map and a risk index for the study area, the flood inundation depth was considered as the hazard component of the risk, and damage factors as hazard index was assigned to the flood depths as depicted in table 8.1. The inundated area (crop fields) was considered as the vulnerability component of the risk, and a vulnerability index was computed for each crop within the flood extents.

As already discussed in the previous steps, the flood depth within a cell was computed through a trend surface and DEM analysis. The cell sizes of the inundated maps were re-sampled through the nearest neighbour interpolation to 100m resolution. This was done to directly convert each cell area to hectare. A hazard index ranging from 1 to 5 was assigned to cells based on the flood depth of the cell. Weights were assigned to the crops based on their resistance or affinity to water. Rice was assigned a weight factor of 4, sorghum 3, millet 2, and maize 1 (Sanyal & Lu, 2003). The higher the resistance of the crop to flooding, the higher the weight factor. For each cell, the risk index was calculated by multiplying the vulnerability and hazard indices assigned to the cell. The risk index was used to create the final risk map, which was then classified into four distinct classes, thus low, medium, high, and very high.

8.1 Flood Hazard Mapping

In this study, the inundation depths and flood extents calculated using a DEM in a trend surface analysis and sentinel radar images respectively were used to prepare a flood hazard map for the area. The inundated area was classified into six categories based on the flood depths using “average continental damage function for Africa – agriculture” as proposed by (Huizinga et al., 2017). The interesting features in this area were the crop fields in the area. The relevant flood depths were within 0 and 2m based on crop heights and developmental stages. The crops under study are arable: maize, millet, sorghum, and rice. Table 8.1 shows the flood depths and assigned damage factors.

Table 8.1: Flood depths and assigned hazard index

Water depth (m)	Damage Factor
0	0
0.5	0.24
1	0.47
1.5	0.74
2	0.92
3+	1.00

Figure 8.1a and 8.1b shows a sample flood hazard maps for the upper Volta, and figure 8.2a and 8.2b for lower Volta. The maps are based on the flood depths of each pixel with the lower flood depths (blue) mostly at the edges of the flood extent, moderate (green) and high (yellow) flood depths in between, and very high flood depths are observed within the river itself as highlighted in red. The flood depths in the hazard maps were determined from the DEMs; hence the poor quality of the results. The images were taken from the 12th of September since these images can be considered for the worst-case scenario. The rest of the dates can be found in Appendix D (figures 16 and 17).

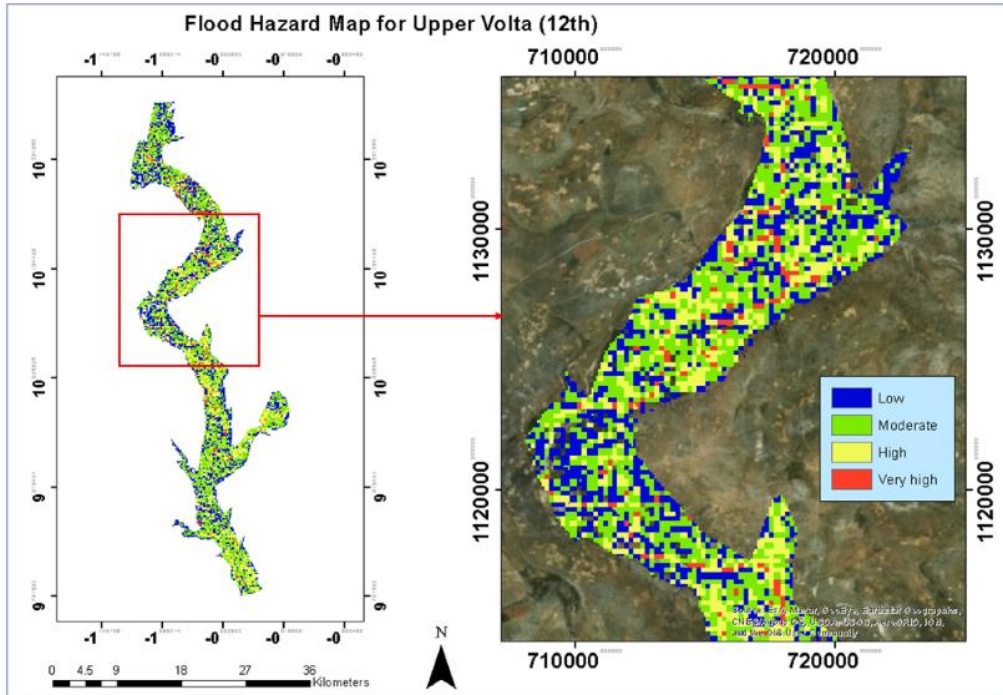


Figure 8.1a: Flood hazard map of the upper Volta, highlighting in detail a section of the flood hazard map.

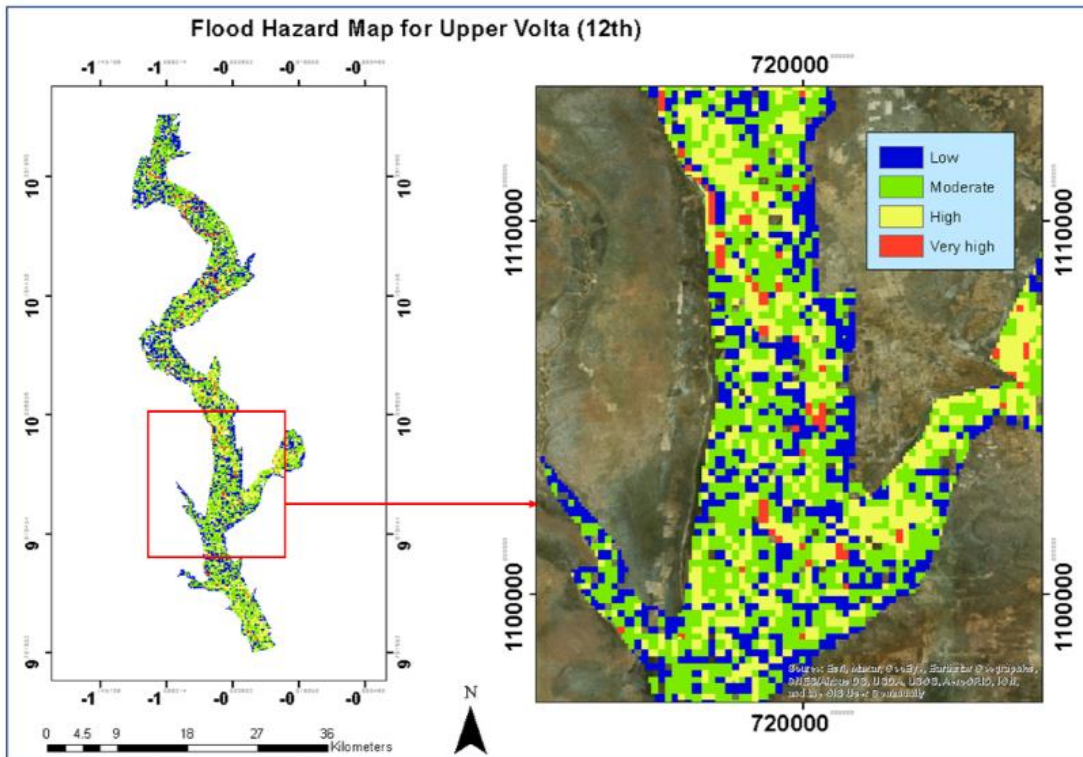


Figure 8.1b: Flood hazard map of the upper Volta, highlighting in detail a section of the map.

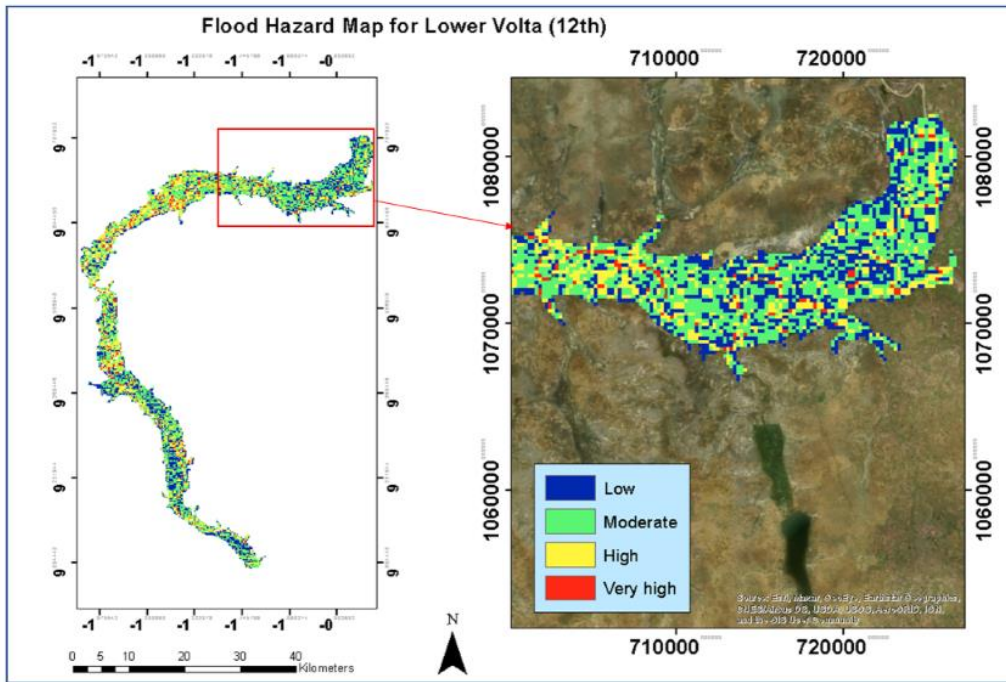


Figure 8.2a: Flood hazard map of the lower Volta, highlighting in detail a section of the map.

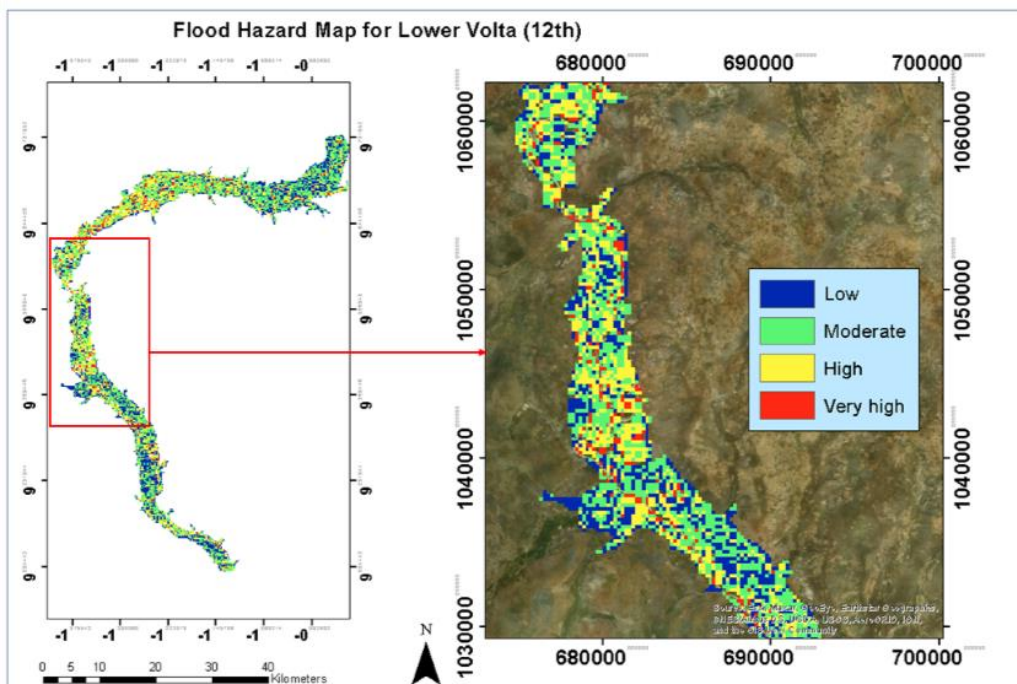


Figure 8.2b: Flood hazard map of the lower Volta, highlighting in detail a section of the map.

Tables 8.2 and 8.3 show the total inundated area within each flood depth, and the associated area percentage for the 12th of September since this day is considered as the worst-case scenario for this analysis

Table 8.2: Flood depths and area covered for the Upper Volta

Flood Depth	Inundated AREA (ha)	PERCENT
Less than 1m	7992	28.7
1 to less than 2m	5272	18.9
2 to less than 3m	5302	19.0
3 to less than 4m	4245	15.2
4m plus	5037	18.1
Total	27850	100

Table 8.3: Flood depths and area covered for the Lower Volta

Flood depth	Inundated Area (hector)	Percentage
Less than 1m	10877	27.5
1 to less than 2m	7274	18.4
2 to less than 3m	7217	18.3
3 to less than 4m	5761	14.6
4m plus	8381	21.2
TOTAL	39511	100

8.2 Flood Return Period

Due to the lack of long-term and quality data, this study could not calculate the return period. However, a study conducted by Udo et al., (2012) in the study area adopted a method to estimate the return periods amidst the data scarcity. They established that it was impossible to reconstruct long-term discharge and historical rainfall data for the area. Historical Landsat images from 2000 to 2010 were therefore used to estimate the flood extents for the period while discharge data from the Nawuni station (figure 18 in appendix D) together with hydraulic model frequency rating curves were used to estimate the return period of the floods for a 10-year period. The study concluded the flood hazard maps for a 10, 25 and 50 years had related maximum discharges of about 2585m³/s (2007 flood). Table 8.4 shows annual maximum discharges and accompanied return periods as recorded from the Nawuni station.

Table 8.4: Annual maximum discharges and their return periods

Discharge	Year	Return period	Discharge	Year	Return period	Discharge	Year	Return period
2593	2010	82.9	1685	1971	2.3	935	1986	0.8
2585	2007	33.9	1669	1967	2.2	924	1977	0.8
2562	1999	21.1	1652	1974	2	917	1958	0.8
2531	1994	15.3	1652	1979	1.9	907	1973	0.7
2523	1989	11.9	1652	1988	1.8	878	2005	0.7
2433	1991	9.7	1604	1953	1.7	831	2006	0.7
2280	2009	8.2	1588	1964	1.6	826	1992	0.6
2162	1963	7.1	1466	1956	1.6	789	2000	0.6
2122	2008	6.2	1451	1996	1.5	675	1990	0.6

2055	1969	5.5	1423	1998	1.4	617	2002	0.5
1940	2003	4.9	1395	1959	1.3	524	1997	0.5
1921	1960	4.5	1323	1995	1.3	510	1976	0.5
1921	1962	4.1	1297	1954	1.2	510	1983	0.4
1884	1970	3.7	1295	1965	1.2	499	1981	0.4
1866	1955	3.4	1199	1968	1.1	444	1982	0.4
1777	2001	3.2	1164	1987	1.1	403	1978	0.3
1759	1961	3	1131	1966	1	328	1984	0.3
1742	1957	2.8	1131	1975	1	309	1972	0.2
1725	1980	2.6	1063	1985	0.9			
1702	1993	2.4	961	2004	0.9			

Source: (Udo. et al., 2012)

The 2018 discharge data for the same Nawuni station recorded 2308.97 m³/s, 2206.94m³/s, and 1949m³/s on the 12th,18th, and 24th of September 2018, respectively. Comparing the maximum discharge of 2308.97 m³/s (12th) to the highlighted (yellow) figures in the table 8.4, for the years 1991 and 2009, it can be inferred that the return period for the flood is about 8 to 10 years; thus 1:9 years flood.

8.3 Vulnerability of crops

Vulnerability analysis here involves the elements at risk in the area of study. The elements at risk, in this case, are crop fields affected by the hazard, which is flooding (Dewan, 2013). Elements at risk were identified from a classified Sentinel-2 image together with google earth images in the GIS environment. This supervised classified map produced a land use/land cover map identifying crop fields, which was then overlaid with the extracted flood depth and extent maps from sentinel-1 images to determine the risk and losses. The classification process and details are described above under sentinel-2 data processing.

To access the vulnerability of the area, weights were assigned to the land uses. The total inundated area was divided into two: crop fields and others (Bare land, grassland, and water bodies). Weights were assigned to the two groups according to the significance. So, the heavier weight of Five (5) was assigned to crop fields and zero (0) to the others. Below in table 8.5 with the areas and assigned weights. To assign the vulnerability weights to the crops, factors such as their water requirement per growing season, stress tolerance (water-logging, heat and drought) and water use efficiency were taken into account (Hadebe et al., 2017; Ofori et al., 2014). Comparing all four crop types, rice and maize had high water requirements with maize requiring less compared to rice. Comparing sorghum and millet, both had about the same water requirements, but sorghum could withstand short periods of flood and had a high-water use efficiency compared to millet. Weights from one to four were assigned to the crops; the higher the vulnerability considering all the above-listed factors, the higher weight. Rice was assigned a weight of one (1), maize-2, Sorghum- 3, and millet – 4. Since the crop distribution in the area is not readily known, the classified cropped area was assumed as the area for the individual crops. A weight of zero was assigned to the area either than crop fields.

Equation one below was used to calculate the vulnerability index. The vulnerability deferred for the different days with the highest vulnerability recorded on 12th, reduced on the 18th, and the least vulnerability was on the 24th for the Upper Volta. This was expected as the flood areas

decreased accordingly. The vulnerability was high for the 12th, decreased on the 18th and spiked again on 24th for the lower Volta due to accumulated volumes and river dynamics. The fluctuation in values is because of the flood extents. For the sake of the analysis, only the worst-case scenarios would be considered; thus, 12th for the upper and lower Volta. Table 8.4 shows the area covered by various land cover from the classified map for the 12th of the Upper Volta. From table 8.4, it shows that grassland covers a larger area. This is not entirely correct as google earth images show that most of the areas classified as vegetation are actually crop fields. Also, the classification error matrix suggests confusion and misclassification between crop fields and vegetation with an overall accuracy of seventy percent.

$$V_{index} = \frac{Weight * (A_c) + 0 * (A_o)}{A_{total}} \dots \dots \dots (1) \text{ (Masood \& Takeuchi, 2012a)}$$

A_c = area of crop, A_o = area either than crop fields, and A_{total} is the total inundated area.

Table 8.5 shows the results of the vulnerability index (V_{index}) analysis for the various crops using the equation above. The results are for the 12th (upper Volta) and 12th (lower Volta). Figure 8.5 and 8.6 respectively shows a graph of the vulnerability index for each crop in the upper and lower Volta.

Table 8.5: Vulnerability index for the upper Volta

Crop	Weight	Total_inundated_area	Crop_area	Vindex
Rice	1	34017	9536	0.28
Maize	2	34017	9536	0.56
Sorghum	3	34017	9536	0.84
Millet	4	34017	9536	1.12

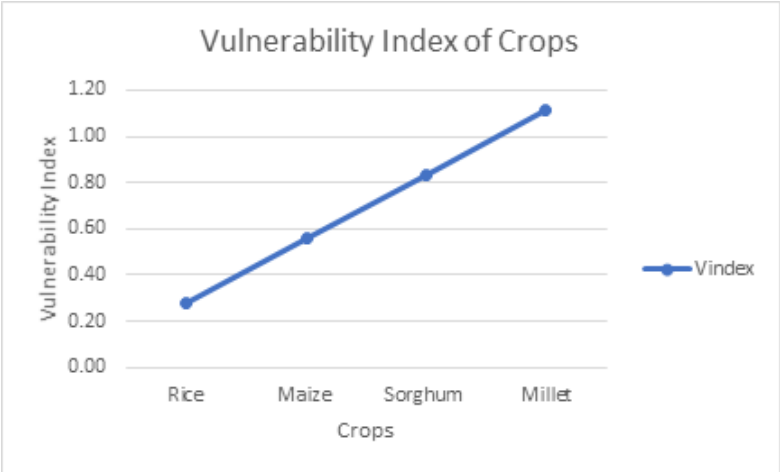


Figure 8.5: Vulnerability index of crops for upper Volta

Table 8.5: Vulnerability index for the lower Volta

Crop	Weight	Total_inundated_area (ha)	Crop_area (ha)	Vulnerability index
Rice	1	11075	4630	0.42
Maize	2	11075	4630	0.84
Sorghum	3	11075	4630	1.26
Millet	4	11075	4630	1.67

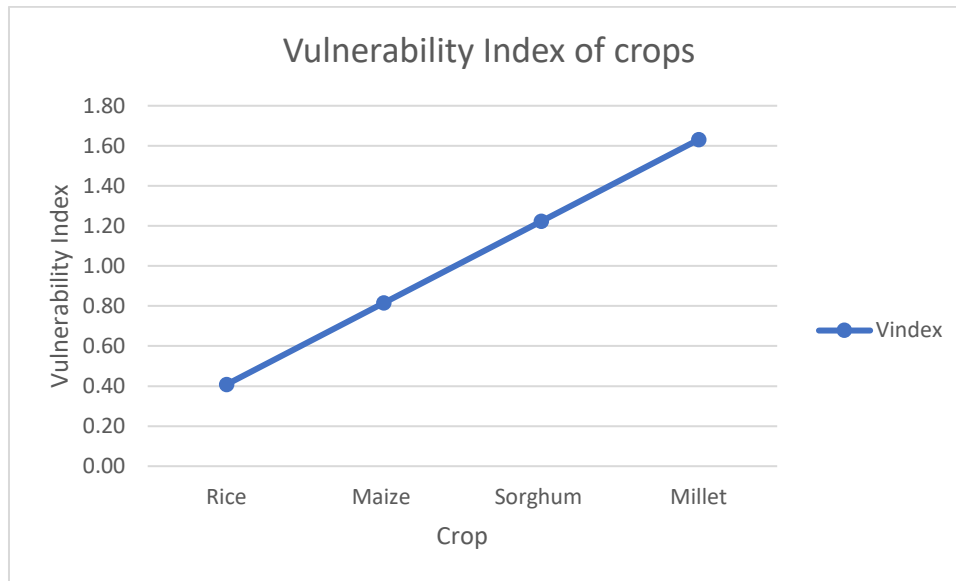


Figure 8.6: Vulnerability index of crops for lower Volta

The results from tables 8.4 and 8.5 show that there are differences in the vulnerability between crops and the area. All the crops are assigned the same varying weights accordingly, but the area has a significant influence on the vulnerability. The upper region shows lower vulnerability values, while the lower region suggests higher vulnerability due to the recorded enormous areas. In all cases, rice has the lowest vulnerability, followed by maize, then sorghum and millet with the highest vulnerability.

This study considered the creation of a risk map for the study area. The vulnerability index (V_{Index}) was multiplied by the hazard index (H_{Index}) to form a risk index (R_{Index}) using the equation (2) (Masood & Takeuchi, 2012b). The depth ranges were considered as the hazard components and weights assigned accordingly; the kind of crop and area covered was taken into consideration as factors of vulnerability. Based on the assigned hazard weights and vulnerability indices, the risk was calculated for each crop at different flood heights. Generally, it can be concluded from the results that the risk increases with increasing flood depth and vulnerability. See table 8.6 and 8.7 respectively for the analysis and results of the 12th (upper) and 12th (lower) Volta.

$$R_{Index} = H_{Index} \times V_{Index} \dots\dots (2)$$

Table 8.6: Risk index for upper Volta

CROP	Vindex	HAZARD index	Risk Index
Rice	0.28	0	0.00
		0.24	0.07
		0.47	0.13
		0.74	0.21
		0.92	0.26
		1	0.28
Maize	0.56	0	0.00
		0.24	0.13
		0.47	0.26
		0.74	0.41
		0.92	0.52
		1	0.56
Sorghum	0.84	0	0.00
		0.24	0.20
		0.47	0.39
		0.74	0.62
		0.92	0.77
		1	0.84
Millet	1.12	0	0.00
		0.24	0.27
		0.47	0.53
		0.74	0.83
		0.92	1.03
		1	1.12

Table 8.7: Risk index for lower Volta

CROP	Vindex	HAZARD index	Risk Index
Rice	0.42	0	0.00
		0.24	0.10
		0.47	0.20
		0.74	0.31
		0.92	0.39
		1	0.42
Maize	0.84	0	0.00
		0.24	0.20
		0.47	0.39
		0.74	0.62
		0.92	0.77
		1	0.84
Sorghum	1.26	0	0.00
		0.24	0.30
		0.47	0.59
		0.74	0.93
		0.92	1.16
		1	1.26
Millet	1.68	0	0.00
		0.24	0.40
		0.47	0.79
		0.74	1.24
		0.92	1.55
		1	1.68

Table 8.8 below summarises the risk categories as computed above from the vulnerability and hazard indices.

Table 8.8: Risk category

Risk index	Class
0 – 0.5	Low
0.5 - 1.0	Medium
1.0 - 1.5	High
1.5 - 2.0	Very high

8.4 Risk assessment

The estimated damages per hectare were also estimated as part of the risk likely to be incurred by the farmers in the event of a flood. An equation that considers the vulnerability, flood depth per cell, and the financial value of the crop per cell were used to calculate the damages using the equation $D = V \times C \times A$, where “D” is the crop damage per cell size, “V” is the Vulnerability, “C” is the financial value of the crop per hectare and “A” is the area per cell.

To simplify the calculations, the cells were re-sampled to a 100m cell size, which is equivalent to a hectare in area, and also most of the measurements are per hectare.

The average yield per hectare was considered in the calculations to determine the financial value per cell. Also, the price per bag (100kg) from Esoko (<https://esoko.com/>) and FAO in Ghana was also used in the calculations. The average yield was multiplied by the inundated cropped area, and the product multiplied by the price per bag to determine the financial value. $C = \text{Area (ha)} * \text{yield/ha} * \text{price per bag (GH\$)}$. An average yield of Maize (5.18/ha), Millet (2.0/ha), Sorghum (4.79/ha), and Rice (4.34/ha) was used. The yields were converted into the number of bags (100kg) per hectare. The total inundated crop area was assumed as the total cultivated area for each crop since data on crop distribution in the area is not readily available. The tables below show the crops and estimated monetary value per inundated cropped area.

Keeping the area constant for all crop types and varying the yield and price per bag, it can be observed that rice recorded the highest values, followed by maize, sorghum, and millet with the least financial value. Rice has a high price compared to the other crops, and so has high financial value even though its yield is lower compared to maize. Maize is second to rice due to its high yields, even though sorghum is more expensive. Sorghum and maize have almost the same amount of yield, and their price range is almost the same. But maize has higher yields and therefore gives it an urge over sorghum. Millet yields are lower than half the yields of sorghum. Millet is more expensive compared to sorghum but yields less compared to the other crops. This, therefore, makes millet the crop with the least financial value. From this analysis, it can be concluded that crops with the lowest vulnerability have the highest financial value and vice versa. In the under listed tables, 8.9 to 8.12 are the calculated financial values of all the crops for both upper and lower Volta.

Table 8.9: The estimated financial value of Rice for the upper and lower Volta

Date	AREA (HA)	BAGS/TOTAL AREA	PRICE(GH\$) /BAG (100kg)	TOTAL AMOUNT (GH\$)
12th	9,536	413,862	328	135,746,867.20
18th	5,050	219,170	328	71,887,760.00
24th	3,519	152,725	328	50,093,668.80
LOWER VOLTA				
12th	4,630	200,942	328	65,908,976.00
18th	3,285	142,569	328	46,762,632.00
24th	4,345	188,573	328	61,851,944.00

Table 8.10: The estimated financial value of Sorghum for the upper and lower Volta

DATE	AREA (HA)	BAGS/TOTAL AREA	PRICE/BAG (GH\$)	TOTAL AMOUNT (GH\$)
12th	9,536	456,774	150	68,516,160.00
18th	5,050	241,895	150	36,284,250.00
24th	3,519	168,560	150	25,284,015.00

LOWER VOLTA				
DATE	AREA (HA)	BAGS/TOTAL AREA	PRICE/BAG (GH\$)	TOTAL AMOUNT (GH\$)
12th	4,630	221,777	150.00	33,266,550.00
18th	3,285	157,352	150.00	23,602,725.00
24th	4,345	208,126	150.00	31,218,825.00

Table 8.11: The estimated financial value of Maize for the upper and lower Volta

DATE	AREA (HA)	BAGS/TOTAL AREA	PRICE/BAG (GH\$)	TOTAL AMOUNT (GH\$)
12th	9,536	493,965	151	74,588,684.80
18th	5,050	261,590	151	39,500,090.00
24th	3,519	182,284	151	27,524,914.20
LOWER VOLTA				
	AREA (HA)	BAGS/TOTAL AREA	PRICE/BAG (GH\$)	TOTAL AMOUNT (GH\$)
12th	4,630	239,834	151	36,214,934.00
18th	3,285	170,163	151	25,694,613.00
24th	4,345	225,071	151	33,985,721.00

Table 8.12: The estimated financial value of Millet

Date	AREA (HA)	BAGS/TOTAL AREA	PRICE/BAG (GH\$)	TOTAL AMOUNT (GH\$)
12th	9,536	190,720	260	49,587,200.00
18th	5,050	101,000	260	26,260,000.00
24th	3,519	70,380	260	18,298,800.00
LOWER VOLTA				
12th	4630	92,600	260	24,076,000.00
18th	3285	65,700	260	17,082,000.00
24th	4345	86,900	260	22,594,000.00

Damages are only estimated for the worse case scenarios, which is the 12th for the upper and lower Volta, respectively, using the equation $D = V \times C \times A$. Below is a table 8.13 outlining the expected damages. Figures 8.7 and 8.8 highlights a graphical representation of the estimated losses and damages for the upper and lower Volta, respectively.

Table 8.13a: Estimated damages of crops for the upper

CROP	Vindex_Upper	Upper_Volta (total amount GHC)	Total Damage cost_Upper (GHC)
Rice	0.28	135,746,867.20	GHC 38,009,122.82
Maize	0.56	74,588,684.80	GHC 41,769,663.49
Sorghum	0.84	68,516,160.00	GHC 57,553,574.40
Millet	1.12	49,587,200.00	GHC 55,537,664.00

Table 8.13b: Estimated damages of crops for the upper

CROP	Vindex_lower	Lower_Volta (total amount GHC)	Total Damage cost_Lower_Volta (GHC)
Rice	0.42	65,908,976.00	GHC 27,681,769.92
Maize	0.84	36,214,934.00	GHC 30,420,544.56
Sorghum	1.26	33,266,550.00	GHC 41,915,853.00
Millet	1.67	24,076,000.00	GHC 40,206,920.00

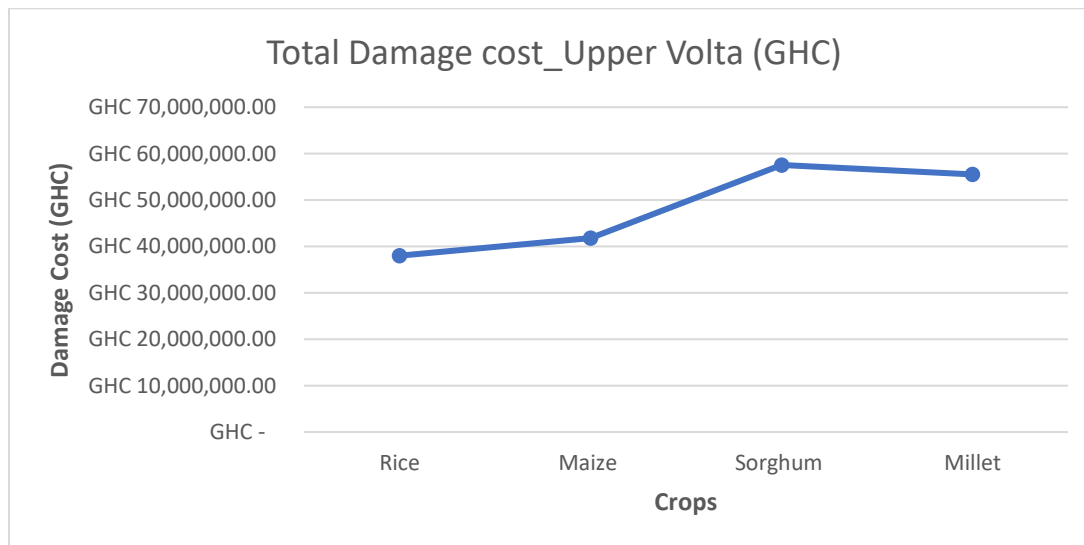


Figure 8.7: Estimated damages per crop for upper Volta

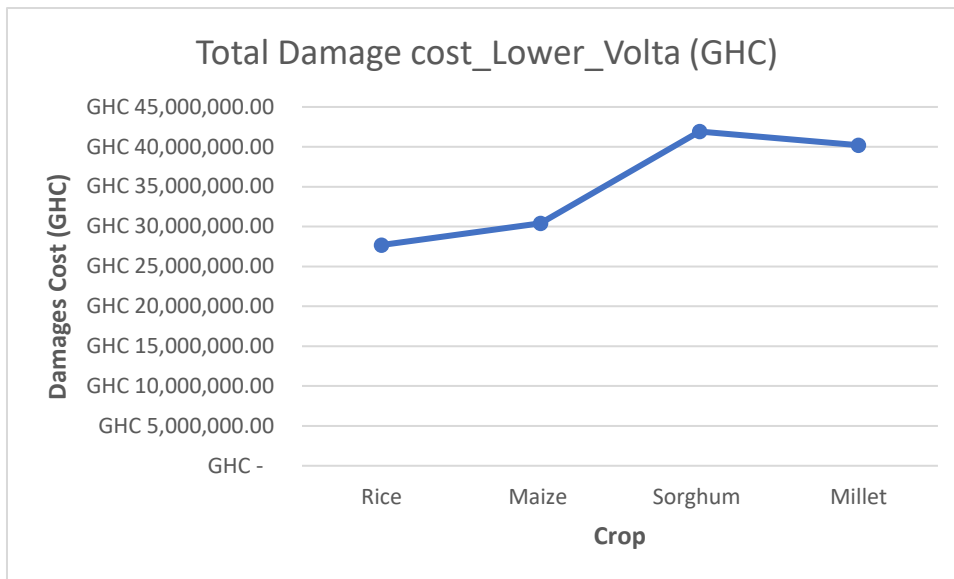


Figure 8.8: Estimated damages per crop for upper Volta

8.5 Discussion

From the graphs above it is obvious that the damage curve has the same pattern for both upper and lower Volta. The damages cost in the upper Volta are more than that of the lower Volta, mostly because of the large crop areas in the upper Volta. Rice has the lowest vulnerability due to its ability to survive in flooded situations compared to the rest of the crops. Rice is followed closely by maize, which also has the next lowest vulnerability. Sorghum ranks highest among all the crops in terms of damages even though millet has the highest vulnerability, and following the trend, millet would have been expected to have the highest vulnerability. Sorghum has a high vulnerability due to its yield. Sorghum has the highest yield of 4.79 after maize and vulnerability of 0.84, which makes it rank higher in terms of damages. Millet, however, even though it sold almost twice the price of sorghum and recorded the highest vulnerability among all, it also has the lowest yields and hence the low expected financial damages.

The analysis conducted above only considered the worst-case scenario with the largest flood extents and deeper flood depths, which occurred on the 12th. This analysis only takes into account crop fields within the flooded extents. The area is also noted to have different flood depths due to the elevation of the terrain and the volume of water over the surface. This analysis further assumed a complete loss because of the total inundation of the fields within the flood extents without considering the flood depths and duration for the damage calculations.

Since the entire process was not modelled, it is, therefore, challenging to time the spreading of the water over the surface and the receding behaviour of the flood in the area. The only timing available is from sentinel-1 satellite images, which are six days apart. The images, however, gives an idea of the increasing and decreasing nature of the flood extents. Even though the flood depths were obtained through the trend surface analysis, the depth alone does not give much information without the duration and timings of the flood.

The elements at risk in this study were crops, and almost all the crops with the exception of rice are better adapted to drought conditions with little rain. Rice, however, can survive in the water close to a week with about 60 to 100% yield loss at the reproductive and maturity stages (Shrestha et al., 2016). Sorghum (red seed) can also withstand a bit of prolonged flooding while millet may only survive about a day's flooding (Dykes et al., 2009), Using the sentinel images for timing the floods would mean that one have to assume a six-day interval between the occurrence of the flood and the receding extent which would mean a 60 to 100% yield loss to the farmers whether partially

or completely inundated. Rice plants may survive better between flood depths of 0 – 1m at the reproductive maturity stages.

Floods in the study area occur in September when the river is at its peak following accumulated heavy rains, especially in August. Rains start in May and planting is mostly done in June, especially in the last two weeks of June when the ground is moist enough. This study, therefore, considered the last week of June as the base for planting. This therefore implies that by the first week of July, the seeds would have germinated. In the case of the September 2018 flood understudy, the floods occurred on the 12th when the plants were about seventy-four days old in their growth stages. This stage is characterized as the reproductive and maturity stage of the crops, which is sensitive to flooding because the yield loss is very high at this stage. The reproductive stage is a very sensitive stage of crop development. At this stage, the crop water requirements are high, and stress is to be avoided as much as possible. This is the stage where the kernels start to develop in the case of maize, sorghum, and millet. That is the final stage of development and filling of grains (PANNAR, 2016). The crops are tall enough at this stage to withstand flood depths between 0 and 1m. Partly submerged plants are likely to continue photosynthesising and may survive between a day to four days, depending on the temperature. Cooler temperatures can increase the chances of survival compared to warmer temperatures (Brandy VanDeWalle, 2011). Since the study area is characterized by high temperatures of up to 33 degrees Celsius, it already limits the chances of survival for partially inundated crops.

The other limiting factor for completely submerged crops and partially submerged crops is the depletion of oxygen in the soil. In the event of a flood, the oxygen within the saturated soil is depleted in about 48 hours (Brandy VanDeWalle, 2011; Wiebold et al., 2013), inhibiting root growth. The lack of oxygen inhibits the plants' ability to undertake critical life activities such as water and nutrient absorption. The saturated soil can also cause leaching and denitrification of nitrogen, leading to nitrogen deficiencies contributing to yield losses. Submerged plants are also prone to diseases such as bacterial stalk, root, and ear rot, which affects crops after a flood event (Nielsen, 2016). In conclusion, once maize, millet, and sorghum are partially or completely inundated, the chances of greater yield losses are very high. The yield loss is estimated between 80 – 100% loss.

The duration, the depths of the flood, the growth stage, soil, and environmental conditions all act together to determine the percentage of yield loss and survival of the crops. The images of the flood extents show a sharp decline in the flood extents between the 12th and the 18th. There is, therefore, the possibility of some crops surviving or all perishing depending on the conditions as mentioned above.

For the upper Volta, for instance, the survival rate of the crops is higher compared to the lower Volta in terms of the flood receding and the elevation in that area. It can be inferred from the images that the flood receded in the three-week period and depending on the rate; the crops may still have a surviving chance. In the case of the Lower Volta However, there were two waves of the flood, and this reduces the chances of crop survival. The water had receded after almost a week on the 18th but there was a second wave of flooding on the 24th almost the same extent and area coverage as the first flood on the 12th. Considering the crops may have still been recovering from the effect of the first flood, this second wave would cause the crops to perish since the soil would have been more saturated. The terrain elevation here too suggests lower elevations, which therefore implies that water is likely to linger longer and move slowly in this region as compared to the upper region.

Considering the maturity days of the crops, millet compared to the other crops is an early maturing crop and is likely to be harvested before the floods sets in. Even if the farmer planted earlier, in the north, open season drying is practised since farmers do not have the means and resources to

harvest, dry, and store the crops properly without risking it rotting away. The crops are left on the field after they are matured to be dried and reduce the moisture content in the seeds and cobs. The abundant sunshine and Sahara winds aid in drying the crops and reducing the moisture content, after which they are then harvested from the field in the months of October to December when there are no rains and stored. Depending on the planting and occurrence of the flood, the crops can be either fully matured or at the reproductive and maturity stages. This, therefore, results in various degrees of yield and financial losses in the event of a flood since it is almost the end of the growing season. IFRC in 2007, reported that 50 to 100% of staple crops were rotten on the field after the floods in the north. The Northern region is known as one of the food baskets in the country. Floods of this nature affect the farmer and the nation as a whole.

9.0 Conclusion

This research basically examined Sentinel-1 Radar data together with selected DEMs in an attempt to assess the accuracy of these data in flood propagation monitoring and flood depth analysis. A risk and loss assessment was also carried out to determine the effect of the floods on crops. The research, therefore, seeks to achieve the under listed and discussed objectives.

1. To investigate how well Sentinel-1 imagery can be used in delineating the extent of riverine floods in an agricultural area.

This study could delineate and extract the flood extents for three dates 12th, 18th, and 24th. September 2018. The images showed a sense of the progression of the flood for the three-week period. A disparity was observed between the Upper and the lower Volta. While a continuous recession of the flood could be observed in the upper Volta, there were fluctuations in the lower Volta with increasing and decreasing flood extents. The timing of the flood could only be assumed from the acquired images; thus, six days apart. This did not allow for monitoring of the gradual recession or progression of the floods on an hourly or daily basis, which is important for flood monitoring in the agricultural field as the duration of the flood determines to a great extent the expected losses.

2. To carry out a flood extent and depth analysis using Sentinel-1 images and DEMs (SRTM 30m, ALOS PALSAR 30m, and a SPOT DEM 30m) together in a trend surfaced analysis

Three DEMs used in determining the flood depths were compared in terms of accuracy through a vertical accuracy assessment using GCP points from the study area. The DEMs were used to determine the flood depths within the flood extents through trend surface interpolation analysis. The trend surface was subtracted from the DEM to determine the flood depths.

The meanderings, vegetation, and oxbows in the river body resulted in negative values that were finally eliminated, and this resulted in some missing pixels in the image which did not give a true reflection of the flood depths within the extents. The quality of the DEMs was not good for an accurate determination of flood depths. The third Interpolation trend represented the flood surface better compared to the first and second trend. The combination of the quality SAR image with the inferior quality DEMs was beneficial in determining the flood depths. The SPOT DEM was considered as the most accurate (best quality) based on the GCP, followed by the SRTM DEM, and the worse of the DEMS was the PALSAR DEM.

Comparing the DEMs and the Sentinel Images (1 & 2) it was observed that the Sentinels give much details of the River characteristics and flood extents and so can be considered as a better choice for flood estimations compared to the DEMs

3. To Investigate the relationship between the different crop cycles and the occurrence of flooding in crop fields along the White Volta river.

This study also looked into the occurrences of floods and the timing of floods. It was observed that the floods usually occur when the crops are at the maturity stage of growth, and this results in high levels of losses since farmers mostly cannot salvage their crops after a flood. The floods usually build up and flow from the North (upper Volta) to the south (lower Volta); this study, therefore, considered the possibility of maybe the farmers in the lower Volta salvaging their crops before floods from the north arrive but this was not the case since the many tributaries of the river coupled with water from the upper Volta resulted in two waves of flood in the area of the lower Volta. The crops in the area are also affected differently by the floods in terms of the depth and duration of floods since some crops were better adapted to flooded conditions than others. Depending on the maturity period of the crops, Millet, for instance, has a higher probability of being harvested before

the floods occur compared to the other crops since it has a shorter maturity period and rice was less perishable compared to the others.

4. To assess the agricultural economic losses of the various crops in the area within the flood extents.

A risk and vulnerability assessment were carried out to determine how the flood affected crops fields within the flood extents and the estimated cost of damages likely to have been incurred by the farmers. The flood depth map was considered as the hazard map, and the vulnerability assessment for maize, millet, sorghum and rice was carried out to determine how the floods affected each crop. Rice was the least vulnerable crop, followed by maize, then sorghum and millet was considered as the most vulnerable crop of all to flood in the area.

The expected financial losses based on the yield per hectare was calculated for each crop. Rice, with the lowest vulnerability, recorded the lowest financial loss, followed by maize with the second-lowest vulnerability after rice. Millet, despite its high vulnerability index, recorded a low financial loss compared to sorghum. Sorghum recorded the highest financial loss due to its high vulnerability index and high price compared to millet. The upper Volta recorded higher financial losses compared to the lower Volta

9.1 Recommendation

High quality data should be used for flood analysis in the region. Open data should be corrected and improved as much as possible using ground data before being used for analysis as these data are not always accurate locally. High quality DEMs such as LiDAR should be used for flood analysis in the region. RADAR images are recommended for flood studies in the region since the area is mostly cloudy in the rainy season.

Farmers should as much as possible desist from farming very close to the river during the rainy season but dry season farming can be adopted in the periods of low tides. Farmers farming close to the river bank in the rainy season are advised to consider the use of early maturing seeds, water resistant crops and farming practices that promote early harvesting of matured crops. This practice if adopted can help minimize the cost and damages associated with floods in the area.

The responsible bodies in the Volta basin should communicate as possible in an attempt to minimize the disaster caused by spillage of dams. This practice if well executed would go a long way to minimize the effect of flooding on the locals along the rivers.

9.2 Limitations of the study

- The lack of field data, insufficient or absence of quality data hampered the accurate reflection of the results as far as ground truth is concerned;
- Timing the floods based on the sentinel-1 Images that were six days apart did not really give a true nature of the gradual time-step progression of the flood in the area. This hindered the determination of the duration of the flood coverage. The flood extent after six days-based on the sentinel-1 images was assumed as the duration of the flood for the three dates observed (12th, 18th and 24th). This affected the actual determination of the effect of floods on the crops.
- The lack of field data on the types and the distribution of the crops in the field hindered a proper assessment of the flooded area according to flood depths and crop types.

- The crop areas are based on the supervised classification results from Sentinel-2 imagery and are also prone to errors; therefore, it might not reflect the actual cropped areas within the flood extent.
- Lack of river discharge data on the Bagre dam management upstream and relevant gauges along the river of the study area prevented me from carrying out flood modelling analysis for the area since the discharge from upstream contributed majorly to the floods in the area.
- The DEMs also used for the study were also of inferior quality and, most of the time, overestimated the elevation values in the area when compared to some ground data collected in the study area from a different study.

LIST OF REFERENCES

- Adam, S., Wiebe, J., Collins, M., & Pietroniro, A. (1998). Radarsat Flood Mapping in the Peace-Athabasca Delta, Canada. *Canadian Journal of Remote Sensing*, 24(1), 69–79.
<https://doi.org/10.1080/07038992.1998.10874693>
- Alfieri, L., Bisselink, B., Dottori, F., Naumann, G., de Roo, A., Salamon, P., Wyser, K., & Feyen, L. (2017). Global projections of river flood risk in a warmer world. *Earth's Future*, 5(2), 171–182.
- Aloba, A. J. (2015). *Assessment of the role of annual flood in the white Volta river on food security*.
- Anayah, F., & Kaluarachchi, J. J. (2009). *Groundwater resources of northern ghana : initial assess ment of data availability*. December, 1–22.
- Anayah, F. M., Kaluarachchi, J. J., Pavelic, P., & Smakhtin, V. (2013). Predicting groundwater recharge in Ghana by estimating evapotranspiration. *Water International*, 38(4), 408–432.
<https://doi.org/10.1080/02508060.2013.821642>
- Andersen, A. N., Braithwaite, R. W., Cook, G. D., Corbett, L. K., Williams, R. J., Douglas, M. M., Gill, A. M., Setterfield, S. A., & Muller, W. J. (1998). Fire research for conservation management in tropical savannas: Introducing the Kapalga fire experiment. *Austral Ecology*, 23(2), 95–110. <https://doi.org/10.1111/j.1442-9993.1998.tb00708.x>
- Andreini, M., Vlek, P., & Van De Giesen, N. (2002). Water sharing in the Volta basin. *FRIEND 2002- Regional Hydrology: Bridging the Gap Between Research and Practice*, 274, 329–336.
- Apel, H., Aronica, G. T., Kreibich, H., & Thielen, A. H. (2009). Flood risk analyses—how detailed do we need to be? *Natural Hazards*, 49(1), 79–98.
- Apel, H., Thielen, A. H., Merz, B., & Blöschl, G. (2006). A probabilistic modelling system for assessing flood risks. *Natural Hazards*, 38(1–2), 79–100.
- Asenso-Okyere, K., Chiang, C., Thangata, P., Andam, K. S., & others. (2012). Two-way links between health and farm labor. *Edited by Shenggen Fan and Rajul Pandya-Lorch*, 121.
- Asumadu-Sarkodie, S., Owusu, P. A., & Jayaweera, M. P. C. (2015). Flood risk management in Ghana: A case study in Accra. *Advances in Applied Science Research*, 6(4), 196–201.
- Atokple, I. D. K. (1995). Current progress towards the utilization of sorghum in brewing lager beer in Ghana. *Processing and Industrial Utilization of Sorghum and Related Cereals in Africa. Ouagadougou: OAU/STRC-SAFGRAD*, 61–69.
- Bagamsah, T. T. (2005). The Impact of Bushfire on Carbon and Nutrient Stocks as Well as Albedo in the savanna of northern Ghana. *Ecology and Development Series 25*, 49(25), 167.
- Barredo, J. I., De Roo, A., & Lavalley, C. (2007). Flood risk mapping at European scale. *Water Science and Technology*, 56(4), 11–17.
- Barry, B., Obuobie, E., Andreini, M., Andah, W., & Pluquet, M. (2005). *The Volta River Basin Comprehensive Assessment of Water Management in Agriculture Comparative study of river basin development and management*.
- Beven, K. J. (2016). EGU Leonardo Lecture: Facets of Hydrology—epistemic error, non-stationarity, likelihood, hypothesis testing, and communication. *Hydrol. Sci. J*, 61(9), 1652–1665.
- Blaikie, P., Cannon, T., Davis, I., & Wisner, B. (2014). *At risk: natural hazards, people's vulnerability*

and disasters. Routledge.

- Blašković, T. (n.d.). *Major floods hit northern Ghana, killing at least 34 people and leaving 100 000 homeless*. Retrieved February 27, 2020, from <https://watchers.news/2018/09/21/ghana-flood-september-2018/>
- Blench, R., Blench, R., & Chapman, R. (2003). *MULTI-AGENCY PARTNERSHIPS (MAPS) FOR TECHNICAL CHANGE IN WEST AFRICAN AGRICULTURE RICE PRODUCTION AND LIVELIHOODS IN GHANA prepared by: G.*
- Boncori, J. P. M. (2016). Caveats concerning the use of SRTM DEM version 4.1 (CGIAR-CSI). *Remote Sensing*. <https://doi.org/10.3390/rs8100793>
- Borga, M., Anagnostou, E. N., Blöschl, G., & Creutin, J.-D. (2011). Flash flood forecasting, warning and risk management: the HYDRATE project. *Environmental Science & Policy*, 14(7), 834–844.
- Brandy VanDeWalle. (2011, May 24). *How Corn Plants Respond to Flooding | CropWatch | University of Nebraska–Lincoln*. IANR Media. <https://cropwatch.unl.edu/how-corn-plants-respond-flooding>
- Brémond, P., & Grelot, F. (2013). Review Article: Economic evaluation of flood damage to agriculture - Review and analysis of existing methods. *Natural Hazards and Earth System Sciences*, 13(10), 2493–2512. <https://doi.org/10.5194/nhess-13-2493-2013>
- Brivio, P. A., Colombo, R., Maggi, M., & Tomasoni, R. (2002). Integration of remote sensing data and GIS for accurate mapping of flooded areas. *International Journal of Remote Sensing*, 23(3), 429–441.
- Brown, J. D., & Damery, S. L. (2002). Managing flood risk in the UK: towards an integration of social and technical perspectives. *Transactions of the Institute of British Geographers*, 27(4), 412–426.
- Cafforio, C., Prati, C., & Rocca, F. (1991). SAR data focusing using seismic migration techniques. *IEEE Transactions on Aerospace and Electronic Systems*, 27(2), 194–207.
- Carrier, M., Lefebvre, R., Racicot, J., & Asare, E. B. (2008). Groundwater recharge assessment in northern Ghana using soil moisture balance and chloride mass balance. *GeoEmonton'08*, 1437–1444.
- Changnon, S. A. (2003). Shifting economic impacts from weather extremes in the United States: A result of societal changes, not global warming. *Natural Hazards*, 29(2), 273–290.
- Chapi, K., Rudra, R. P., Ahmed, S. I., Khan, A. A., Gharabaghi, B., Dickinson, W. T., Goel, P. K., & others. (2015). Spatial-temporal dynamics of runoff generation areas in a small agricultural watershed in southern Ontario. *Journal of Water Resource and Protection*, 7(01), 14.
- Clement, M. A., Kilsby, C. G., & Moore, P. (2017). *Multi-temporal synthetic aperture radar flood mapping using change detection*. <https://doi.org/10.1111/jfr3.12303>
- Coveney, S., & Roberts, K. (2017). Lightweight UAV digital elevation models and orthoimagery for environmental applications: data accuracy evaluation and potential for river flood risk modelling. *International Journal of Remote Sensing*, 38(8–10), 3159–3180.
- Curlander, J. C., & McDonough, R. N. (1991). *Synthetic aperture radar* (Vol. 11). Wiley, New York.
- Darfour, B., & Rosentrater, K. A. (2016). Agriculture and food security in Ghana. *2016 American Society of Agricultural and Biological Engineers Annual International Meeting, ASABE 2016*.

<https://doi.org/10.13031/aim.20162460507>

- Davies, O. (1968). The origins of agriculture in West Africa. *Current Anthropology*, 9(5, Part 2), 479–482.
- De Zan, F., & Guarnieri, A. M. (2006). TOPSAR: Terrain observation by progressive scans. *IEEE Transactions on Geoscience and Remote Sensing*, 44(9), 2352–2360.
<https://doi.org/10.1109/TGRS.2006.873853>
- Dewan, A. M. (2013). Floods in a megacity: Geospatial techniques in assessing hazards, risk and vulnerability. In *Floods in a Megacity: Geospatial Techniques in Assessing Hazards, Risk and Vulnerability*. <https://doi.org/10.1007/978-94-007-5875-9>
- Dewan, A. M., Kumamoto, T., & Nishigaki, M. (2006). Flood hazard delineation in greater Dhaka, Bangladesh using an integrated GIS and remote sensing approach. *Geocarto International*, 21(2), 33–38.
- Dewan, A. M., & Yamaguchi, Y. (2009). Land use and land cover change in Greater Dhaka, Bangladesh: Using remote sensing to promote sustainable urbanization. *Applied Geography*.
<https://doi.org/10.1016/j.apgeog.2008.12.005>
- Dhar, O. N., & Nandargi, S. (1998). Floods in Indian rivers and their meteorological aspects. *MEMOIRS-GEOLOGICAL SOCIETY OF INDIA*, 1–26.
- Di, L., Eugene, G. Y., Kang, L., Shrestha, R., & BAI, Y. (2017). RF-CLASS: A remote-sensing-based flood crop loss assessment cyber-service system for supporting crop statistics and insurance decision-making. *Journal of Integrative Agriculture*, 16(2), 408–423.
- Dovie, D. B. (2010). Climate Change, Water and Disasters: Perspectives from Ghana's Three Northern Regions. *WRC-CCA Report Series, 1Water*.
- Duy, N. B. (2016). Automatic detection of surface water bodies from Sentinel-1 SAR images using Valley-Emphasis method. *Vietnam Journal of Earth Sciences*, 37(4), 328–343.
<https://doi.org/10.15625/0866-7187/37/4/8298>
- Dykes, L., Seitz, L. M., Rooney, W. L., & Rooney, L. W. (2009). Flavonoid composition of red sorghum genotypes. *Food Chemistry*, 116(1), 313–317.
<https://doi.org/10.1016/j.foodchem.2009.02.052>
- Ekekpi, G. K., Aalangdong, O. I., Yakubu, S. M., & Agyare, W. A. (2000). *A review of natural resources management for agricultural production in the Northern Region*.
- FAO. (2013). Analysis of incentives and disincentives for Sorghum in Ghana. Technical note series. *Mafap, June*, 1–30. <http://www.fao.org/mafap>
- FAO, I. (1996). World Sorghum and Millet Economy Facts, trends and outlook. *A Joint FAO and ICRISAT Study*, 68.
- Farr, T. G., Rosen, P. A., Caro, E., Crippen, R., Duren, R., Hensley, S., Kobrick, M., Paller, M., Rodriguez, E., Roth, L., & others. (2007). The shuttle radar topography mission. *Reviews of Geophysics*, 45(2).
- Fernández-Lavado, C., Furdada, G., & Marqués, M. A. (2007). *Geomorphological method in the elaboration of hazard maps for flash-floods in the municipality of Jucuaran (El Salvador)*.
- Flood disaster profile of Ghana since 1968 - Graphic Online*. (n.d.). Retrieved October 6, 2020, from <https://www.graphic.com.gh/news/general-news/flood-disaster-profile-of-ghana.html>

- Forkuo, E. K. (2010). Digital elevation modelling using ASTER stereo imagery. *J Environ Sci Eng*, 52, 81–92.
- Forkuo, E. K. (2011). Flood hazard mapping using aster image data with GIS. *Internacional Journal Of Geomatics And Geociences*, 1(4), 932–950. <https://doi.org/ISSN 0976-4380>
- Forkuo, E. K., & others. (2008). Digital terrain modeling in a GIS environment. *第 21 届国际摄影测量与遥感大会 (ISPRS 2008)*, 2230–2236.
- Gan, T. Y., Zunic, F., Kuo, C.-C., & Strobl, T. (2012). Flood mapping of Danube River at Romania using single and multi-date ERS2-SAR images. *International Journal of Applied Earth Observation and Geoinformation*, 18, 69–81.
- Gesch, D., Oimoen, M., Zhang, Z., Meyer, D., & Danielson, J. (2012). VALIDATION OF THE ASTER GLOBAL DIGITAL ELEVATION MODEL VERSION 2 OVER THE CONTERMINOUS UNITED STATES. *ISPRS - International Archives of the Photogrammetry, Remote Sensing and Spatial Information Sciences*. <https://doi.org/10.5194/isprsarchives-xxxix-b4-281-2012>
- Geudtner, D., Torres, R., Snoeij, P., Davidson, M., & Rommen, B. (2014). Sentinel-1 System capabilities and applications. *International Geoscience and Remote Sensing Symposium (IGARSS)*. <https://doi.org/10.1109/IGARSS.2014.6946711>
- Ghana, M. (2013). Basic Agricultural Public Expenditure Diagnostic Review. *Report under Strengthening National Comprehensive Agricultural Public Expenditure in Sub-Saharan Africa Implemented by the World Bank*.
- Ghana Statistical Service. (2010). Population & Housing Census. *Regional Analytical Report - Upper East Region*, 1–194.
- Gong, D. Y., Wang, S. W., & Zhu, J. H. (2001). East Asian winter monsoon and Arctic Oscillation. *Geophysical Research Letters*, 28(10), 2073–2076. <https://doi.org/10.1029/2000GL012311>
- Goovaerts, P. (2000). Geostatistical approaches for incorporating elevation into the spatial interpolation of rainfall. *Journal of Hydrology*, 228(1–2), 113–129.
- Hadebe, S. T., Modi, A. T., & Mabhaudhi, T. (2017). Drought Tolerance and Water Use of Cereal Crops: A Focus on Sorghum as a Food Security Crop in Sub-Saharan Africa. *Journal of Agronomy and Crop Science*, 203(3), 177–191. <https://doi.org/10.1111/jac.12191>
- Han, P., Long, D., Han, Z., Du, M., Dai, L., & Hao, X. (2019). Improved understanding of snowmelt runoff from the headwaters of China's Yangtze River using remotely sensed snow products and hydrological modeling. *Remote Sensing of Environment*, 224, 44–59. <https://doi.org/10.1016/j.rse.2019.01.041>
- Hirabayashi, Y., Mahendran, R., Koirala, S., Konoshima, L., Yamazaki, D., Watanabe, S., Kim, H., & Kanae, S. (2013). Global flood risk under climate change. *Nature Climate Change*, 3(9), 816–821.
- Home - National Seed Trade Association of Ghana. (n.d.). Retrieved June 15, 2020, from <https://nastag.org/>
- Honda, K. C., Francis, X. J., & Sah, V. P. (1997). Flood monitoring in central plain of Thailand using JERS-1 SAR data. In *Proc. 18th Asian Conference of Remote Sensing*.

- Huizinga, J., de Moel, H., & Szewczyk, W. (2017). Global flood depth-damage functions : Methodology and the Database with Guidelines. In *Joint Research Centre (JRC)*. <https://doi.org/10.2760/16510>
- IFRC. (n.d.-a). *Ghana: Emergency Plan of Action (EPoA) Floods in Upper East Region DREF Operation n° MDRGH015 / PGH031 - Ghana | ReliefWeb*. Reliefweb. Retrieved September 19, 2020, from <https://reliefweb.int/report/ghana/ghana-emergency-plan-action-epoa-floods-upper-east-region-dref-operation-n-mdrgh015>
- IFRC. (n.d.-b). *Northern Ghana in urgent need of food after devastating floods - IFRC*. Retrieved June 15, 2020, from <https://www.ifrc.org/ar/news-and-media/news-stories/africa/ghana/northern-ghana-in-urgent-need-of-food-after-devastating-floods/>
- James B. Campbell, R. H. W. (2011). *Introduction to Remote Sensing*, (Fifth). The Guilford Press. https://books.google.nl/books?hl=en&lr=&id=NkLmDjSS8TsC&oi=fnd&pg=PP1&dq=Campbell+%26+Wynne,+2011&ots=s2Ekz7s0-x&sig=OXARVajcs1lbCeiwQTSazEBJrLg&redir_esc=y#v=onepage&q=Campbell+%26+Wynne%2C+2011&f=false
- Jawak, S. D., Bidawe, T. G., & Luis, A. J. (2015). A Review on Applications of Imaging Synthetic Aperture Radar with a Special Focus on Cryospheric Studies. *Advances in Remote Sensing*, 04(02), 163–175. <https://doi.org/10.4236/ars.2015.42014>
- Jaybhay, J., & Shastri, R. (2015). A Study of Speckle Noise Reduction Filters. *Signal & Image Processing : An International Journal*. <https://doi.org/10.5121/sipij.2015.6306>
- Jia, K., Liu, J., Tu, Y., Li, Q., Sun, Z., Wei, X., Yao, Y., & Zhang, X. (2019). Land use and land cover classification using Chinese GF-2 multispectral data in a region of the North China Plain. *Frontiers of Earth Science*, 13(2), 327–335.
- Jjemba, J. W. and E. W. (2015). “Historic Flood Events Uganda by text mining local newspapers,” *FloodTags, Uganda*.
- Jonkman, S. N. (2005). Global perspectives on loss of human life caused by floods. *Natural Hazards*, 34(2), 151–175. <https://doi.org/10.1007/s11069-004-8891-3>
- Jorg Haarpaintner. (2019). *Ghana Sentinel 1 Change Detection v3*. Skopptest.Maps.Arcgis.Com. <https://hub.arcgis.com/datasets/ace55b26c27344b6b7e7a4026a549237>
- Karley, N. K. (2009). Flooding and physical planning in urban areas in West Africa: situational analysis of Accra, Ghana. *Theoretical and Empirical Researches in Urban Management*, 4(4 (13), 25–41.
- Kasei, R. A., Ampadu, B., Sapanbil, G. S., & others. (2013). Relationship between rainfall-runoff on the White Volta River at Pwalugu of the Volta Basin in Ghana. *J. Environ. Earth Sci*, 3(11), 92–99.
- Kablouti, M., Ouerdachi, L., & Boutaghane, H. (2012). Spatial interpolation of annual precipitation in Annaba-Algeria-comparison and evaluation of methods. *Energy Procedia*, 18, 468–475.
- Kesse, & O, G. (1985). *The mineral and rock resources of Ghana*. A.A. Balkema Publishers, Accord, MA.
- Khalil, H. P. S. A., Jawaaid, M., & Bakar, A. A. (2011). Woven hybrid composites: water absorption and thickness swelling behaviours. *BioResources*, 6(2), 1043–1052.

- Kiel, B., Alsdorf, D., & LeFavour, G. (2006). Capability of SRTM C-and X-band DEM data to measure water elevations in Ohio and the Amazon. *Photogrammetric Engineering & Remote Sensing*, 72(3), 313–320.
- Komi, K., Neal, J., Trigg, M. A., & Diekkrüger, B. (2017). Modelling of flood hazard extent in data sparse areas: a case study of the Oti River basin, West Africa. *Journal of Hydrology: Regional Studies*, 10, 122–132.
- Kotera, A., & Nawata, E. (2007). Role of plant height in the submergence tolerance of rice: a simulation analysis using an empirical model. *Agricultural Water Management*, 89(1–2), 49–58.
- Kubal, C., Haase, D., Meyer, V., & Scheuer, S. (2009). Integrated urban flood risk assessment - Adapting a multicriteria approach to a city. *Natural Hazards and Earth System Science*. <https://doi.org/10.5194/nhess-9-1881-2009>
- Kudadjie, C. Y., Struik, P. C., Richards, P., & Offel, S. K. (2004). Assessing production constraints, management and use of sorghum diversity in north-east Ghana: A diagnostic study. *NJAS - Wageningen Journal of Life Sciences*. [https://doi.org/10.1016/S1573-5214\(04\)80022-8](https://doi.org/10.1016/S1573-5214(04)80022-8)
- Kundzewicz, Z. W., Kanae, S., Seneviratne, S. I., Handmer, J., Nicholls, N., Peduzzi, P., Mechler, R., Bouwer, L. M., Arnell, N., Mach, K., & others. (2014). Flood risk and climate change: global and regional perspectives. *Hydrological Sciences Journal*, 59(1), 1–28.
- Kwang, C., & Osei, E. M. (2017). Accra Flood Modelling through Application of Geographic Information Systems (GIS). *Remote Sensing Techniques and Analytical Hierarchy Process. J Remote Sensing & GIS*, 6(191), 2.
- Lee, G., Jun, K. S., & Cung, E. S. (2014). Group decision-making approach for flood vulnerability identification Group decision-making approach for flood vulnerability identification using the fuzzy VIKOR method Group decision-making approach for flood vulnerability identification Group decision-making approach for flood vulnerability identification. *Nat. Hazards Earth Syst. Sci. Discuss*, 2, 6141–6171. <https://doi.org/10.5194/nhessd-2-6141-2014>
- Lee, J. S., & Pottier, E. (2009). Introduction to the polarimetric target decomposition concept. *Polarimetric Radar Imaging: From Basics to Applications; CRC Press: Boca Raton, FL, USA*, 1–422.
- Li, Jin, & Heap, A. D. (2008). A Review of Spatial Interpolation Methods for Environmental Scientists. *Australian Geological Survey Organisation*. https://doi.org/http://www.ga.gov.au/image_cache/GA12526.pdf
- Li, Jing, & Wong, D. W. S. (2010). Effects of DEM sources on hydrologic applications. *Computers, Environment and Urban Systems*, 34(3), 251–261.
- Liew, S. C. (2011). Principles of remote sensing. *Centre for Remote Imaging, Sensing and Processing, National University of Singapore, Singapore*, 119260.
- Maillard, P., Alencar-Silva, T., & Clausi, D. A. (2008). An evaluation of Radarsat-1 and ASTER data for mapping veredas (palm swamps). *Sensors*, 8(9), 6055–6076.
- Marechal, C., Pottier, E., Hubert-Moy, L., & Rapinel, S. (2012). One year wetland survey investigations from quad-pol RADARSAT-2 time-series SAR images. *Canadian Journal of Remote Sensing*, 38(3), 240–252.
- Marti-Cardona, B., Lopez-Martinez, C., Dolz-Ripolles, J., & Bladè-Castellet, E. (2010). ASAR polarimetric, multi-incidence angle and multitemporal characterization of Doñana wetlands

- for flood extent monitoring. *Remote Sensing of Environment*, 114(11), 2802–2815.
- Martinis, S., & Twele, A. (2011). Unsupervised flood detection in X-band SAR data using multi-contextual Markov image modeling on irregular graphs. *TerraSAR-X Science Team Meeting*. <https://elib.dlr.de/69780/>
- Masood, M., & Takeuchi, K. (2012a). Assessment of flood hazard, vulnerability and risk of mid-eastern Dhaka using DEM and 1D hydrodynamic model. *Natural Hazards*, 61(2), 757–770. <https://doi.org/10.1007/s11069-011-0060-x>
- Masood, M., & Takeuchi, K. (2012b). Assessment of flood hazard, vulnerability and risk of mid-eastern Dhaka using DEM and 1D hydrodynamic model. *Natural Hazards*, 61(2), 757–770. <https://doi.org/10.1007/s11069-011-0060-x>
- Masoudian, M. (2009). *The topographical impact on effectiveness of flood protection measures Bündnisse zur* (Vol. 18). kassel university press GmbH.
- Mastin, M. (2009). Watershed models for decision support for inflows to potholes reservoir. *Washington: US Geological Survey Scientific Investigations Report*, 5081, 54.
- Matgen, P., Schumann, G., Henry, J.-B., Hoffmann, L., & Pfister, L. (2007). Integration of SAR-derived river inundation areas, high-precision topographic data and a river flow model toward near real-time flood management. *International Journal of Applied Earth Observation and Geoinformation*, 9(3), 247–263.
- Mazzorana, B., Levaggi, L., Keiler, M., & Fuchs, S. (2012). *Towards dynamics in flood risk assessment*.
- McCusker, B., & Carr, E. R. (2006). The co-production of livelihoods and land use change: Case studies from South Africa and Ghana. *Geoforum*, 37(5), 790–804.
- Meenakshi, A. V., & Punitham, V. (n.d.). *Performance of Speckle Noise Reduction Filters on Active Radar and SAR Images*.
- Merryman Boncori, J. P. (2016). Caveats concerning the use of SRTM DEM version 4.1 (CGIAR-CSI). *Remote Sensing*, 8(10), 793.
- Merz, B., Kreibich, H., Schwarze, R., & Thielen, A. (2010). Review article'Assessment of economic flood damage?. *Natural Hazards and Earth System Sciences (NHESS)*, 10(8), 1697–1724.
- Merz, B., Thielen, A. H., & Gocht, M. (2007). Flood risk mapping at the local scale: concepts and challenges. In *Flood risk management in Europe* (pp. 231–251). Springer.
- Messner, F. (2007). *Evaluating flood damages: guidance and recommendations on principles and methods*. T09-06-01.
- Meyer, V., Becker, N., Markantonis, V., Schwarze, R., Van Den Bergh, J. C. J. M., Bouwer, L. M., Bubeck, P., Ciavola, P., Genovese, E., Green, C., Hallegatte, S., Kreibich, H., Lequeux, Q., Logar, I., Papyrakis, E., Pfuerscheller, C., Poussin, J., Przyluski, V., Thielen, A. H., & Viavattene, C. (2013). Review article: Assessing the costs of natural hazards-state of the art and knowledge gaps. *Natural Hazards and Earth System Science*, 13(5), 1351–1373. <https://doi.org/10.5194/nhess-13-1351-2013>
- Meyer, Volker, Scheuer, S., & Haase, D. (2009). A multicriteria approach for flood risk mapping exemplified at the Mulde river, Germany. *Natural Hazards*. <https://doi.org/10.1007/s11069-008-9244-4>
- Minh, H. V. T., Avtar, R., Mohan, G., Misra, P., & Kurasaki, M. (2019). Monitoring and mapping

- of rice cropping pattern in flooding area in the Vietnamese Mekong Delta using Sentinel-1A data: a case of an Giang Province. *ISPRS International Journal of Geo-Information*, 8(5), 211.
- MoFA (Ministry of Food and Agriculture). (2009). National Rice Development Strategy-Draft. *A Draft Report of the Ministry of Food and Agriculture of the Republic of Ghana*.
- Moreira, A., Prats-Iraola, P., Younis, M., Krieger, G., Hajnsek, I., & Papathanassiou, K. P. (2013). A tutorial on synthetic aperture radar. *IEEE Geoscience and Remote Sensing Magazine*, 1(1), 6–43.
- Morris, J., & Brewin, P. (2013). *The impact of seasonal flooding on agriculture: the spring 2012 floods in Somerset, England*. *J. Flood Risk Manage.*
- Morris, J., & Hess, T. M. (1988). Agricultural flood alleviation benefit assessment: a case study. *Journal of Agricultural Economics*, 39(3), 402–412.
- Morris, Joe, & Wheeler, H. (2007). Catchment land-use. Ed) Thorne, C. R., et Al. *Future Flooding and Coastal Erosion Risks*. London, Thomas Telford, 64–95.
- Motsumi, S., Magole, L., & Kgathi, D. (2012). Indigenous knowledge and land use policy: Implications for livelihoods of flood recession farming communities in the Okavango Delta, Botswana. *Physics and Chemistry of the Earth*. <https://doi.org/10.1016/j.pce.2012.09.013>
- Musah, B. A., Mumuni, E., Abayomi, O., & Jibreel, M. B. (2013). Effects of Floods on the Livelihoods and Food Security of Households in the Tolon/Kumbungu District of the Northern Region of Ghana. *American Journal of Research Communication*, 1(8), 160–171.
- Namara, R. E., Horowitz, L., Nyamadi, B., & Barry, B. (2011). *Irrigation development in Ghana: Past experiences, emerging opportunities, and future directions*.
- Nielsen, D. C. (2016). *Water in Dryland Cropping Systems* *Water in Dryland Cropping Systems*. January 2003.
- Nkwunonwo, U., Whitworth, M., & Baily, B. (2016). A review and critical analysis of the efforts towards urban flood risk management in the Lagos region of Nigeria. *Natural Hazards and Earth System Sciences*, 16(2), 349–369.
- Nyarko, B. K. (2007). Floodplain wetland-river flow synergy in the White Volta River basin, Ghana. *Thesis*, 214.
- O’Grady, D., Leblanc, M., & Bass, A. (2014). The use of radar satellite data from multiple incidence angles improves surface water mapping. *Remote Sensing of Environment*, 140, 652–664.
- OECD. (2010). *Cities and climate change*. OECD Publishing Paris.
- Ofori, E., Oteng-Darko, P., Berchie, J. N., Nimako, F. O., Yeboah, S., Danquah, E. O., & others. (2014). Monitoring of soil moisture regime and water use efficiency under maize cowpea cropping system. *Int. J. Curr. Microbiol. App. Sci*, 3(10), 837–848.
- Okuyama, Y. (2007). Economic modeling for disaster impact analysis: past, present, and future. *Economic Systems Research*, 19(2), 115–124.
- Osei-Asare, Y. B. (2010). Mapping of poverty reduction strategy papers (PRSPs), Sector strategies and policies related to rice development in Ghana. *Coalition for African Rice Development (CARD) c/o AGRA, Nairobi, Kenya*.
- Otieno, J. A. (2004). Scenario study for Flood Hazard Assessment in the lower Bicol Floodplain

- Philippine using A 2D Flood model. *International Institute for Geo-Information Science and Earth Observation*.
- Owusu, G. (2014). Re-engineering DEM to extract geomorphologic parameters for flood prediction in Ghana. *J Geomatics*, 8, 153–163.
- PANNAR. (2016, November 14). *MANAGE THE GROWTH STAGES OF THE MAIZE PLANT WITH PANNAR*.
https://www.pannar.com/index.php?/blog/detail/manage_the_growth_stages_of_the_maize_plant
- Peltonen-Sainio, P., Jauhiainen, L., Trnka, M., Olesen, J. E., Calanca, P., Eckersten, H., ... & Kumar, S. (2010). Coincidence of variation in yield and climate in Europe. *Agriculture, Ecosystems & Environment*, 139(4), 483–489.
- Penning-Rowsell, E. C., Yanyan, W., Watkinson, A. R., Jiang, J., & Thorne, C. (2013). Socioeconomic scenarios and flood damage assessment methodologies for the Taihu Basin, China. *Journal of Flood Risk Management*, 6(1), 23–32. <https://doi.org/10.1111/j.1753-318X.2012.01168.x>
- Premachandra, G. S., Hahn, D. T., Rhodes, D., & Joly, R. J. (1995). Leaf water relations and solute accumulation in two grain sorghum lines exhibiting contrasting drought tolerance. *Journal of Experimental Botany*, 46(12), 1833–1841.
- Programme, U. N. H. S., & for Africa, U. N. E. C. (2008). *The State of African Cities 2008: A Framework for Addressing Urban Challenges in Africa*. UN-HABITAT.
- Puech, C., & Raclot, D. (2002). Using geographical information systems and aerial photographs to determine water levels during floods. *Hydrological Processes*, 16(8), 1593–1602.
- Pultz, T. J., Lseonte, R., St-Maurent, L., & Piters, L. (1991). Flood mapping with airborne sar imagery: Case of the 1987 saint-john river flood. *Canadian Water Resources Journal*, 16(2), 173–189. <https://doi.org/10.4296/cwrj1602173>
- Rahman, M., Di, L., Yu, E., Zhang, C., Mohiuddin, H., & others. (2019). In-Season Major Crop-Type Identification for US Cropland from Landsat Images Using Crop-Rotation Pattern and Progressive Data Classification. *Agriculture*, 9(1), 17.
- Rahman, M. M., Lamb, D. W., & Samborski, S. M. (2019). Reducing the influence of solar illumination angle when using active optical sensor derived NDVIAOS to infer fAPAR for spring wheat (*Triticum aestivum* L.). *Computers and Electronics in Agriculture*, 156, 1–9.
- Rahman, M. R., & Thakur, P. K. (2018). Detecting, mapping and analysing of flood water propagation using synthetic aperture radar (SAR) satellite data and GIS: A case study from the Kendrapara District of Orissa State of India. *Egyptian Journal of Remote Sensing and Space Science*, 21, S37–S41. <https://doi.org/10.1016/j.ejrs.2017.10.002>
- Ranum, P., Peña-Rosas, J. P., & Garcia-Casal, M. N. (2014). Global maize production, utilization, and consumption. *Annals of the New York Academy of Sciences*, 1312(1), 105–112.
- Rehman, S., Sahana, M., Hong, H., Sajjad, H., & Ahmed, B. Bin. (2019). A systematic review on approaches and methods used for flood vulnerability assessment: framework for future research. *Natural Hazards*, 1–24.
- Reliefweb. (n.d.). *Ghana: Floods - Aug 2018 | ReliefWeb*. Reliefweb. Retrieved September 19, 2020, from <https://reliefweb.int/disaster/fl-2018-000154-gha>

- Richard Davies. (2018, September 25). *Ghana – Dozens Killed by Flooding in Northern Regions – FloodList*. Floodlist . <http://floodlist.com/africa/ghana-floods-northern-regions-september-2018>
- Sahana, M., Hong, H., & Sajjad, H. (2018). Analyzing urban spatial patterns and trend of urban growth using urban sprawl matrix: A study on Kolkata urban agglomeration, India. *Science of the Total Environment*, 628, 1557–1566.
- Santillan, J. R., & Makinano-Santillan, M. (2016). Vertical accuracy assessment of 30-M resolution ALOS, ASTER, and SRTM global DEMs over Northeastern Mindanao, Philippines. *International Archives of the Photogrammetry, Remote Sensing and Spatial Information Sciences - ISPRS Archives*, 41(July), 149–156. <https://doi.org/10.5194/isprsarchives-XLI-B4-149-2016>
- Sanyal, J., & Lu, X. X. (2003). Application of GIS in flood hazard mapping : a case study of Gangetic Map Asia 2003 Poster Session. *Map Asia 2003, September 2016*, 8.
- Sanyal, J., & Lu, X. X. (2005). Remote sensing and GIS-based flood vulnerability assessment of human settlements: A case study of Gangetic West Bengal, India. *Hydrological Processes*, 19(18), 3699–3716. <https://doi.org/10.1002/hyp.5852>
- Sayers, P., Yuanyuan, L., Galloway, G., Penning-Rowsell, E., Fuxin, S., Kang, W., Yiwei, C., & Le Quesne, T. (2013). *Flood risk management: a strategic approach*. Asian Development Bank, GIWP, UNESCO and WWF-UK.
- Scheuer, S., Haase, D., & Meyer, V. (2011). Exploring multicriteria flood vulnerability by integrating economic, social and ecological dimensions of flood risk and coping capacity: From a starting point view towards an end point view of vulnerability. *Natural Hazards*, 58(2), 731–751. <https://doi.org/10.1007/s11069-010-9666-7>
- Schreier, G. (Ed. . (1993). *SAR geocoding: data and systems*. Wichmann.
- Shrestha, B. B., Okazumi, T., Miyamoto, M., & Sawano, H. (2016). Flood damage assessment in the Pampanga river basin of the Philippines. *Journal of Flood Risk Management*, 9(4), 355–369. <https://doi.org/10.1111/jfr3.12174>
- Siauw, D., & others. (2001). State of forest genetic resources in Ghana. *Forest Genetic Resources Working Papers. Working Paper FGR E*, 17.
- Skinner, J. M. S. (n.d.). *Global Water Initiative: Burkina Faso | International Institute for Environment and Development*. Retrieved September 18, 2019, from <https://www.iied.org/global-water-initiative-burkina-faso>
- Smith, K., & Ward, R. (1998). *Floods: physical processes and human impacts*. John Wiley and Sons Ltd.
- SRID. (2004). *Production of major crops in Ghana, 2003*.
- Subramanya, K. (2009). *Flow in open channels*. Tata McGraw-Hill Education.
- Suwandana, E., Kawamura, K., Sakuno, Y., Kustiyanto, E., & Raharjo, B. (2012). Evaluation of ASTER GDEM2 in comparison with GDEM1, SRTM DEM and topographic-map-derived DEM using inundation area analysis and RTK-dGPS data. *Remote Sensing*, 4(8), 2419–2431.
- Symeonakis, E., Bonifácio, R., & Drake, N. (2009). A comparison of rainfall estimation techniques for sub-Saharan Africa. *International Journal of Applied Earth Observation and Geoinformation*, 11(1), 15–26.
- Taylor, A. (2011). The Role of Leadership for Environment and Sustainability. *Perspectives on Environment and Sustainability*, April.

<http://www.watercentre.org/education/leadership/attachments/5.pdf>

- Twele, A., Cao, W., Plank, S., & Martinis, S. (2016). Sentinel-1-based flood mapping: a fully automated processing chain. *International Journal of Remote Sensing*.
<https://doi.org/10.1080/01431161.2016.1192304>
- Udo., E. A., C., O. O., N., B. C., & A., G. U. (2015). Flood Hazard Analysis and Damage Assessment of 2012 Flood in Anambra State Using GIS and Remote Sensing Approach. *American Journal of Geographic Information System*, 4(1), 38–51.
<https://doi.org/10.5923/j.ajgis.20150401.03>
- Udo, J., Hartman, M., & Wolters, E. (n.d.). *Flood Hazard Assessment White Volta*.
- Udo, Ms. J., Klopstra, Ms. D., Hartman, Ms. M., Andah, D. W., Giessen, P. D. Ms. N. van de, Termes, Ms. P., & Bijkerk, Ms. T. (2012). *North Ghana Sustainable Development , Disaster Prevention and Water Resources Management*. December.
- UNISDR, C., & others. (2015). *The human cost of natural disasters: A global perspective*.
- UNISDR, U. (2004). Environmental Protection and Disaster Risk Reduction: A Community Leader's Guide. *UN/ISDR African Educational Series*, 2(2), 54.
- USAID. (2009). West Africa Rice Value Chain Analysis: Global Food Security Response - Senegal Rice Study. *Analysis*, February, 45.
- van Aalst, M. K., Cannon, T., & Burton, I. (2008). Community level adaptation to climate change: The potential role of participatory community risk assessment. *Global Environmental Change*, 18(1), 165–179. <https://doi.org/10.1016/j.gloenvcha.2007.06.002>
- Van de Giesen, N., Andreini, M., Van Edig, A., & Vlek, P. (2001). Competition for water resources of the Volta basin. *LAHS-AISH Publication*, 268, 199–205.
- Voigt, S., Martinis, S., Zwenzner, H., Hahmann, T., Twele, A., & Schneiderhan, T. (2009). Extraction of flood masks using satellite based very high resolution SAR data for flood management and modeling. *RIMAX Contributions at the 4th International Symposium on Flood Defence (ISFD4)*.
- Wang, B., & LinHo. (2002). Rainy Season of the Asian–Pacific Summer Monsoon*. *Journal of Climate*, 15(4), 386–398. [https://doi.org/10.1175/1520-0442\(2002\)015<0386:RSOTAP>2.0.CO;2](https://doi.org/10.1175/1520-0442(2002)015<0386:RSOTAP>2.0.CO;2)
- Wang, Y., Hess, L. L., Filoso, S., & Melack, J. M. (1995). Understanding the radar backscattering from flooded and nonflooded Amazonian forests: Results from canopy backscatter modeling. *Remote Sensing of Environment*, 54(3), 324–332. [https://doi.org/10.1016/0034-4257\(95\)00140-9](https://doi.org/10.1016/0034-4257(95)00140-9)
- Wechsler, S. P. (1999). Digital Elevation Model (DEM) uncertainty: evaluation and effect on topographic parameters. *ESRI User Conference*, 1081–1090.
- Westen, C. Van. (2009). Guide Book Session 6 : Risk Analysis. *Guide Book*, 1–33.
- Wiebold, W. J. (William J. 1949-, Mason, H. S., Knerr, D. R., Schwab, D. M., Angotti, J., & Schelp, W. C. (2013). 2013 Wiebold. In *University of Missouri--Columbia. University Extension. Extension website*. University of Missouri Extension.
<https://mospace.umsystem.edu/xmlui/handle/10355/37953>
- Winsemius, H. C., Aerts, J. C. J. H., Van Beek, L. P. H., Bierkens, M. F. P., Bouwman, A., Jongman, B., Kwadijk, J. C. J., Ligtoet, W., Lucas, P. L., Van Vuuren, D. P., & others.

- (2016). Global drivers of future river flood risk. *Nature Climate Change*, 6(4), 381–385.
- Wisner, B. (2004). *Assessment of Capacity and Vulnerability*. In, BANKKOFF, G., FRERKS, G. AND HILHORST D.(ed.) *Mapping Vulnerability: Disaster, Development and People*. London: Earthscan.
- WMO. (2013). Flood Mapping. *Integrated Flood Management Tools Series*, 20, 88. www.apfm.info
- Wolski, P., Murray-Hudson, M., Thito, K., & Cassidy, L. (2017). Keeping it simple: Monitoring flood extent in large data-poor wetlands using MODIS SWIR data. *International Journal of Applied Earth Observation and Geoinformation*, 57, 224–234.
- Yaro, J. A. (2004). Theorizing food insecurity: building a livelihood vulnerability framework for researching food insecurity. *Norsk Geografisk Tidsskrift-Norwegian Journal of Geography*, 58(1), 23–37.
- Zele\vnáková, M., Ga\vnová, L., Purcz, P., & Satrapa, L. (2015). Methodology of flood risk assessment from flash floods based on hazard and vulnerability of the river basin. *Natural Hazards*, 79(3), 2055–2071.
- Zwet, J. Van Der. (2012). The creation of a reservoir in the White Volta River, Ghana: An analysis of the impact on river morphology. *Thesis, May*, 1–160.

APPENDIX A: literature review / datasets

Table 1.0: Microwave bands and their frequencies

Frequency band Identification	Wavelength [cm]	Frequency [GHz]
Ka	0.8–1.1	40–26.5
K	1.1–1.7	26.5–18
Ku	1.7–2.4	18–12.5
X	2.4–3.8	12.5–8
C	3.8–7.5	8–4
S	7.5–15	4–2
L	15–30	2–1
P or UHF	30–100	1–0.3

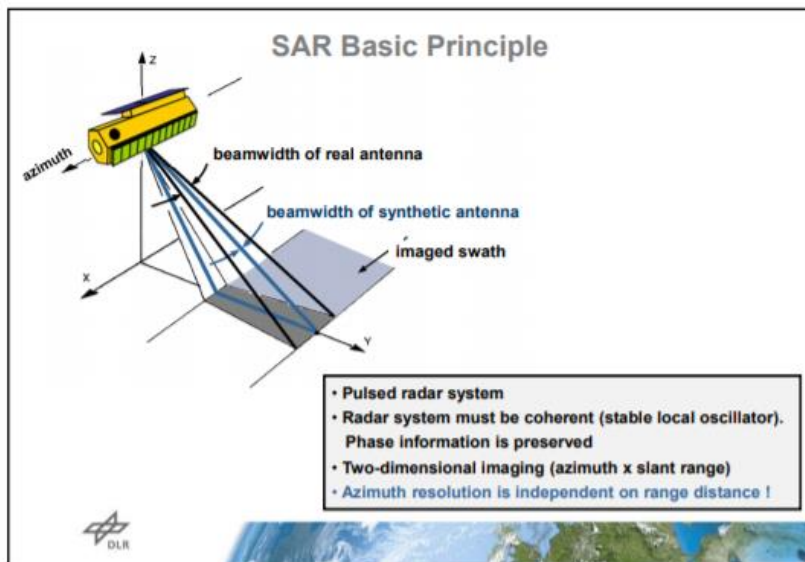


Figure 1.0: Basic operating principle of SAR (adopted from Alberto Moreira 2013)

1.0 Sentinel-2 Data

Orthorectified Sentinel-2 C (Multispectral Instrument Level 1C (MSI L1 C) downloaded or accessed from Copernicus Open Access Hub from March to June 2020 was the Main data used for the analysis in this study. Sentinel-2 data has 13 spectral bands in the Near InfraRed (NIR) Visible (VIS) and Shortwave Infrared Spectral Range (SWIR). Details of the bands are summarized in Table 2.2

Table 1.2 Characteristics of Sentinel-2A MSI bands.

Band Number	Central Wavelength (nm)	Bandwidth (nm)	Spatial Resolution (m)
1	443	20	60
2	490	65	10
3	560	35	10
4	665	30	10
5	705	15	20
6	740	15	20
7	783	20	20
8	842	115	10
8a	865	20	20
9	945	20	60
10	1375	30	60
11	1610	90	20
12	2190	180	20
TCI	RGB	Composite	10

The NDVI is the measure of the difference between red light (absorbed by vegetation) and near-infrared (reflected) channels. The near-infrared and green light is reflected most by the chlorophyll, while red and blue light is mostly absorbed. The formula below is used to calculate NDVI from Sentinel-2

$$\text{NDVI} = \text{Index (B8, B4)} = \frac{B8 - B4}{B8 + B4}$$

The Sentinel-1 images used for this study are listed in Table 3.3

Table 1.3: Satellite Images used for the analysis

Sentinel-1 image	Acquisition Date	Acquisition model	Season	Purpose
S1A_IW_GRDH_1SDV_20190311T181914	11/03/2019	VV +VH	Dry	Preflood event
S1A_IW_GRDH_1SDV_20180912T181851	12/09/2018	VV +VH	Wet	Observation and mapping of flood extents
S1A_IW_GRDH_1SDV_20180912T181916	12/09/2018	VV +VH	Wet	Observation and mapping of flood extents
S1B_IW_GRDH_1SDV_20180918T181833	18/09/2018	VV +VH	Wet	Observation and mapping of flood extents
S1B_IW_GRDH_1SDV_20180918T181808	18/09/2018	VV +VH	Wet	Observation and mapping of flood extents
S1A_IW_GRDH_1SDV_20180924T181852	24/09/2018	VV +VH	Wet	Observation and mapping of flood extents

S1A_IW_GRDH_1SDV_20180924T181917	24/09/2018	VV +VH	Wet	Observation and mapping of flood extents
Sentinel -2	14/09/2018		Wet	Land-use/landcover classification

Table 1.5: Characteristics and mode of acquisition of Sentinel-1

Mode	Incidence Angle	Resolution	Swath Width	Polarization (H = Horizontal V = Vertical)
Stripmap	20 - 45	5 x 5 m	80 km	HH+HV, VH+VV, HH, VV
Interferometric Wide swath	29 - 46	5 x 20 m	250 km	HH+HV, VH+VV, HH, VV
Extra Wide swath	19 - 47	20 x 40 m	400 km	HH+HV, VH+VV, HH, VV
Wave	22 - 35 - 38	5 x 5 m	20 x 20 km	HH, VV

Source: <https://sentinel.esa.int/web/sentinel/missions/sentinel-1/instrument-payload/resolution-swath>

APPENDIX B: Description of Crops considered in this study

Table 1.6: Genetically Improved Maize Varieties as adopted from CSIR/SARI

Variety	Type of Variety	Grain Colour/Texture	Maturity Days	Average Yield	
				Tonnes/Hectare	Bags/Acre
Abontem	QPM drought and Striga tolerant	yellow/flint	80	4.0	15
Aburohema	QPM drought and Striga tolerant	White/flint	95	4.5	18
Aseda	Normal/Hybrid	White/Flint dent	110	6.5	26
Bihilifa	drought tolerant	Yellow/flint dent	90	4.6	19
Dodzi	OPV	White/dent	75	3.4	14
Dorke-SR	Normal	White/dent	95	3.8	15
Eni-pibi	QPM/Hybrid	White/flint	110	5.5	22
Etubi	Normal/hybrid	White/dent	110	5.0	20
Ewul-Boyu	drought tolerant	White/flintdent	110	5.6	23
Golden Jubilee	OPV	Yellow/dent	110	5.0	20
Mamaba	QPM Hybrid	White/flint	110	6.0	24
Obatanpa	QPM OPV	White/dent	105	4.6	19

Omankwa	QPM drought and Striga tolerant	White/flint	95	4.5	18
OpeEbu	Normal/Hybrid	White/Flintdent	110	7.5	30
Sanzal-Sima	drought tolerant	White/flintdent	110	5,4	22
Tigli	drought tolerant	Yellow/flintdent	120	5.2	21
Tintim	Normal/Hybrid	White/Flintdent	110	7.5	30
Wang-Dataa	drought and Striga tolerant	White/flint dent	90	4.7	19

Table 1.7: Genetically improved sorghum varieties.

Variety	Type of Variety	Grain Colour/Texture	Maturity Days	Average Yield	
				Tonnes/Hectare	Bags/Acre
Framida	Striga tolerant	yellow/flint	100 -110	4.0	15
Naga White	High yielding/early maturing	White/flint	100-110	4.5	18
Kapaala	High yielding/early maturing	White/Flint dent		6.5	26
Kadaga	High yielding/early maturing	Yellow/flint dent	100-110	4.6	19
Fadda	OPV	White/dent	75	3.4	14
Dorado	Normal	White/dent	95	3.8	15

Table 1.8: Millet varieties in Ghana

Source: CSIR 2015

Variety	Type of Variety	Grains	Maturity Days	Yield Potential
Kaanati	Tolerant to Downy mildew	Mean 1000 seed weight 11.4g,	70	2 t/ha
Afribeh-naara	Drought/ Downy mildew tolerant	Mean 1000 seed weight 12 g	70	1.9 t/ha
Waapp-naara	Drought tolerant/ Downy mildew Resistant	Mean 1000 seed weight 8 g,	80	2.1 t/ha
Akad-kom	Drought tolerant, Tolerant to Downy mildew	Mean 1000 seed weight 11.4g	70	2 t/ha
Naad-kohblug	Insect and bird damage resistant, Tolerant to Downy mildew	Mean 1000 seed weight 12 g,	75	2 t/ha

Table 1.9: Rice varieties developed by CSIR-SARI

Variety	Grain yield (kg/ha)	Plant height at maturity (cm)	Maturity days
Exbaika	4291.0	97.2	123.2
Hybrid	3276.6	105.5	119.0
IR841	4331.5	108.5	123.2
Jasmine 85	3403.5	90.5	120.5
Long grain ordinary 2	4343.6	110.8	130.5

APPENDIX C: Flood Depth Analysis and Digital Elevation Model (DEM) Interpolation Processing

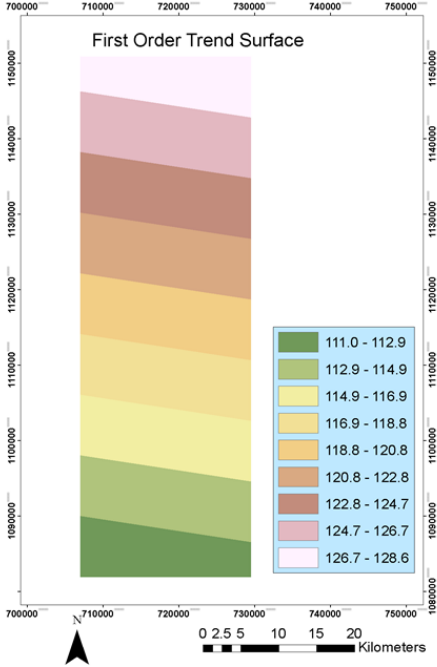


Figure 2.0 : First order polynomial interpolated surface (linear) of the study area showing elevation. This interpolation resulted in a poor representation.

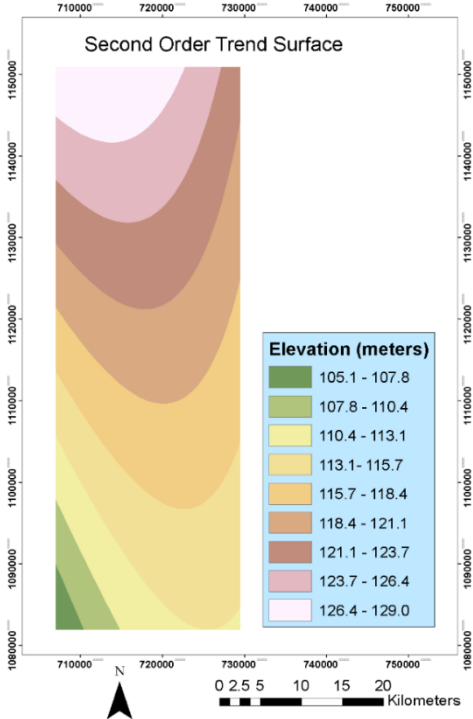


Figure 3.0 : Second order polynomial interpolated surface (quadratic) representation of the study area showing elevation

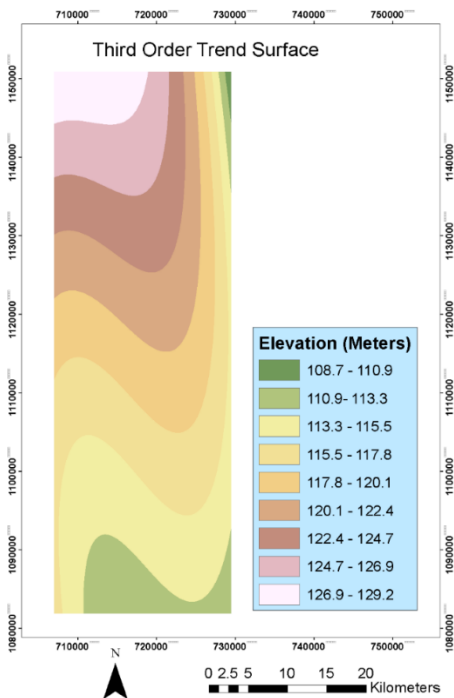


Figure 4.0: Third order polynomial interpolated surface (cubic) of the study area showing elevation. The best representation of the water surface.

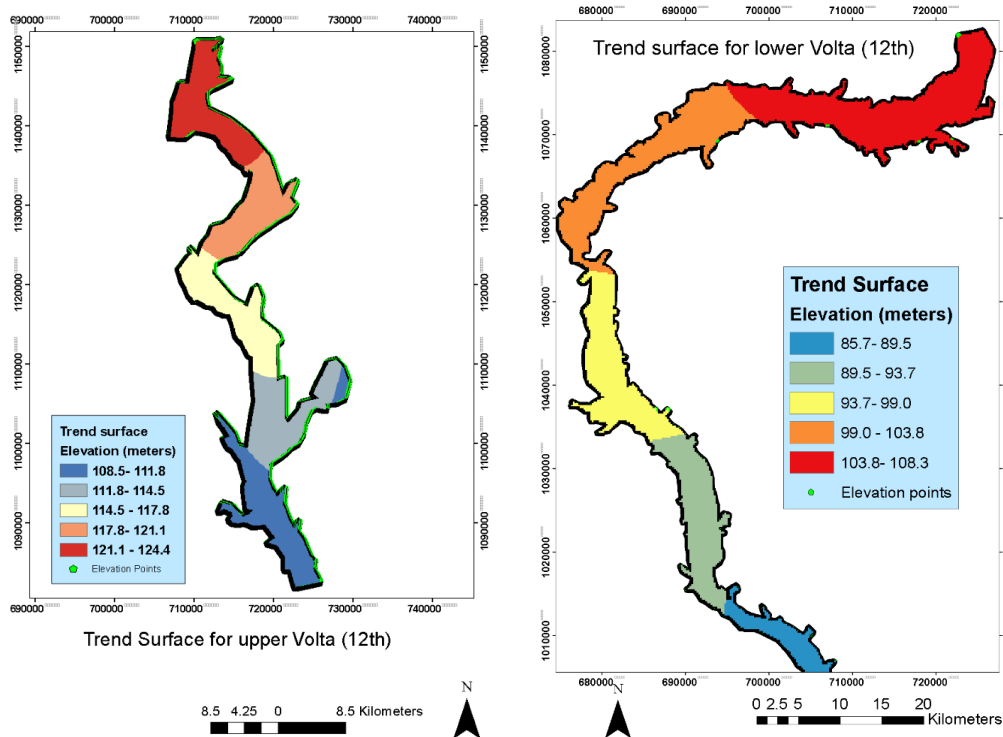


Figure 5.0: Interpolated third-order trend surface for the flood extent of the 12th showing elevation (meters) and generated points (in green) at the edge of the flood extents used to extract elevation values for upper and lower respectively

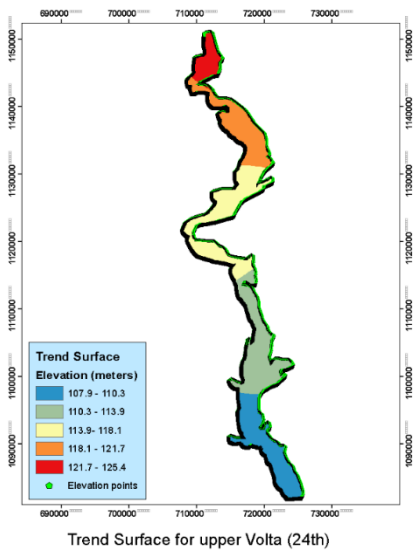


Figure 6.0: Interpolated third order trend surface for the flood extent of the 18th showing elevation (meters) and generated points (in green) at the edge of the flood extents used to extract elevation values.

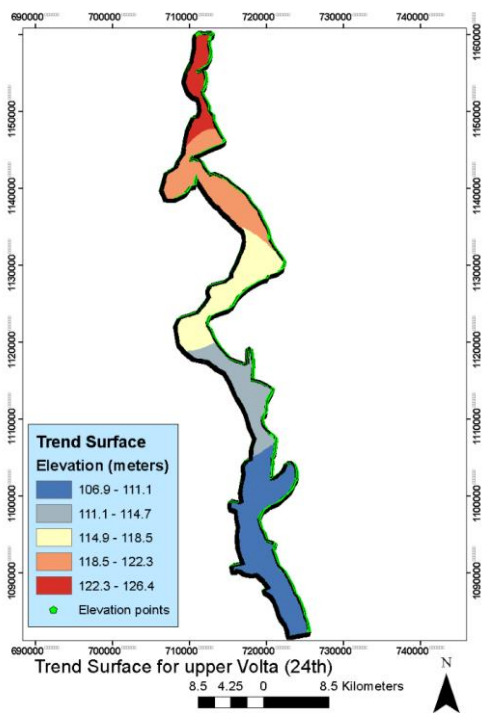


Figure 7.0: Interpolated third-order trend surface for the flood extent of the 24th showing elevation (meters) and generated points (in green) at the edge of the flood extents used to extract elevation values. (upper Volta)

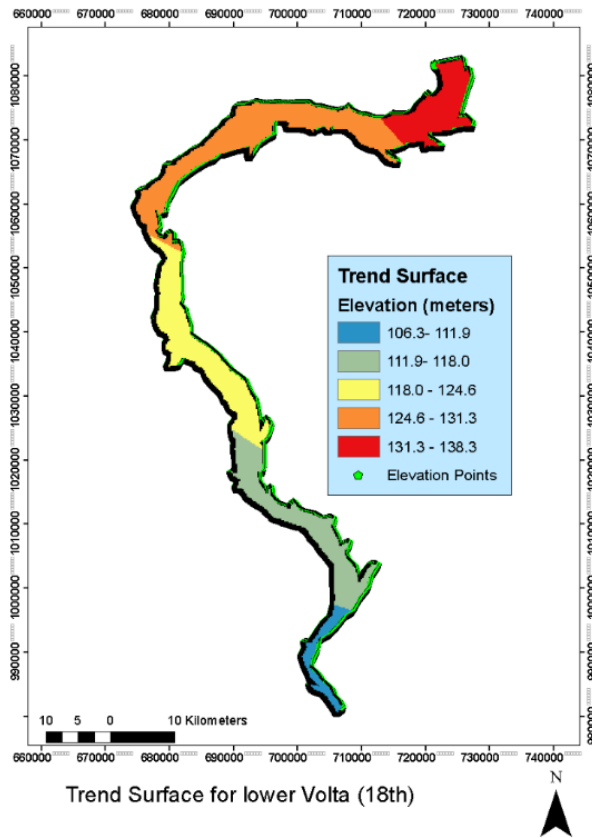


Figure 8.0: Interpolated third-order trend surface for the flood extent of the 18th showing elevation (meters) and generated points (in green) at the edge of the flood extents used to extract elevation values. (lower Volta)

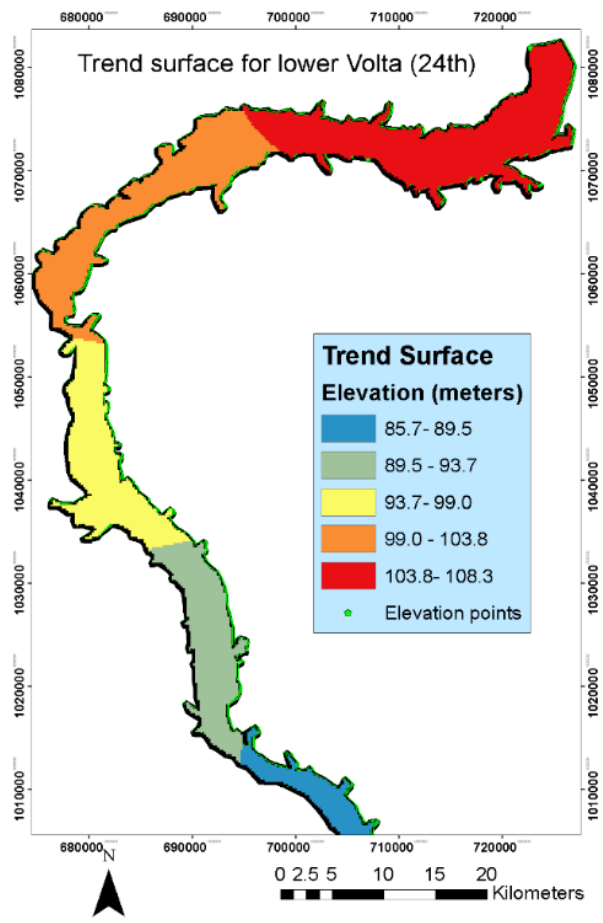


Figure 9.0: Interpolated third-order trend surface showing elevation (meters) and generated points (in green) at the edge of the flood extents used to extract elevation values. (lower Volta)

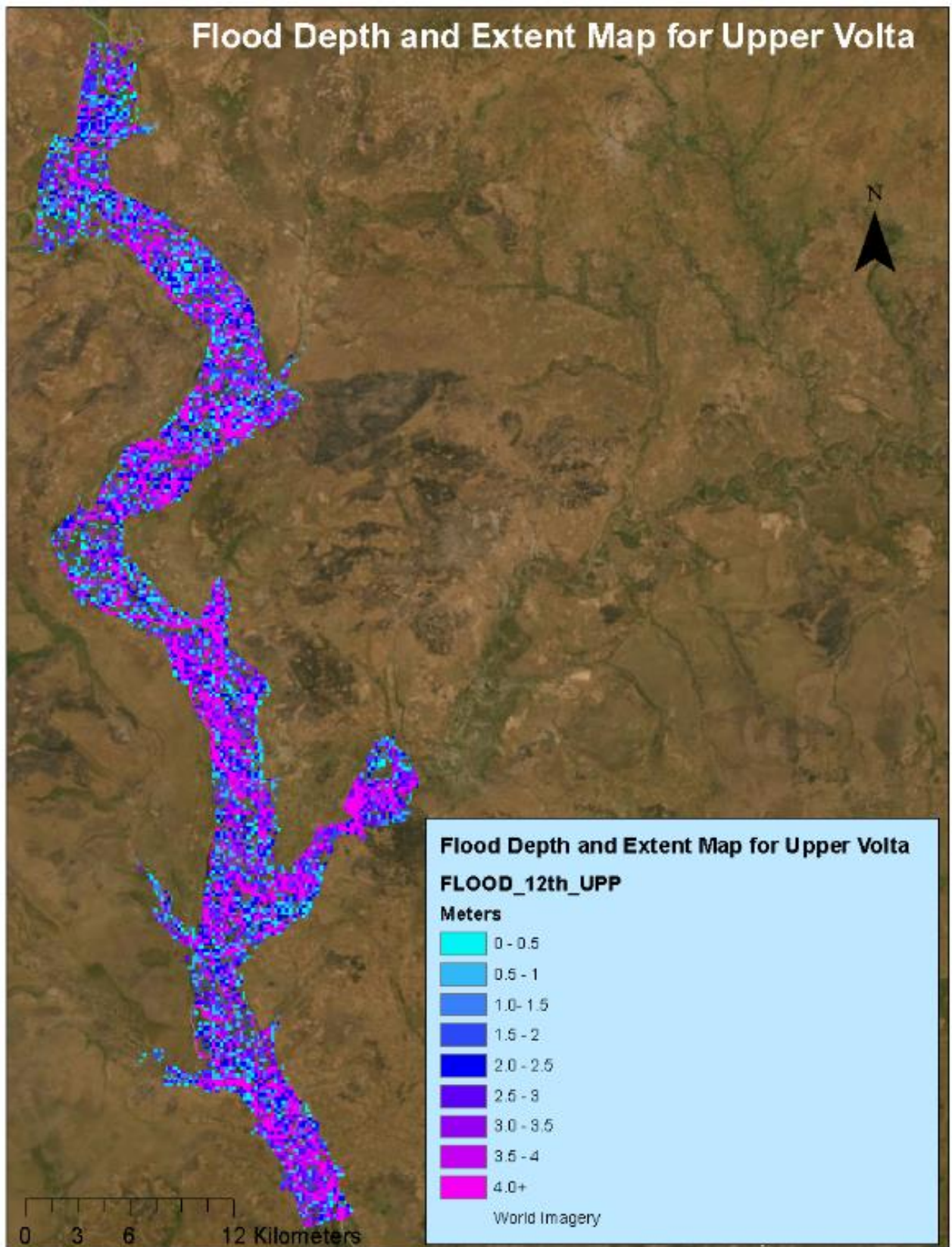


Figure 10.0: Flood depth and extent map for Upper Volta (12th)

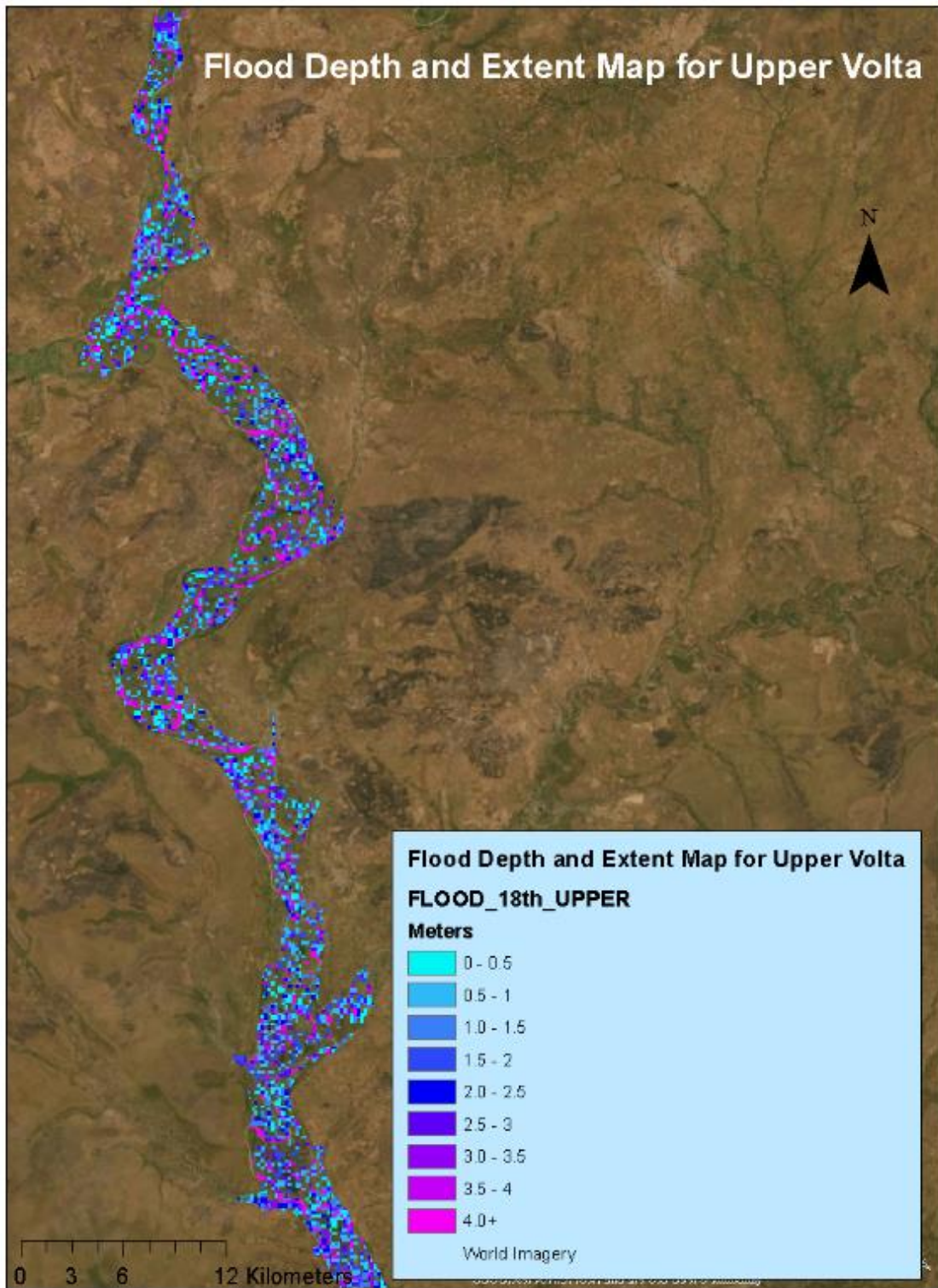


Figure 11.0: Flood depth and extent map for Upper Volta (18th)

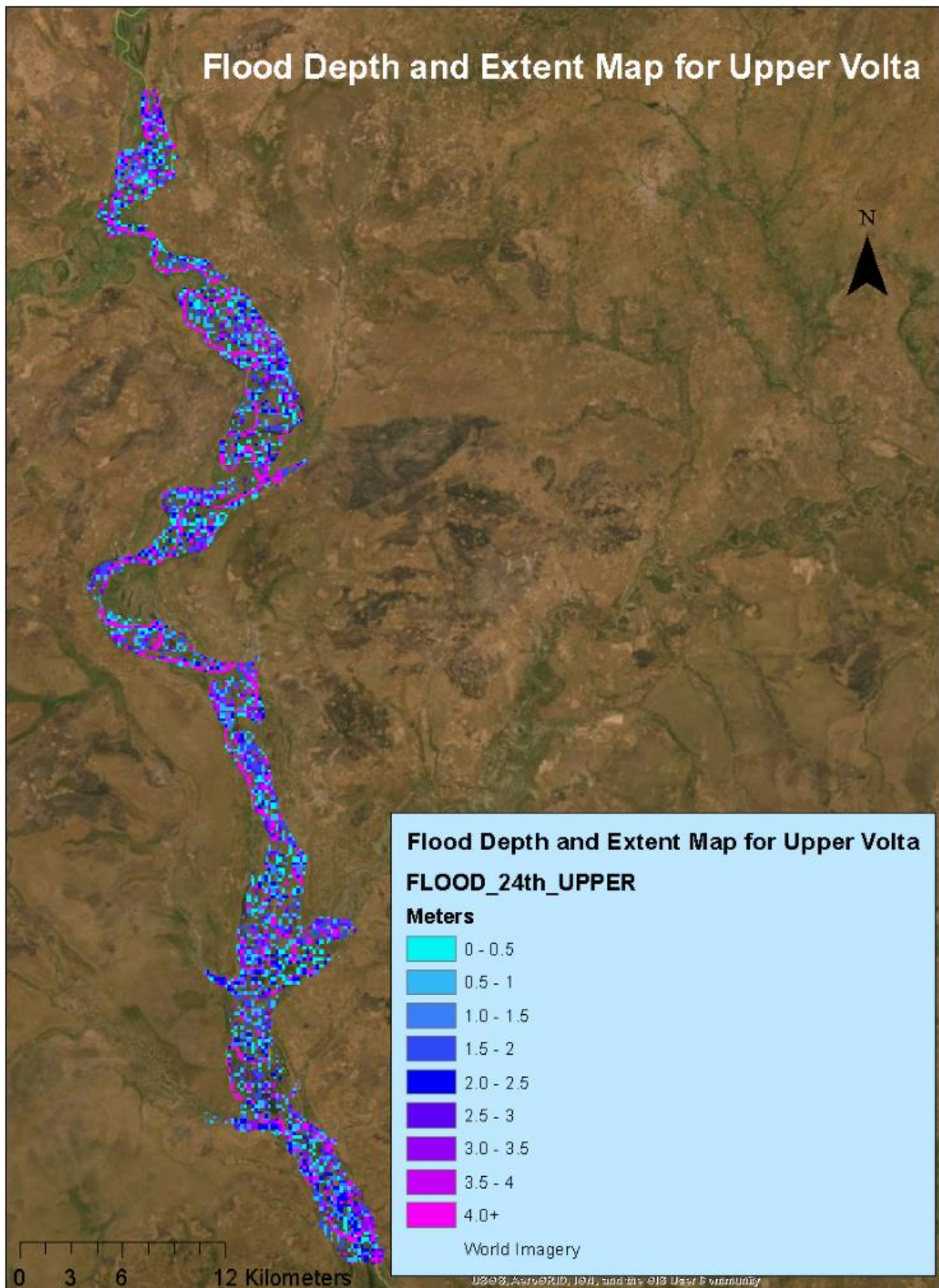


Figure 12.0: Flood depth and extent map for Upper Volta (24th)

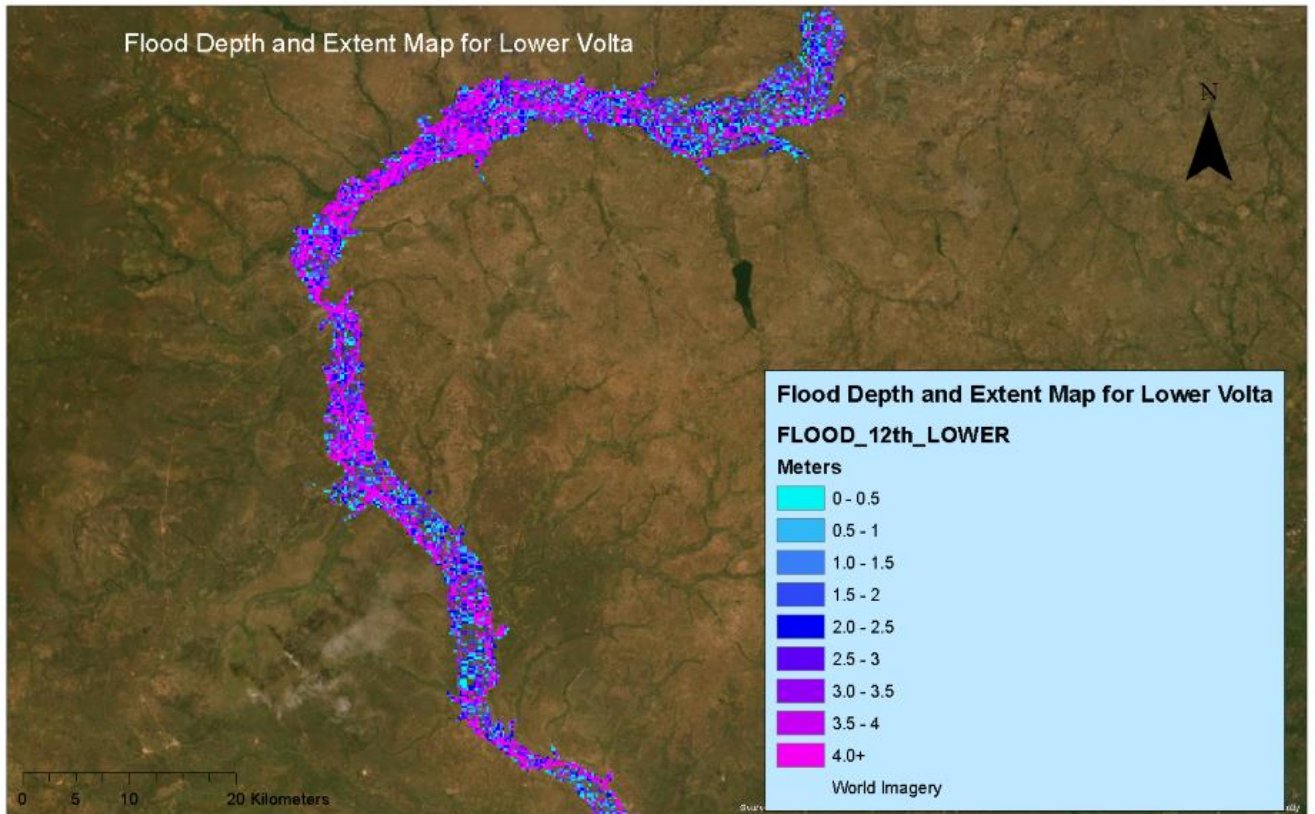


Figure 13.0: Flood depth and extent map for Lower Volta (12th)

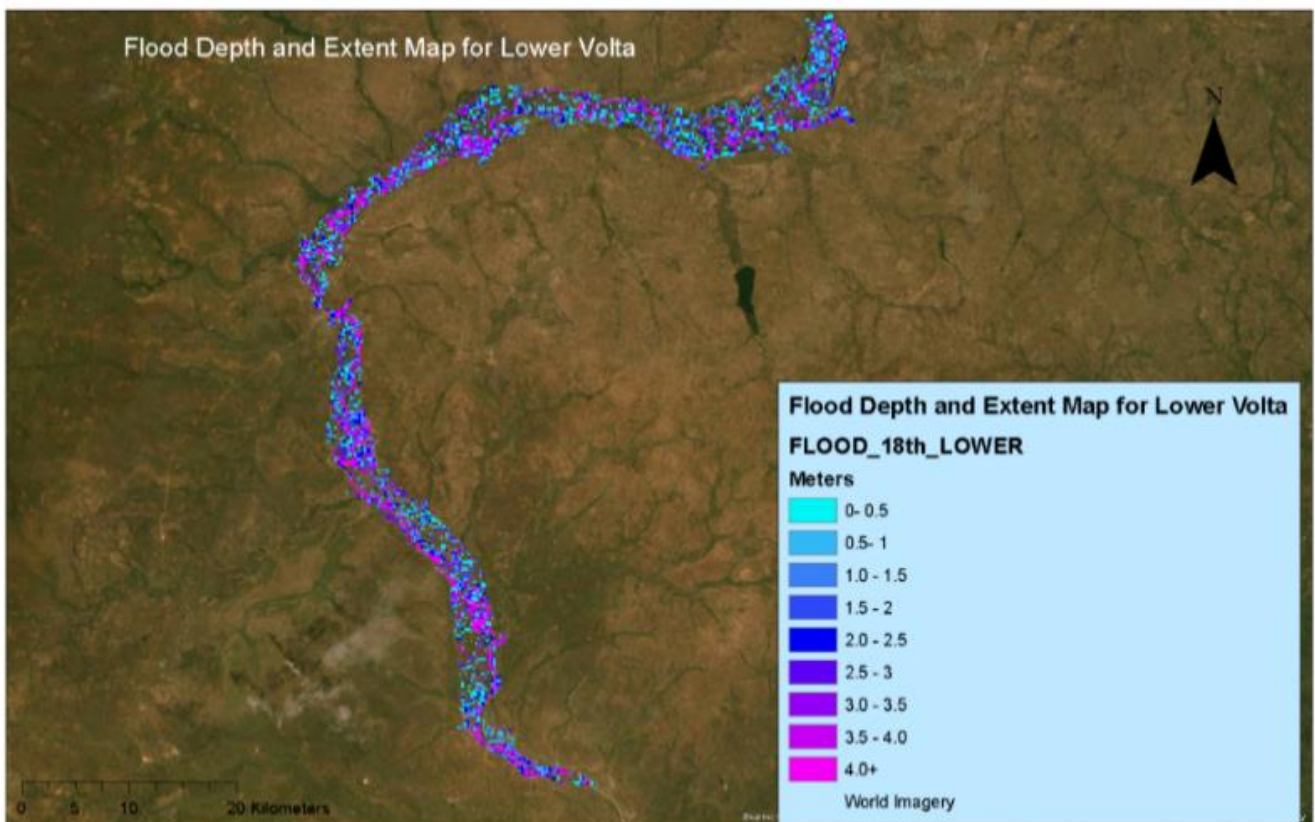


Figure 14.0: Flood depth and extent map for Lower Volta (18th)

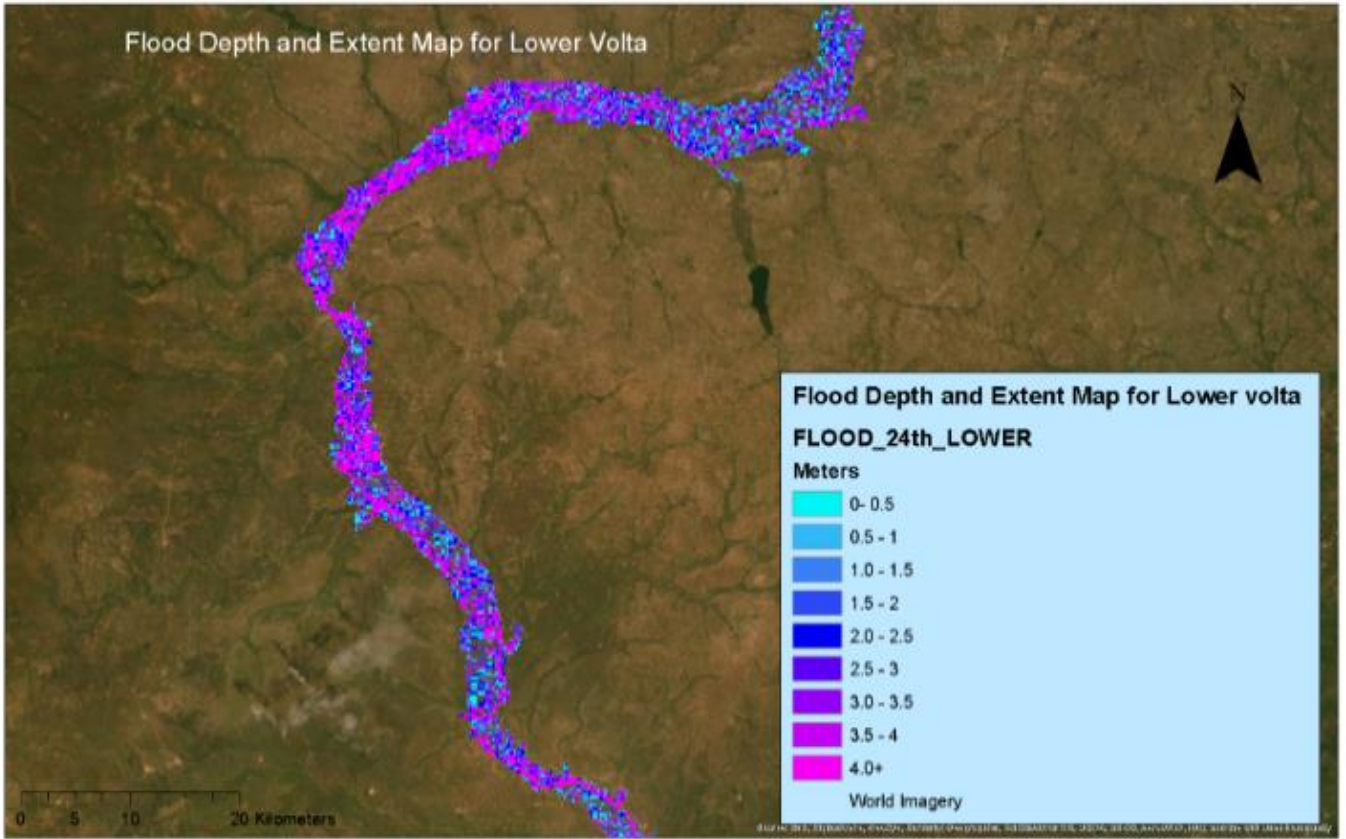


Figure 15.0: Flood depth and extent map for Lower Volta (24th)

APPENDIX D: Vulnerability, Hazard and Risk Assessment

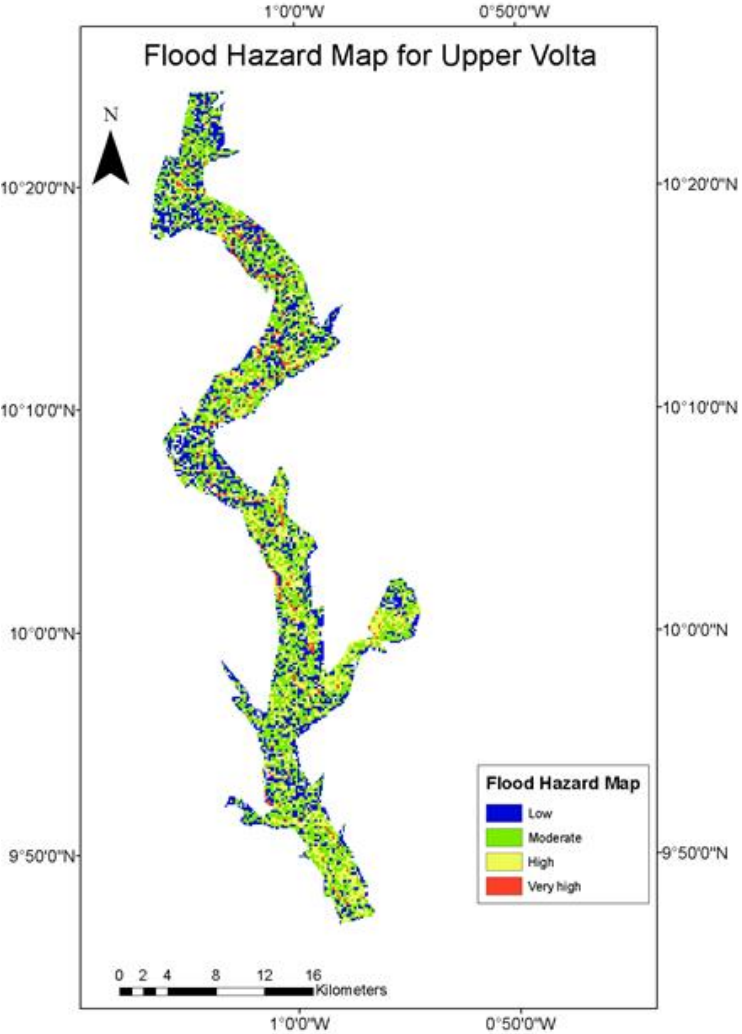


Figure 16.0: Flood Hazard Map for the upper Volta (full extent)

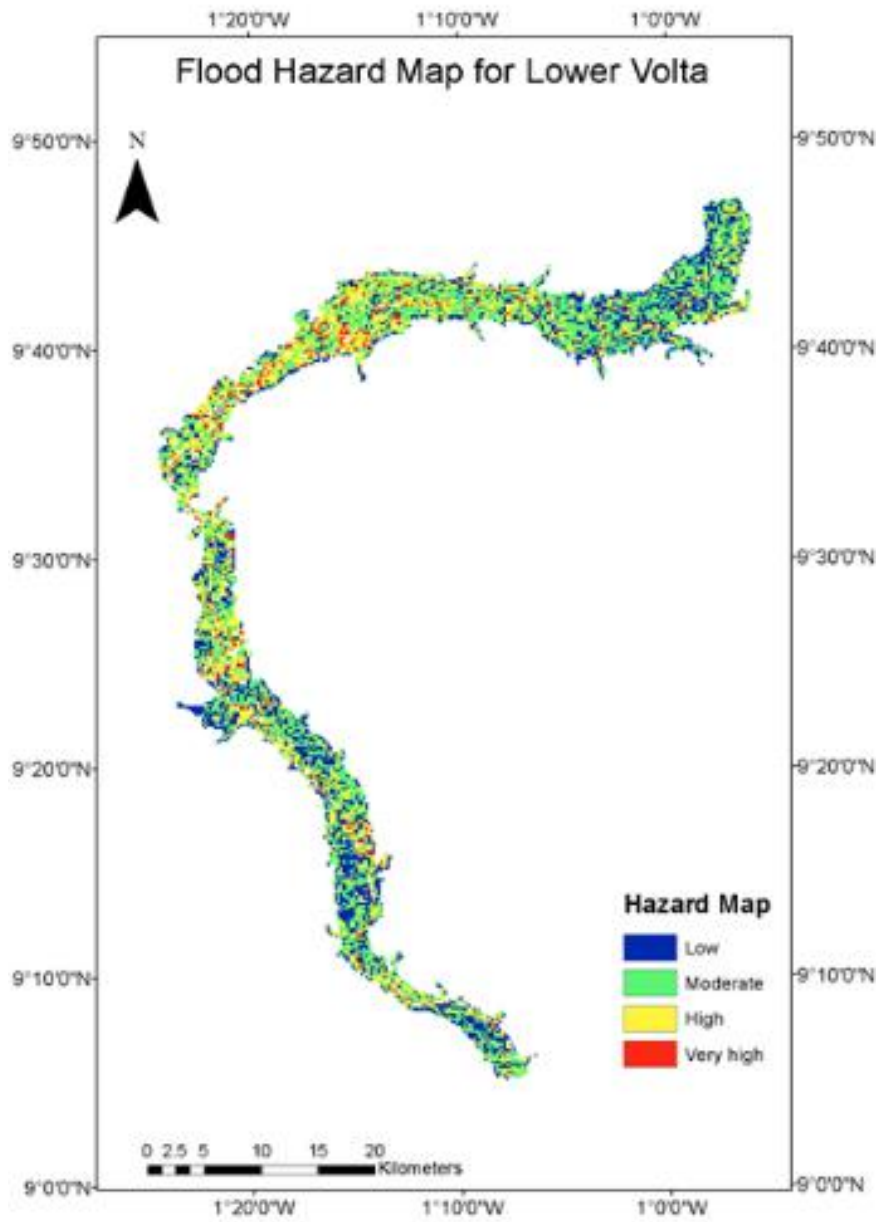


Figure 17.0: Flood Hazard Map for the lower Volta (full extent)

<https://www.youtube.com/watch?v=ftB1kLFI7mQ>

Table 1.10: Accuracy Assessment Of Landcover Classification

		Error Matrix				
		Reference Data				
		Cultivated	Water	Grassland	Woodland	Row Sum
Classified Data	Cultivated	5467	64	1220	1971	8722
	Water	923	2602	122	4154	7801
	Grassland	341	38	8124	240	8743
	Woodland	694	0	0	7691	8385
	Col Sum	7425	2704	9466	14056	33651
		Commission %	Omission Estimated	Kappa		
1		37.319422	26.37037	0.521149		
2		66.645302	3.772189	0.275316		
3		7.07995	14.177055	0.90149		
4		8.276685	45.283153	0.857862		
Kappa		Kappa Variance				
0.611463		0.00001				
Observed Correct		Total Observation	% Observed Correct			
23884		33651	70.975603			

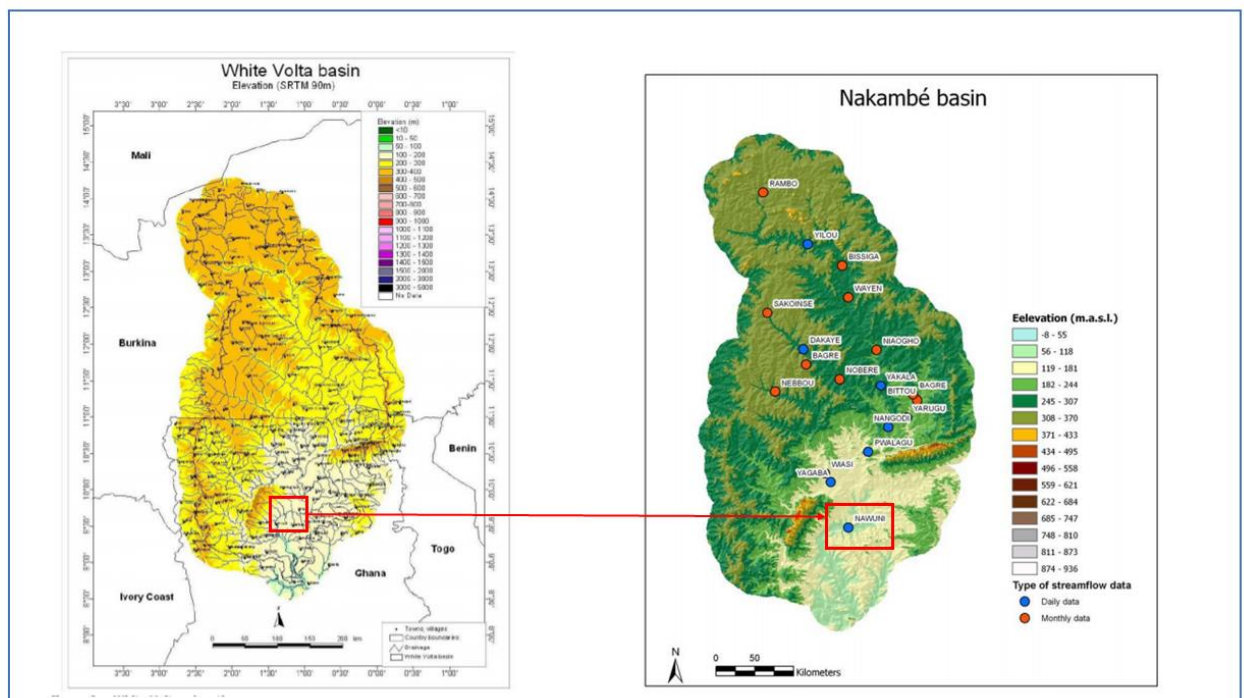


Figure 18: Location of the Navuni measuring station in the White Volta basin

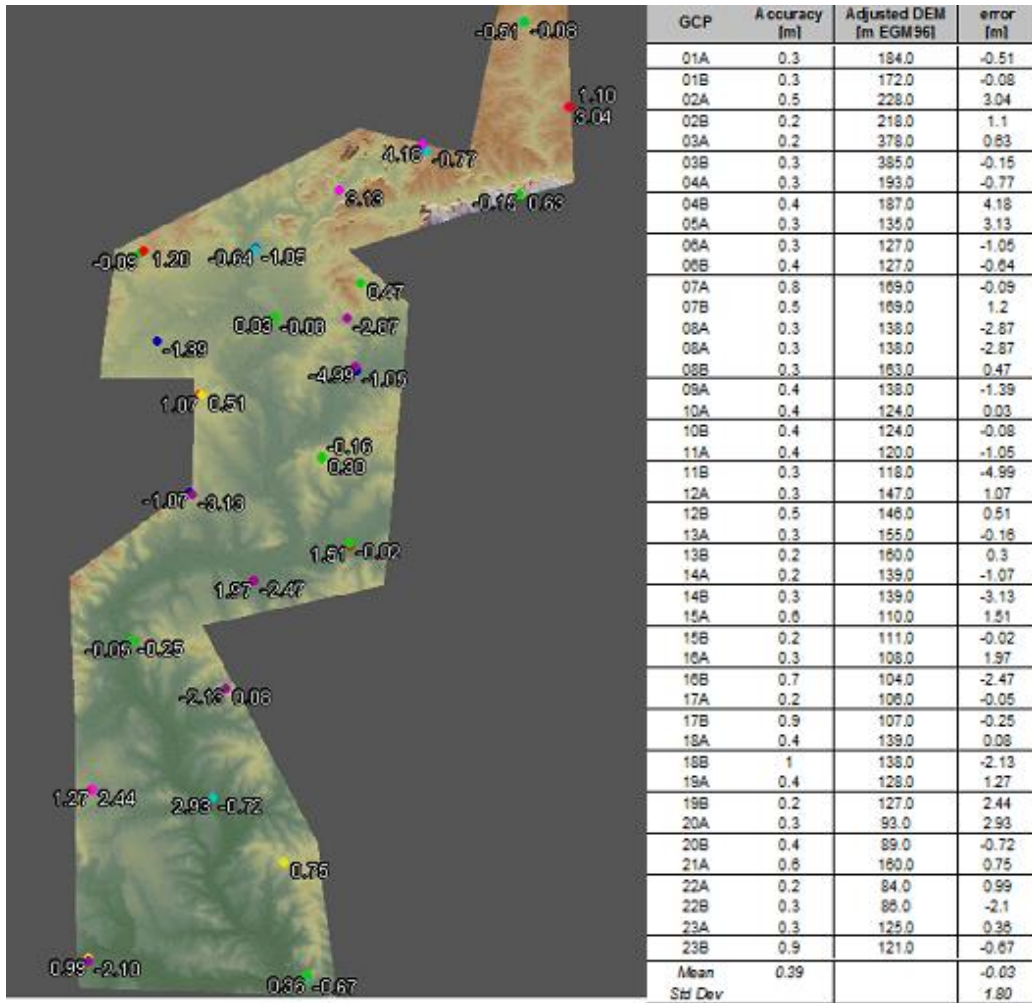


Figure 19: Location and correction by ground control points on DEM. Adopted from Udo et al., (2012)

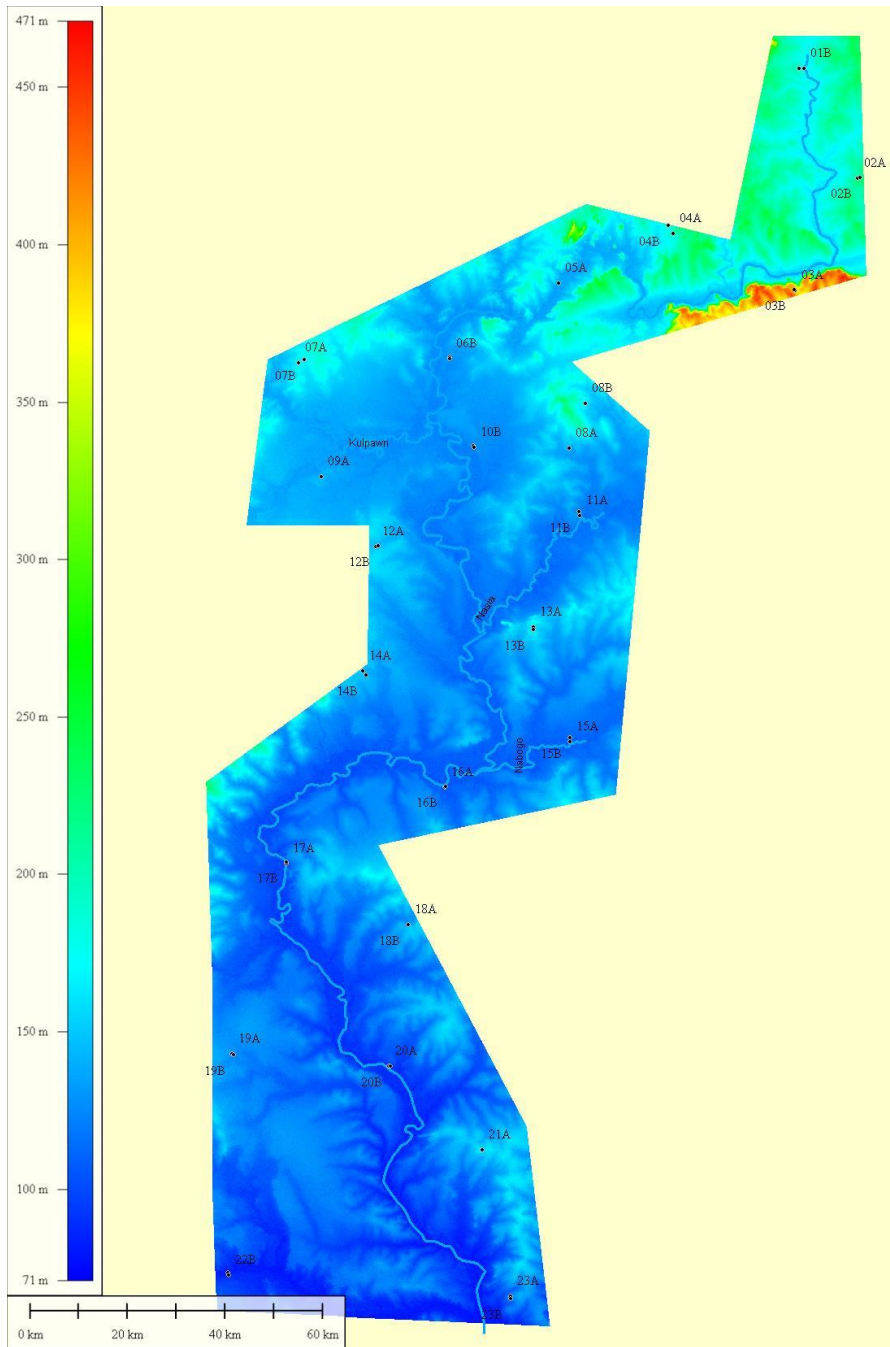


Figure 20: SPOT DEM of the Study area and GCP's. Source: Udo et al., (2012)



Figure 21: Flooded Maize farms

